PB 290870

REPORT NO.
UCB/EERC-77/30
DECEMBER 1977

EARTHQUAKE ENGINEERING RESEARCH CENTER

AN APPROACH FOR IMPROVING SEISMIC BEHAVIOR OF REINFORCED CONCRETE INTERIOR JOINTS

by
BRANKO GALUNIC
VITELMO V. BERTERO
EGOR P. POPOV

Report to Sponsors:
National Science Foundation

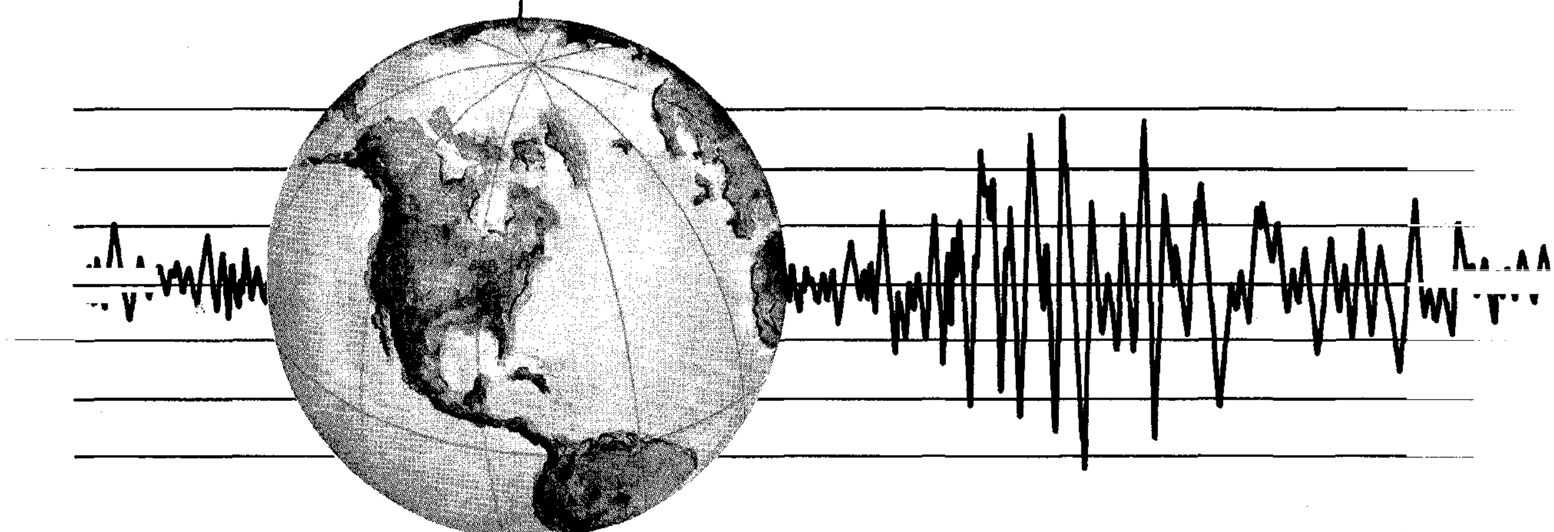

COLLEGE OF ENGINEERING

UNIVERSITY OF CALIFORNIA · Berkeley, California

BIBLIOGRAPHIC DATA SHEET	1. Report No. NSF/RA-770799	2.	3. Recipient's Accession No. PB290870

4. Title and Subtitle An Approach for Improving Seismic Behavior of Reinforced Concrete Interior Joints	5. Report Date December 1977 6.
7. Author(s) B. Galunic, V. V. Bertero, and E. P. Popov	8. Performing Organization Rept. No. UCB/EERC-77/30
9. Performing Organization Name and Address Earthquake Engineering Research Center 47th. St. and Hoffman Blvd. Richmond, CA 94804	10. Project/Task/Work Unit No. 11. Contract/Grant No. AEN-7307734 A02 ENV-7604263 A02
12. Sponsoring Organization Name and Address National Science Foundation 1800 G St., N. W. Washington, D. C. 20550	13. Type of Report & Period Covered 14.

15. Supplementary Notes

16. Abstracts

The interior joints of reinforced concrete moment-resisting frames are vulnerable to severe bond deterioration of the beam main bars passing through the column during severe cyclic loadings such as might occur in a major earthquake. In conventionally designed interior joints, cracks form on the beams at both faces of a column and if their main reinforcing bars are sufficiently strained, these bars can be simultaneously pulled from one side and pushed from the other. The bars could then slip through the columns, greatly reducing the stiffness in the beam-column assemblies. An approach for obviating this problem by avoiding the high straining of the bars at the face of the column by forming the plastic hinges with the resulting significant cracking away from the column faces is suggested. Two schemes for achieving this by proper detailing of the main beam reinforcement are reported. One such scheme involves bending some of the main beam bars at a properly computed distance from the column. In the alternative scheme some of the bars are cut off at a properly determined distance from column faces. Experimental results show that the approach of forcing the development of the plastic hinges away from the column is very promising for solving the problem of severe bond deterioration of the main bars passing through the column, and that for the subassemblage tested, either of the schemes used gave excellent results.

17b. Identifiers/Open-Ended Terms

17c. COSATI Field/Group

18. Availability Statement	19. Security Class (This Report)	21. No. of Pages
Release Unlimited	UNCLASSIFIED	116
	20. Security Class (This Page) UNCLASSIFIED	22. Price A06 - A01

AN APPROACH FOR IMPROVING SEISMIC BEHAVIOR OF REINFORCED CONCRETE INTERIOR JOINTS

By

Branko Galunic
Research Assistant
University of California
Berkeley

Vitelmo V. Bertero
Professor of Civil Engineering
University of California
Berkeley

Egor P. Popov
Professor of Civil Engineering
University of California
Berkeley

A report on research sponsored by
the National Science Foundation

Report No. UCB/EERC-77/30
Earthquake Engineering Research Center
College of Engineering
University of California
Berkeley, California

December 1977

ABSTRACT

The interior joints of reinforced concrete moment-resisting frames are vulnerable to severe bond deterioration of the beam main bars passing through the column during severe cyclic loadings such as might occur in a major earthquake. In conventionally designed interior joints, cracks form on the beams at both faces of a column and if their main reinforcing bars are sufficiently strained, these bars can be simultaneously pulled from one side and pushed from the other. The bars could then slip through the columns, greatly reducing the stiffness in the beam-column assemblies. An approach for obviating this problem by avoiding the high straining of the bars at the face of the column by forming the plastic hinges with the resulting significant cracking away from the column faces is suggested. Two schemes for achieving this by proper detailing of the main beam reinforcement are reported. One such scheme involves bending some of the main beam bars at a properly computed distance from the column. In the alternative scheme some of the bars are cut off at a properly determined distance from column faces. Experimental results show that the approach of forcing the development of the plastic hinges away from the column is very promising for solving the problem of severe bond deterioration of the main bars passing through the column, and that for the subassemblage tested, either of the schemes used gave excellent results.

ACKNOWLEDGMENTS

The authors are grateful for the financial support provided for this investigation by the National Science Foundation under Grants AEN-7307734 A02 and ENV-7604263 A02. The work reported herein is a phase of an ongoing investigation at the University of California, Berkeley, under the supervision of Professors E. P. Popov and V. V. Bertero. Many individuals contributed to the efforts described. The original configuration of the subassemblage and the experimental setup followed the design by graduate student D. Soleimani. Graduate students G. Lantaff and S. Viwathanatepa, as well as B. Lotz, assisted with the experiments.

L. Tsai and R. Kaack provided editorial assistance and L. Hashizume made the technical illustrations.

TABLE OF CONTENTS

Table of Contents (Continued)

LIST OF TABLES

LIST OF FIGURES

List of Figures (Continued)

List of Figures (Continued)

List of Figures (Continued)

1. INTRODUCTION

1.1. General

Strength is not the sole criterion in designing a building to withstand earthquake loading. To obtain an efficient building, a structure must also be ductile, that is, it should be able to undergo large inelastic deformations without collapse. The input earthquake energy is thus absorbed and dissipated by the hysteretic behavior of the structural system. In order to develop large inelastic deformations, special care must be taken in the detailing and placing of the reinforcement, especially in the lower levels of the structure where the shears in the girders and columns, caused by lateral earthquake loads, are largest. To achieve ductility in concrete the potential brittle types of failure, such as crushing of confined concrete, sudden loss of bond and anchorage, and shear failure must be prevented, and loss of stiffness under cyclic loading delayed and minimized.

It has been shown that under present detailing practices one of the most critical regions in a ductile moment-resisting space frame, which requires a strong column - weak beam design approach, may be the interior beam-column joint [1,2]. Present methods of designing, proportioning, and detailing members of these ductile frames result in inelastic deformations concentrated in regions of beams, usually called plastic hinges, which develop near the column face. In these cases the bond of the beam main reinforcement along the beam-column joint deteriorates under cyclic loading [2,3]. Under seismic loading reversals the alternating yielding of the beam main reinforcing bars at both faces of the interior column and the concomitant cracking cause bars to be pulled from one side and simultaneously pushed from the other with forces equal to or higher than their yielding forces. In addition, the total anchorage provided for the continuous bars is reduced to a length somewhat smaller than the width of the column at the joint. Reduced anchorage and repeated reversals of the simultaneous push and pull action on the bars can ultimately cause complete loss of bond, enabling the bars to slip with very little resistance through the column at the joint. The attendant drop in stiffness of the joint can be detrimental to the behavior of the whole building. Large deformations can lead to very expensive nonstructural damage and, in certain cases, to collapse of the structure.

Based on observations of the above behavior in experiments conducted at Berkeley, Bertero and Popov [1,3] have recommended methods to minimize or avoid the problems created by the slippage of the beam main bars through the interior joint. The suggested approach requires that plastic hinges form away from the face of the columns. According to this approach, significant bar slippage could then be prevented, or at least delayed, until very large displacements occurred. The purpose of this study was to investigate the feasibility of this approach.

1.2. Objectives and Scope

This study is a continuation of one reported in references 2 and 3. The objective was to study the effects of forming the critical section of the beam away from the face of the column using two different detailing techniques. The model used was a beam-column subassemblage prototype taken from a third-story level of a 20-story office building that was used in the earlier studies. The parameters studied included the strength, stiffness, ductility, and energy absorption and dissipation of the subassemblages. Two specimens, BC5 and BC6, were constructed and tested.

Specimen BC5 was designed so that the plastic hinge would form 406 mm (16 in.) away from the column face. The critical section was formed by bending two of the top beam bars downward and the corresponding bottom bars upward, to intersect 406 mm (16 in.) from the column face. After additional bending, the bars extended to the end of the beam. The beam bars located in the outer corners of the stirrups were continuous.

Specimen BC6 was designed to form plastic hinges 610 mm (24 in.) away from the column faces on both sides. The critical sections were designed to occur at the selected locations by cutting off the two interior bars on the top and bottom of the beam 610 mm (24 in.) from the column faces. Both specimens were subjected to the same loading program so that their behavior could be compared.

2. TEST SPECIMENS

2.1. Design of Specimens

The specimens used in this investigation were designed to model, as effectively and economically as possible, the behavior of a multistory reinforced concrete structure when subjected to large lateral deformations due to seismic loads. A 20-story office building (Fig. 1) was chosen as the prototype for determining the dimensions and appropriate loading conditions [2]. The structure was designed as a ductile reinforced concrete moment-resisting frame according to UBC and ACI codes [4,5].

To model the behavior of a structure as complex as the one outlined above, it is insufficient to study the behavior of each element separately because of the complex interaction between the various elements, such as beams, columns, and joints. Therefore, a beam-column subassemblage was chosen as an effective model for determining overall structural behavior (Figs. 1 and 2).

The beam-column subassemblage consists of a column cut off at midheight above and below floor level, and two beams connected to the column and cut off at the midspan of both bays (Fig. 2). The models used in these tests were made to one-half scale.

The models were designed to correspond to the third floor level of the 20-story building. It is in the lower levels where the most serious damage usually occurs during a severe earthquake, due in part to the high shear and moments that are developed as well as in part to the large vertical forces which develop in the columns due to dead and live loads in the upper levels. When the structure is subjected to lateral forces, these vertical forces cause additional moments to occur at the joints. At large displacements this well-known $P-\delta$ effect is important in designing tall structures for earthquake loads.

Under these conditions the plastic hinges in the lower stories of a tall building tend to form near the column faces because the effect of the gravity load is small in comparison to that of the lateral load. Therefore, the points of zero moment would lie very near the midspan of the beams and the midheight of the columns, which justifies the pinned ends in the columns and beams used in these experiments (Figs. 3-5).

2.2. Description of Test Specimens

The 20-story reinforced concrete prototype building used in this study was designed according to the UBC for a zone 3 location [4]. Each half-scale beam-column subassemblage consisted of two beams, 229 mm (9 in.) wide by 406 mm (16 in.) deep ($I_B = 3073\ in^4$), on either side of a square column 432 mm by 432 mm (17 in. by 17 in.). The effective lengths of the column and each beam were 1.83 m (6 ft), Fig. 5. (See Table 1 for specimen properties.)

The columns for both specimens were reinforced with the same amount of steel. The longitudinal reinforcement consisted of 12 #6 bars (area of steel = 1.8% gross area). Three overlapping closed transverse ties were placed at one section to offer proper lateral restraint to the main bars as well as proper confinement and shear strength. These ties were formed from #2 bars and spaced 40.6 mm (1.6 in.) apart.

The major difference between the two specimens was in the detailing of the main beam reinforcement. For both specimens the beam reinforcement at the column face consisted of 4 #6 bars on top and bottom. Thus, top and bottom steel were equal, which is more conservative than the minimum required by ACI 318-71 [5]. Section A.5.3 of this code states: "The positive moment capacity of flexural members at column connections shall not be less than 50% of the negative moment capacity." The beam steel ratio at the column face was 0.0135.

The plastic hinges for the specimens were designed using two different schemes. In specimen BC5 the two top interior main bars were bent downward, and the two corresponding bottom bars were bent upward, to cross 406 mm (16 in.) from the face of the column as shown in Fig. 6. All inclined bars were bent 60 degrees from the horizontal. After additional bending the bars extended horizontally to the end of the beam. All corner bars were both straight and continuous. In the second specimen, BC6, the interior bars on the top and bottom of the beams were cut off 610 mm (24 in.) from the face of the column. The plastic hinge was located by the requirement that the steel at the column faces begin strain hardening just before the critical section reaches its maximum strength (see Appendix A).

The plastic hinge in BC5 was closer to the column because the large amount of diagonal steel at that section substantially increased the moment capacity of the section. In BC6 the bars were cut off at a point slightly beyond where analysis indicated that the plastic hinge would occur because it was anticipated that with bond deterioration the plastic hinge would gradually move toward the column face. In both specimens the beams were reinforced against shear with #2 double stirrups placed 89 mm (3.5 in.) apart, except in the plastic hinge region where a more conservative stirrup spacing of 4.5 times the bar diameter or 51 mm (2 in.), was used to prevent buckling of the main reinforcement (Fig. 7). Grade 60 steel was used for all reinforcement. Shear transducers were attached at the ends of the beams to measure vertical reactions. Steel plates were attached at the top and bottom of the columns and were used to connect the specimens to the testing frame and the loading device.

2.3. Materials

A summary of the main mechanical characteristics of the materials are given in Table 1. The specimens were designed for a 28-day concrete strength of 27.6 MPa (4000 psi). Because of an error in the mixing process, the concrete for specimen BC5 was not of uniform quality. Whereas the concrete in the columns reached the specified strength, that obtained in the beams was only 14.5 MPa (2100 psi). However, since the tests were conducted primarily to study the behavior of the subassemblages after the steel has yielded, the steel had a far greater influence on the specimen's performance in the inelastic range than the concrete, and the overall results were not greatly affected. In this design, the bond at the joint was not critical. The yield strength for the #6 bars was 441 MPa (64 ksi), and the ultimate strength was 731 MPa (106 ksi).

--

2.4. Fabrication of Test Specimens

The concrete specimens were cast in place in plywood forms stiffened with battens. The concrete was compacted with a high-frequency vibrator. The reinforcement cage was constructed to close tolerance and was securely tied with 16-gage wire. Plastic chairs were used to hold the reinforcement cage in position in the oiled wooden frame.

The specimens were cast in a vertical position in the course of one day, in three separate lifts with a delay after each to allow for settlement of the concrete. The lower section of the column was cast first, up to the bottom of the beams. Later the beams and finally the top part of the column were cast to finish the process. After the specimens were cured and the forms removed, metal hinge assemblies were attached at all four ends of the specimens. These were made of steel for the column and of aluminum for the beams. The aluminum hinge assemblies were designed to act as transducers for measuring the reaction forces acting on the beams during the experiments. (See reference 6 for further details on transducers, clip gages, and other experimental procedures.)

3. EXPERIMENTAL TEST SETUP AND INSTRUMENTATION

3.1. General

A large steel testing frame, designed and constructed for studying steel beam-column subassemblages [6], was used. The top hinge of the column was connected to the frame and prevented from translating. A 2090-kN (470-kip) axial load was applied to the bottom hinge by means of a hydraulic jack supported on a movable cart. This load represented the dead and live forces acting on the column and was kept constant during the experiments. After the axial load was applied and the column permitted to undergo the consequent contraction, the ends of the beams were connected to the frame on horizontal guides in such a way as to permit rotation and lateral translation but not vertical displacement.

The effect of lateral load was simulated by applying a force or displacement at the bottom hinge by means of a double-acting hydraulic cylinder which moved the hinge back and forth in the plane of the frame. The applied forces and reactions are shown schematically in Fig. 5b. As can be seen from that figure, the reactions in the beams were caused, not only by the applied lateral load H, but also, by the additional moment due to the $P-\delta$ effect.

By summing the moment about the top hinge of the column, each beam reaction became $V = H/2 + P\delta/(2h)$, assuming $V_E = V_W = V$ and noting that $L = h$. Thus, each beam had an additional force due to the vertical load equal to $P\delta/(2h)$, where P was the total vertical load, δ was the bottom hinge displacement measured from the top of the column, and h was the story height measured from top to bottom hinges. Since the subassemblage corresponded to a lower story of a building, the axial load was large. Therefore, the $P-\delta$ effects were very significant for large story displacements.

To eliminate errors due to the effects of friction on the rollers of the cart, a transducer was used to measure directly the horizontal force H transmitted to the specimen. With this arrangement, the actual horizontal load applied to the lower column hinge was accurately measured.

3.2. Instrumentation

The main parameters studied in these experiments were the loads, i.e., the applied loads, the reactions in the beams and columns, the strains in concrete and reinforcement, the rotations (average curvature) and shear deformation at the critical regions, and the displacements of the beams under applied loading. Special instrumentation was used for obtaining reliable data on each of these parameters.

3.2.1. Load and Reaction Measurements

Load transducers were used to measure the horizontal and vertical forces H and P applied to the bottom hinge of the column. As mentioned above, specially designed aluminum transducers were bolted to the ends of beams to measure their reactions, V_E and V_W (Fig. 5b) [6].

3.2.2. Column and Displacement Measurements

During the experiments, the displacement of the bottom hinge was measured by a 381-mm (15-in.) linear potentiometer and was recorded continuously on an XYY' recorder. The lower column hinge displacements were measured periodically by a precision theodolite to check the accuracy of the deflection readings by the recording equipment.

Readings were also taken at the top hinge using the theodolite. The lateral load applied to the specimens induced some deformations of the steel testing frame. The horizontal displacement of the top hinge could be calculated from the theodolite readings and that measurement was used to determine the true displacement of the bottom hinge relative to the top hinge.

3.2.3. Rotations or Average Curvature Measurements

Average curvatures were calculated from measurements made at five different locations on both the east and west beams. These measurements were made using clip gages [6]. These clip gages were attached to pins embedded in the concrete. Five long steel pins were placed vertically in the vertical plane of symmetry of each beam before the concrete was poured and thus cast with the specimen. The first pin was placed 76.2 mm (3 in.) from the column face, the second 146 mm (5-3/4 in.) from the first, and the remaining three at 184-mm (7-1/4-in.) intervals. The first pin was placed close to the column face in order to measure possible cracks there or to measure slippage or yielding of the main bars in the region of largest moment. The clip gages were then attached to the tops and bottoms of the pins for curvatures C2 to C5 inclusive (Figs. 8 and 9). The gages were connected to a low-speed scanner powered by a NOVA computer to measure the relative displacements of the pin ends. Knowing the relative displacements of the tops and bottoms of the pins and their respective length, it was possible to determine the rotations of the sections, providing data for calculating the average curvatures. The rotation at the region adjacent to the columns (first curvature C1), was measured by means of linear potentiometers, whose output was plotted continuously on an XY recorder.

Other curvatures were also measured by means of clip gages attached to steel pins soldered directly to the main longitudinal reinforcement bars. By comparing the rotations determined from the bars and those from the concrete, slippage of the bars could be determined.

Because the column was much stiffer than the beams, no appreciable column deformation was expected, and no extensive measurements were made over the length of the column.

3.2.4. Shear Deformation Measurements

Shear deformation was measured at the critical location on each beam. At each critical section two diagonally crossing clip gages, D1 and D2, were attached to pins soldered to the main bars (Figs. 8 and 9), and then connected to the low-speed scanner. By measuring the relative movement of the two diagonal points, the average shear distortion can be determined from the following relationship:

$$\gamma_{av} = \left(\frac{\Delta + \bar{\Delta}}{2}\right)\left(\frac{d}{bh}\right)$$

where Δ and $\bar{\Delta}$ are the diagonal displacements, d is the undistorted diagonal distance; and b and h are the respective horizontal and vertical distances between the points (Fig. 10). This equation is valid only for uncracked sections, or regions with vertical flexural cracking; it does not apply to inclined cracks traversing only one diagonal clip gage. Nonetheless, the equation does give an idea of the average shear even after a diagonal crack crossed the instrumented region.

The cracking history of the west beam in the region of the plastic hinge was monitored by taking photogrammetric pictures of a rectangular grid drawn on the beams. The grid consisted of lines drawn horizontally and vertically at 89-mm (3.5-in.) spacing, extending from a point 25.4 mm (1 in.) from the column face to 825.5 mm (32.5 in.) away. Before the lines were drawn, the beams were whitewashed to heighten the contrast for ease of reading. There were also five targets placed in the shape of a cross on the face of the column at the beam-column joint. These provided reference points for determining relative distortions of the beam (column distortion was negligible). The grid pattern was also helpful in serving as a check of the beam curvatures and tip displacements. The photogrammetric camera was mounted on a separate steel tripod away from the testing frame.

3.2.5. Strain and Deformation Measurements

Strain measurements in the main bars were made by means of strain gages attached at a number of critical points in the specimens. For BC5, the gages were placed at the face of the column on all main bars. They were also placed inside the joint 89 mm (3.5 in.) from the column face on two of the continuous bars. The bent bars had a number of gages in the areas of the plastic hinge on both sides of the column (Fig. 11).

The strain gage readings were recorded on the low-speed scanner at the end of each cycle of load application, at maximum displacements, and also at the point of zero column displacement.

In specimen BC6 strain gages were placed at the face of the column on the continuous and cutoff bars to monitor any possible yielding in that region. Gages were also placed on the continuous bars in the middle of the plastic hinge area 419 mm (16.5 in.) from the face of the column of specimen BC6 and recorded continuously on the XY recorders to determine the onset of yielding for the main bars. Additional gages were placed at various locations, as shown in Fig. 12.

3.2.6. Pull-Out Measurements

Pull-out of the main longitudinal bars from the columns was measured by linear potentiometers attached to pins soldered to each main bar 76 mm (3 in.) from the face of the column, and recorded continuously on XY recorders.

3.3. Data Acquisition System

The loads, displacements, and strains were continuously plotted by XY and XYY' recorders and at particular stages of loading, by the low-speed scanner in the NOVA computer. Since the number of XY recorders was limited, only the most important results were plotted, while the majority was read with the scanner. The output from the clip gages used to measure curvatures and shear deformations and nearly all output from the strain gages were recorded on the scanner. Eight XY and XYY' recorders were used in each experiment to obtain continuous plots of displacement δ, pull-out, and strains of the main bars in the plastic hinge region versus the measured horizontal load H.

3.4. Test Procedure

After the specimens were placed in the steel testing frame and before applying axial load, the column had to be plumbed in order to eliminate undesirable forces.

As pointed out in section 3.1, the column was allowed to contract before the hinges at the ends of the beams were secured in position. When all the hinges were securely fastened, the lateral load was applied to the bottom hinge. The magnitude of the applied lateral load H and the bottom hinge deflection δ were continuously plotted on an XYY' recorder. The $H-\delta$ record served as a guide for controlling the loading history throughout the test. The first few lateral load cycles were conducted in the working range primarily to check the working condition of the instrumentation and recording equipment. The loading program shown in Fig. 13 was used for both BC5 and BC6 and indicates the deflection applied to the bottom hinge at each load cycle. At LP 9 there was enough lateral displacement to induce first yielding of the main bars in the plastic hinge region. The strain in those bars was continuously plotted on XYY' recorders. A sudden and rapid increase in strain signified the onset of yielding, and the lateral displacement was immediately stopped. The column was then displaced in the opposite direction until yielding of the main bars in the plastic hinge was again observed. The experiment proceeded at progressively increasing displacements after the first yield as shown in Fig. 13. Two cycles were made at each peak displacement selected in the test program.

4. EXPERIMENTAL RESULTS

4.1. General

One of the most important measures of the specimen's overall performance is determined from the curves of the bottom hinge lateral displacement δ versus the applied lateral load H. Figure 5b indicates that if there were no axial load, the horizontal load could be easily determined from the load transducer at the bottom column hinge. If axial load is neglected, then from the summation of moments about the top column hinge:

$$(V_E + V_W)\,L = Hh$$

Since in this case $L = h$:

$$V_E + V_W = H$$

Thus, the horizontal load can be determined by adding the shears in each beam. When axial load P is included, the summation of moments about the top hinge yields:

$$(V_E + V_W)L = Hh + P\delta$$

which reduces to:

$$V_E + V_W = H + \frac{P\delta}{h} = H_{eq}$$

Thus, the sum of the beam shears represents the total horizontal load H plus the $P\!-\!\delta$ effect, giving a total equivalent horizontal load, H_{eq}.

The shear values at the two beam hinges were added together automatically during the experiment by connecting the leads from their respective transducers in series and plotting the sum continuously on an XYY' recorder. The value of H was recorded on the same instrument using the lateral load transducer at the bottom column hinge. Since lateral force H must overcome the frictional forces in all four metal hinges, the measured force H was greater than the actual one. To correct for this error it was possible to work in reverse by calculating the $P\!-\!\delta$ effect in the $H_{eq}\!-\!\delta$ diagram (Figs. 14 and 15), and then to construct the actual $H\!-\!\delta$ curves.

As mentioned earlier, the H_{eq} force was obtained by summing the shears of the beams so that the frictional effect did not enter into the results. Since the deflection, δ, was continuously recorded, the $P-\delta$ effect could be determined at each point on the $H_{eq}-\delta$ curve. Horizontal load H could be calculated from the equation:

$$H = H_{eq} - \frac{P\delta}{h}$$

The frictional effects are excluded from this equation. The two $H-\delta$ curves so obtained are shown in Figs. 16 and 17. The $H-\delta$ curves including frictional effects are shown in Figs. 18 and 19. As can be seen, these effects accounted for approximately 13.3 to 22.2 kN (3 to 5 kips) of additional horizontal load. The $H-\delta$ and $H_{eq}-\delta$ curves are compared in Figs. 20 and 21. Note that the $H-\delta$ curve gives the erroneous impression that the structure loses lateral resistance after LP 13, whereas the $H_{eq}-\delta$ curve indicates an increase in strength up to LP 21.

The $H_{eq}-\delta$ curves give the most direct measure of performance for the subassemblage during cyclic loading because H_{eq} represents the combined action of the lateral force and the $P-\delta$ effect on the subassemblage, i.e., it gives the real measure of the lateral resistance (strength) of the subassemblage. During the first few cycles of tip displacement in the working stress range, the slope of the $H_{eq}-\delta$ curve was nearly linear for both specimens, and only a very small amount of energy was dissipated due to hysteresis. Hairline cracks began to form at LP 1 for both beams, but they were essentially vertical flexural cracks at this stage of loading.

4.2. Overall Behavior

4.2.1. Specimen BC5

Initial yielding of the main longitudinal bars in the plastic hinge region of specimen BC5 occurred at LP 9 at a displacement of the bottom column hinge of about 15 mm (0.59 in.). This displacement represents a lateral drift of 0.008 times the story height of 1.82 m (6 ft), which is about 64% greater than the recommended 0.005 [7]. It should be noted that these values are not directly comparable because (1) the value recommended by code is not at first yielding of the bars but represents the displacement calculated from the applied code lateral forces multiplied by a factor equal to $1/k$, and (2) the subassemblage tested failed to incorporate the contribution of the floor slab to lateral stiffness. The subassemblage was able to sustain a 178-kN (40-kip) horizontal load at that deflection. When the subassemblage was loaded in the opposite direction, yielding of the bars on the opposite sides of the beams began at a displacement of 15.2 mm (0.60 in.). After one or more cycles at this yielding displacement, successively larger displacements were applied at multiples of the deflection ductility ratio, μ. In this report the ductility ratio is understood to be the ratio of the imposed displacement (of the bottom hinge) to the displacement at first yield of the main reinforcing bars. The following observations can be made from the $H_{eq}-\delta$ graph [Fig. 14].

First, the strength of the subassemblage increased after first yielding of the main bars. The largest increase occurred between LP's 9 and 13, i.e., between $\mu = 1$ and $\mu = 2$. At LP 13 the specimen resistance was 212 kN (47.6 kips), 18% greater than LP 9. The peak strength occurred at a ductility ratio of 5 (LP 21). The 235-kN (52.5-kip) force was 31% greater than the value of H_{eq} at first yield. A ductility ratio of 5 for this member corresponded to a story drift of 0.040 times the story height, or more than 8 times the recommended code value of 0.005. Although at ductility ratios greater than 5 the capacity of the subassemblage under cyclic loading began to decrease at a higher rate than before, the specimen was capable of resisting a lateral load corresponding to an H_{eq} of 218 kN (49 kips) when forced at LP 25 to a deformation of 102 mm (4 in.), which corresponded to a displacement ductility of 7.1.

Secondly, the capacity of the subassemblage was reduced at each repeated cycle at the same displacement. The drop in strength between the first and second cycles after first yielding ranged from about 2% to 6.7% of the first load. However, at a ductility of 7 (LP's 25 and 27), the drop in strength of the second load cycle was about 24% of the first value at that displacement. Although only two complete cycles were made at any one displacement, the capacity of the specimen for a third displacement can be determined from the curve at the point where the succeeding cycle passes through the previous displacement. Although the capacity of the section continues to decrease for ductility ratios of 5 or less, the percentage decrease is of the same order of magnitude as it was for the previous cycle.

Thirdly, the initial loading stiffness of the subassemblage, represented in these graphs by the slope of the curves, decreased after each loading cycle, as can be seen in the graph of Fig. 14, which was generated in a clockwise manner. On the other hand, during unloading the stiffnesses of two cycles at the same ductility were nearly identical. The largest drop in stiffness occurred in the loading portion of the graph between LP's 26 and 27.

4.2.2. Specimen BC6

The behavior of BC6 was similar to that of BC5. Most of the general observations made above are applicable. The first yield of the main bars in the plastic hinge occurred at LP 9 at a displacement of 15.2 mm (0.60 in.) and a load, H_{eq}, of 190 kN (42.8 kips), see Fig. 15. The maximum strength of this subassemblage occurred, as it did in BC5, at a ductility ratio of about 5 at 73.7-mm (2.9-in.) displacements (LP 21). The 233-kN (52.4-kip) maximum H_{eq} load was nearly identical to that of BC5. At LP 25 the experiment was temporarily halted because of significant damage and shear distortion at the critical region. However, after analysis of the $H_{eq}-\delta$ plots, it was decided that it would be advantageous to force this specimen to the same maximum lateral displacement as that for specimen BC5, δ_{max} = 102 mm (4 in.). The results from these additional tests are represented by the dashed lines in Figs. 15, 17, and 21.

Upon subsequent cycling as shown in Figs. 15 and 17, the resistance of the specimen started to deteriorate and at a lateral displacement of 102 mm (4 in.) at LP 27, the resistance was 165 kN (37 kips), which was considerably smaller than that observed for specimen BC5, 218 kN (49 kips), at the same displacement. At this load point a nearly horizontal slope of the hysteretic loop could be observed, indicating that the capacity of the specimen had been exhausted. Similar observations apply to the largest reversal cycle, where a definite decrease in the capacity of the subassemblage appeared, first at LP 28 and finally, at LP 29 (Fig. 15).

As in BC5, the capacity of the subassemblage was reduced at the second cycle of the same deflection. The drop in strength ranged from less than 1% to about 6.7% of the first cycle capacity. In general, the reductions tended to be somewhat less than those recorded for BC5. As in BC5, the stiffness of BC6 degraded in successive cycles. While unloading, the stiffnesses of two successive cycles at the same displacement were often nearly identical. However, after the first loading at a displacement of about 76 mm (3 in.) after unloading, and at the initiation of reversed loading, the stiffness of the second cycle suddenly dropped. The sudden loss at this point was due primarily to large shear distortion at the plastic hinge region and slippage of the main bars in this region. This observation will be commented upon later.

4.3. Energy Dissipation

The area enclosed in the $H_{eq}-\delta$ curves is a measure of the subassemblage's energy dissipation characteristic, which in turn is one the best indices for judging the structure's performance during an earthquake. The $H_{eq}-\delta$ graphs show that just as the strength of the specimen increased for higher ductility ratios, μ, to maximum strength at a μ of about 5 and decreased at each repeated cycle, energy dissipation increased with higher ductility ratios and decreased at a repeated cycle of the same displacement. The energy dissipated during the different cycles have been measured and are given in Tables 2 and 3.

4.3.1. Specimen BC5

The drop in area from the first to second cycle at a ductility ratio of 2 was about 10%. At a ductility ratio of 5 the drop in area of the second cycle was still only 9.2% of the first cycle. However at a ductility ratio of 7, the area of the second cycle was 33% smaller. This considerable drop was a consequence of deterioration in strength [which decreased from 217 kN (48.8 kips) to 165.5 kN (37.2 kips)] and stiffness. As can be seen by comparing the increases in the areas of the first cycle loops with the increase in the ductility ratios, although the areas are increasing, they are increasing at a slower rate.

4.3.2. Specimen BC6

The hysteretic loops of BC6 had properties similar to those of BC5. For repeated cycles at the same displacement the energy absorption capacity dropped about 10% at a ductility ratio of 2 and about 14% at a ductility ratio of 4.8. As shown in Tables 2 and 3 and Fig. 22, this latter drop was higher (14% vs. 9%) than that observed in specimen BC5. At a ductility of 7 the energy dissipation capacity of BC6 was only 22.2 kN-m (196.3 k-in.), which represents a drop of 38% with respect to that obtained for specimen BC5. It is interesting to note the large increase in energy dissipation in the cycles after initial yield. Although the displacement at cycle 13-14 was only twice that at cycle 9-10, the energy dissipation increased by a factor of more than 7 (Table 3). Comparison of the energy dissipations of BC5 and BC6 shows that despite the more stable, rounder shapes of the curves for BC5 (see Fig. 22), the total energy dissipated was nearly the same up to $\mu = 5$. After LP 16 and up to LP 24 the BC5 areas were larger by about 2% to 7%. It should be remembered that the concrete strength of BC5 was much lower than that of BC6 so that the capacity of BC5 might have been larger had the correct design concrete strength been obtained for this specimen.

4.4. Beam Deflections

If the whole subassemblage were allowed to rotate as a rigid body about the top hinge, it can be concluded from geometry that the total vertical movement of the end of either beam would be equal to the horizontal displacement of the bottom hinge (Fig. 23). In this experiment the ends of the beams were constrained from displacing in the vertical direction. Therefore, the deflection of the beams as measured from the tangent to the beam at the beam-column joint is approximately equal to the horizontal displacement of the bottom column hinge. The actual tangential deflection of the beam was somewhat smaller due to (1) flexibility of the columns and (2) possible beam-bar pull-out at the column face (fixed-end beam rotation). However, both sources of deformation were small and the error was negligible since the columns were so much stiffer than the beams. Most of the beam deflections were accounted for by flexural and shear deformations in the critical regions of the plastic hinge. Clip gages placed at the top and bottom of the beams measured the relative displacements between sections, from which the rotations could be calculated and the tip displacements (due to flexural deformations) determined. These beam deflections are given in Tables 4 and 5 and shown graphically in Figs. 24 and 25. The shear distortion at the plastic hinge region was measured by the diagonally crossing clip gages (Figs. 8 and 9).

4.4.1. Specimen BC5

The results for BC5 indicate that very little deflection was caused by shear deformation. Table 4 also indicates that most of the rotation was contained in the C3 and C4 regions (see Figs. 24a and 25), corresponding to the location of the plastic hinge, which for BC5 was at the diagonal crossing of the main bars. The deflection due to rotation of region C3 accounted for nearly 50% of the total beam displacement. This indicates that the plastic hinge formed very close to the desired location. At larger displacements the contribution of the first curvature C1 to the total displacement increased to about 16% of the total. This was due to the large strain of the main bars at the face of the column. The rotation of the C1 region more than doubled from LP 19 to 21, whereas the increase in other regions was no greater than 45%. The strain history of the west top bar is shown in Fig. 26a. Yielding of the bar at the section where the gage was placed started at LP 12.

Figure 24a and Tables 4a and 4b show a significant amount of error between the actual deflection and that calculated from the beam displacement measurements. Part of the error is due to the fact that not all of the rotations in the beam were captured by the installed instrumentation. There was some cracking in the vicinity of the beam ends where the metal transducers were attached.

Total rotation in the C3 and C4 regions at maximum load (LP 21) was 0.0396 rad. From LP 21 to LP 22, i.e. for a complete reversal deformation (see Fig. 14), the plastic hinge rotated 0.078 rad., which, for a length of 15.5 in. is an extremely significant inelastic rotation. At LP 26 these rotations had increased even further to 0.058 rad., or 0.115 rad. for the cycle from LP 26 to LP 27.

4.4.2. Specimen BC6

Tables 5a and 5b give the components of tip displacement due to different sources. The plastic hinges in specimen BC6 were located at the bar cut off 610 mm (24 in.) from the column faces. It is in this region that the largest rotations occurred. Initially, most of the curvature formed in the C5 region (see Fig. 9 and Table 5), which measured the curvatures of the beam just beyond the point where the bars were cut off. Later in the experiment at larger displacements, the curvature in the C4 region, whose center was 498 mm (19.6 in.) from the column face, became larger as the plastic hinge moved toward the face of the column. During the last few cycles that region contributed to about 67% of the total flexure. (See Fig. 24b for the contributions to the tip displacement from the five measured regions of rotations.)

For BC6 shear distortion in the plastic hinge region contributed a significant amount of tip displacement, over 30% of the total measured tip displacement at the last few cycles. At the end of the cycle at $\mu = 5$ (LP 25) a shear offset of about 19 mm (3.4 in.) was measured at the plastic hinge where the two parts of the cracked beam slipped relative to each other (Fig. 60). There was practically no yielding of the main bars at the column face (Figs. 35 and 36) so that the curvature at that region was small for the full duration of the test and contributed little to the total tip displacement. Although there were some errors between the calculated and observed values of the tip displacement, they were considerably smaller than those observed for specimen BC5. From the photographs of Figs. 56 through 60, one can observe that the large number of cracks in the beams beyond the points where measurements were being made could account for some of the discrepancies in deflection calculations.

4.5. Reinforcing Steel Strain Measurements

The strain history of the reinforcing steel offers valuable insight into the mechanical behavior of the specimens. The strains of the main bars in the plastic region were plotted continuously on XYY' recorders for both BC5 and BC6. Those in other locations were recorded with the aid of the low-speed scanner. Graphs plotted from the scanner are only approximations of the true behavior since for any one cycle the readings at only four loading points were available, giving the strains at maximum displacement and zero lateral force. However, in most cases these readings gave a good indication of the overall behavior. Selected strain gage results for BC5 are plotted in Figs. 26 through 34. Those for BC6 are plotted in Figs. 35 through 43.

4.5.1. Specimen BC5

Figure 26 represents the strain history for one of the continuous top bars on the west beam at the column face. The graph shows the strain versus the reaction at the beam end. The bar was in tension at even-numbered load points and in compression at odd ones. As evident from the graphs, as LP 12 the bar started to yield at the column face, and at LP 22 significant yielding occurred which corresponded to the large rotation recorded by the potentiometers (Table 4). The graphs also indicate that no full reversals of steel strains occurred. Under tension the bars were free to elongate because the concrete was cracked and could provide no resistance. However, when the load on the beam was reversed, the crack closed and from then on concrete carried most of the induced compressive forces. Therefore, only at the beginning of loading does the steel develop the major part of its compressive stress, and because of crack closure no significant strain reversal in the steel can take place.

Significant yielding of the main bars at the column face observed at LP 22 was therefore delayed until large frame displacement had been achieved (Fig. 26). At LP 22 bottom hinge displacement was about 77 mm (3 in.). In previous tests on beam-column subassemblages significant beam steel bar yielding at the column face occurred very early. It was this early and significant inelastic straining that was the main reason for the large stiffness reduction eventually leading to early failure of the specimen [2]. When the beam main bars on both sides of the column face underwent a large amount of yielding during one full cycle of deformation reversal, simultaneous pushing and pulling of the bars, with forces at yielding or a higher intensity, occurred. These caused, upon subsequent cycling of the specimen, deterioration of the bond of these main bars along their embedment (or anchorage) length, which was reduced to just, or somewhat less than, the width of the joint.

As pointed out before, in the experiment of specimen BC5 this type of behavior at the joint faces was delayed (by forcing the plastic hinges to form away from the column faces) up to LP 22, i.e., until large frame displacement had been achieved. This means that up to LP 22 the bond was only destroyed at the plastic hinge region forming away from the column face, which left the beam main bars with an anchorage length substantially larger than the width of the column joint.

Figure 27 shows the strain history of one of the continuous bottom bars at a point 76 mm (3 in.) near the face of the column but inside the joint. These curves indicate no yielding of the main bars occurred through LP 22; hence, little, if any, slippage occurred at the joint up to this load point. Unfortunately, at that point the strain gage ceased to function. The strain at LP 22 was about 2200 microstrains, which was close to yielding. It is possible that at the next cycle it would have yielded. However, this load point corresponded to the last cycle of the test, which represented a displacement of about 102 mm (4 in.), or a displacement ductility of nearly 7.

An interesting observation can be made from analyzing the results presented in Figs. 29 and 31, which show the strain history of the diagonally crossing bars in the plastic hinge region of the east beam. Figure 29 is a graph of the strain in bar B2 measured by a gage located 356 mm (14 in.) from the face of the column; Fig. 31 shows the strain of the crossing bar T2, being the strain measured by a gage located 444 mm (17.5 in.) from the column face. These graphs indicate that these two bars were in tension throughout the test, regardless of the direction of the shear force. In Fig. 29 when V_E was applied downwards, the neutral axis shifted to a point low enough to induce tensile force in the bar. For example, at LP 21 the shear on the east beam was downward-acting and the neutral axis was below the intersecting point of the bars. Hence, both inclined bars were stressed in tension by bending. The bars were also stressed by the effect of shear acting in the region where the bars were bent. Because the effectiveness of concrete in resisting shear at this region was reduced at large displacements, most of the shear resistance had to be provided by the diagonally crossing bars. Therefore, the downward-acting shear caused compression in the instrumented bar of Fig. 29 and tension in the instrumented bar of Fig. 31. At LP 22, when the shear was acting in the opposite direction, the bar in Fig. 29 had larger tension than the bar in Fig. 31, which explains the different patterns in the crescent shape of these graphs.

To observe the variation of strains in the bent bars a short distance from the plastic hinge, a strain gage was placed on bar B2 in the west beam at 572 mm (22.5 in.) from the column face. The strain history is shown in Fig. 33. The largest strain, 1440 microstrains, indicates that no yielding occurred in this region. The large difference in strains between LP's 12 and 14 was caused by cracking of the concrete in the nearby region. At LP 13 the bar was in tension. When the load was reversed the cracks in the concrete closed before large compressive forces could be taken up by the bar. Thus, the previously induced tensile deformation could not be overcome, which led to the well-known phenomenon of beam elongation.

The graphs in Fig. 34 show the variation of strain along the length of bar B2 in the west beam. This bar was one of the two that were bent. These graphs were constructed from gage readings at 572 mm, 444 mm, 229 mm, and 0 mm (22.5, 17.5, 9, and 0 in.) from the column face at two different load points: LP 9 (first yield) and LP 21 (maximum strength). The graphs show large strains at the column face where the moment was largest, with the strains getting smaller due to the moment gradient as the distance from the column face increased There was bond loss in the plastic hinge region due to significant concrete cracking, which caused a sharp drop in the strain at that region. As the bond developed in the region outside the plastic hinge, the strains reached a maximum and then decreased as the moment approached zero at the end of the beam. The two curves are similar in shape but the strains are larger at LP 21 by nearly one order of magnitude.

4.5.2. Specimen BC6

Figures 35 and 36 indicate that the strains in the continous beam bars at the face of the column did not reach their yield value during the test. However, the strains at the last load point, LP 24, were very nearly the yield value for the steel. There was an observable, but negligible, amount of slippage of the bars in the columns, as can be seen from the results in Fig. 37. Slippage is shown by the migration of the strain at odd-numbered load points. When the bar is in tension at even-numbered load points, it slips a small amount. When the load is reversed and the bar is in compression the slippage cannot be reversed completely, leaving a residual elongation strain in the bar.

The strain gage placed on the cutoff bar on the east beam 520.7 mm (20.5 in.) from the column face clearly indicates that this bar began to slip began at LP 14 (Fig. 39). The explanation for the large change in strain between LP's 12 and 14 is similar to that of BC5 in Fig. 33 given earlier. The strain history of the cutoff bars at 330 mm (13 in.) from the column face was similar (Fig. 38), indicating some slippage, but the tensile strains were larger due to the larger moments at that region and also to more bond strength since it was farther away from the cutoff point.

The continuous bars underwent somewhat larger strains at the critical regions than did the continuous bars of BC5. The plastic hinge for BC6 was 610 mm (24 in.) away from the column face while that of BC5 was only 406 mm (16 in.) . Therefore, for the same beam tip displacement, the beam of BC6 had to rotate more in its plastic hinge than did BC5. This is reflected in the larger strains in the critical regions. The strain gage placed at 737 mm (29 in.) from the column face on bar T1 of the east beam showed that yielding began at LP 9 and became significant at LP 15 (Figs. 41 and 42).

The variation of strain along the length of bar T1, which was a continuous bar throughout the beam, is shown in Fig. 43. Since readings were taken at only four locations, the actual shape of the curve can differ from that drawn in the figure. The graphs drawn for LP's 9 and 21 show the large strain in the main bar in the plastic hinge region as was explained above.

4.6. Beam Crack Patterns

Cracking in the beams was determined from the photogrammetric results. The crack pattern and deformations in the critical region are shown in an exaggerated scale in Figs. 44

through 51. The photographs of the same load points are shown in Figs. 52 through 59. Figure 60 shows the state of the whole subassemblage BC6 after LP 25 of the experiment.

4.6.1. Specimen BC5

Figures 44 to 47 show that the dominant cracks in BC5 were the vertical flexural cracks. Not until the last cycle at LP 25 (Fig. 47) were any signfificant diagonal shear cracks visible. The figures show a significant amount of distortion at the plastic hinge region, which, however, was localized. As can be seen from Fig. 47, even at the last cycle the last vertical line at the ends of the grid remains nearly plane after a considerable beam tip displacement. Spalling occurred in the concrete at the top of the beams in practically all the region located from the plastic hinge to the column face, but not until near the end of the test at LP 25. Vertical cracks stayed open after load reversal following LP 17.

4.6.2. Specimen BC6

Figures 48 through 51 show the cracking in the critical region of the west beam of specimen BC6. The major difference between the performance of specimens BC5 and BC6 was the large diagonal shear cracks which were visible in BC6 at LP 9 and the larger shear distortion that occurred at the plastic hinge region. The shear resistance and shear stiffness in BC6 was much less than in BC5, which had 4 #6 bars diagonally crossing in the critical region. Shear distortion at LP 24 was so large and the damage at the critical region so extensive that the test was temporarily halted at LP 25 with a displacement of about 76 mm (3 in.) (Fig. 15).

Under repeated cycling in the inelastic range, the vertical cracks at the top of the beam interesected those at the bottom. At larger displacements the cracks stayed open the full depth of the beam and only the top and bottom bars resisted the moment, causing a drop in the member stiffness. Shear was resisted only by some aggregate interlocking and friction between the two faces and by dowel action of the main bars. During shear reversal at small shear forces there was a small amount of slippage between the two sides which caused a sharp drop in overall stiffness, as shown in Fig. 15.

The largest cracks occurred at a point just to the right of the cutoff point 610 mm (24 in.) from the column face (Figs. 50 and 51).

5. CONCLUSIONS AND RECOMMENDATIONS

There is documentation indicating that severe bond deterioration can occur in conventionally designed interior beam-column joints during large cyclic lateral displacements such as those which occur during a major earthquake [1-3]. In extreme cases the continuous bars of the two adjoining beam spans may begin to slide with very little frictional resistance through the column, thereby providing negligible resistance to the lateral inertial forces. This study addressed itself to the problem of avoiding or eliminating this serious condition.

Two alternative schemes for resolving the problem were proposed, and two specimens were fabricated and tested. Both specimens were successful in showing how to obviate the problem of bond loss in the main beam bars within the column. This was achieved by designing the plastic hinges to occur away from the column faces. Equal amounts of top and bottom steel were used in the beams at the column faces, and special web reinforcement was provided in the regions of anticipated hinges.

In one specimen, BC5, the two top interior main bars were bent downward, and the two corresponding bottom bars were bent upward, intersecting 406 mm (16 in.) away from the face of the column. These bars were inclined 60 degrees from the horizontal. After reverse bending of the bent bars at the bottom and top of the beam, the bars extended horizontally to the end of the beam. All four corner bars were straight and continuous. In the second specimen, BC6, two of the four main bars on the top and bottom of the beam were cut off 610 mm (24 in.) away from the face of the column.

Both designs performed well, but BC6 was certainly the simpler of the two to fabricate. However, several important advantages of BC5 should be noted. At large lateral displacements, the cracking pattern in BC5 was well distributed throughout the beams. Because only vertical stirrups were used in BC6, they were ineffective in preventing significant localized shear distortion in the hinge regions. In contrast, the crossing steel of BC5 offered excellent resistance to shear. The diagonal cracks due to shear stresses did not open up in this specimen until the very end of a test and no sliding shear through vertical cracks was observed. In BC6, immediately after yielding of the main bars at the hinge, the hinge was weakened by the shear-flexure cracking. Moreover, the cracking pattern was more random and concentrated in the proximity of the hinge, resulting in large local shear distortions. At a ductility of 4.8 considerable sliding shear was observed. This shear distortion contributed to nearly one-half of the total displacement of the beam. Specimen BC5, with the crossing steel, was especially ductile, with the cracked region spreading virtually over the entire beam; shear distortion in the critical regions and therefore in the whole beam was negligible.

Both specimens generated excellent hysteretic loops that became pinched only at the very end of an experiment, indicating good energy dissipation capabilities. The maximum nominal shear stress v_u developed in specimens BC5 and BC6 did not exceed 1.5 MPa (215 psi). Since the f_c' of concrete in the beams of these two specimens were 14.5 MPa (2100 psi) and 27.6 MPa (4000 psi), respectively, the resulting v_u for BC5 was about $0.39\sqrt{f_c'}$ MPa ($4.7\sqrt{f_c'}$ psi), while the value for BC6 was only about $0.28\sqrt{f_c'}$ MPa ($3.4\sqrt{f_c'}$ psi). Thus, either design scheme appears acceptable for avoiding bond failure of beam bars in the columns when the shear acting in the critical regions is small [say, $v_{u_{max}} < 0.29\sqrt{f_c'}$ MPa ($3.5\sqrt{f_c'}$ psi)]. Note, however, that when the value of shear is high [say, $v_{u_{max}} > 0.29\sqrt{f_c'}$ MPa ($3.5\sqrt{f_c'}$ psi), only the scheme used in BC5 is recommended.

The ACI Code does not require calculations of anchorage for top and bottom reinforcement that is continuous through a beam-column connection; Section A.5.4 of the code specifies only that anchorage be computed within each flexural member. Because tests have shown that there is considerable bond degradation of the beam main bars in which inelastic deformation takes place, the soundness of the code provision should be investigated.

It is recommended that the design schemes considered in this study be the subject of a more comprehensive experimental and analytical investigation. Parameters to be studied include: (1) effect of high shear stresses; (2) use of higher strength concrete; (3) use of light-weight concrete; and (4) effect of the interaction between slab of floor system and beam.

Studies should be carried out that will permit practical guidelines to be formulated for establishing the proper location of the plastic hinges. Other schemes, such as the use of haunched beams to force the formation of platic hinges away from the face of the column, should also be investigated. Methods of improving bond and anchorage of the beam main reinforcing bars or delaying and minimizing their bond deterioration at the joint if plastic hinges form at the face of the column should be explored. For example, the possibility of bending the beam bars at the joint, or using plates welded to the bars could be studied to assess their effects on anchorage.

REFERENCES

1. Bertero, V. V., E. P. Popov, and T. Y. Wang, "Hysteretic Behavior of Reinforced Concrete Flexural Members with Special Web Reinforcement," *Report No. EERC 74-9,* Earthquake Engineering Research Center, University of California, Berkeley, 1974 (PB 236 797); a summary of the report is published in *Proceedings,* U. S. National Conference on Earthquake Engineering, University of Michigan, Ann Arbor, June 1975.

2. Popov, E. P., V. V. Bertero, and S. Viwathanatepa, "Analytic and Experimental Hysteretic Loops for R/C Subassemblages," *Proceedings,* Fifth European Conference on Earthquake Engineering, Istanbul, Turkey, September 1975.

3. Bertero, V. V. and E. P. Popov, "Hysteretic Behavior of Ductile Moment-Resisting Reinforced Concrete Frame Components," *Report No. EERC 75-16,* Earthquake Engineering Research Center, University of California, Berkeley, 1975 (PB 246 388).

4. *Uniform Building Code,* International Conference of Building Officials, Whittier, California, 1973 ed.

5. ACI Committee 318, *Building Code Requirements for Reinforced Concrete,* ACI 318-71, American Concrete Institute, Detroit, Michigan, May 1972.

6. Krawinkler, H., V. V. Bertero, and E. P. Popov, "Inelastic Behavior of Steel Beam-to-Column Subassemblages," *Report No. EERC 71-7,* Earthquake Engineering Research Center, University of California, Berkeley, 1971 (PB 211 355).

7. *Uniform Building Code,* International Conference of Building Officials, Whittier, California, 1976 ed.

TABLES

Preceding page blank

TABLE 1 SPECIMEN PROPERTIES

PARAMETER		SPECIMEN BC5	SPECIMEN BC6
Beam length (in.)		72	72
Column height (in.)		72	72
Column:			
Area	(in^2)	289	289
A_s	(in^2)	5.28	5.28
f	(%)	1.83	1.83
f_y	(ksi)	64	64
f'_c	(ksi)	4.0	4.0
Beam:			
b	(in.)	9.0	9.0
h	(in.)	16.0	16.0
d	(in.)	14.5	14.5
d'	(in.)	1.5	1.5
A_s	(in^2)	1.76	1.76
A'_s	(in^2)	1.76	1.76
ρ		0.0135	0.0135
ρ'		0.0135	0.0135
f_y	(ksi)	64	64
$f_{s\,max}$		106	106
f'_c	(ksi)	2.1	4.0

1 in. = 25.4 mm
1 ksi = 6.895 MPa

TABLE 2 ENERGY DISSIPATION OF SPECIMEN BC5

CYCLE	$H_{eq}^{Top}/H_{eq}^{Bottom}$ kips/kips	μ	TOP AREA (K-IN.)	BOTTOM AREA (K-IN.)	TOTAL AREA (K-IN.)
9-10	40.0/40.6	1.0	--	--	8.6
11-12	39.3/39.7	1.0	--	--	8.7
13-14	47.3/45.1	2.0	22.5	32.3	54.8
15-16	44.4/44.4	2.0	25.2	24.1	49.3
17-18	50.7/52.2	3.4	59.4	76.0	135.4
19-20	47.9/50.2	3.4	64.3	65.5	129.8
21-22	52.5/53.4	5.0	103.7	132.6	236.2
23-24	49.0/48.2	5.0	112.0	102.6	214.5
25-26	48.8/44.2	7.1	154.8	160.0	314.7
27-28	37.2/36.7	7.1	108.1	102.0*	210.1

*estimated.

TABLE 3 ENERGY DISSIPATION OF SPECIMEN BC6

CYCLE	$H_{eq}^{Top}/H_{eq}^{Bottom}$ kips/kips	μ	TOP AREA (K-IN.)	BOTTOM AREA (K-IN.)	TOTAL AREA (K-IN.)
9-10	42.8/42.3	1.0	--	--	8.6
11-12	41.7/41.4	1.0	--	--	8.7
13-14	46.1/45.5	2.0	25.4	35.5	60.9
15-16	46.2/45.6	2.0	28.6	26.1	54.7
17-18	50.5/49.0	3.25	57.1	76.4	133.5
19-20	49.5/48.5	3.25	65.7	59.1	124.8
21-22	52.4/52.4	4.8	100.6	129.7	230.3
23-24	50.5/48.9	4.8	102.0	96.5	198.5
25-26	47.1/43.9	4.8	99.0	81.7	180.7
27-28	37.1/31.1	6.6	93.0	103.3	196.3

1 in = 25.4 mm

1 kip = 4.448 kN

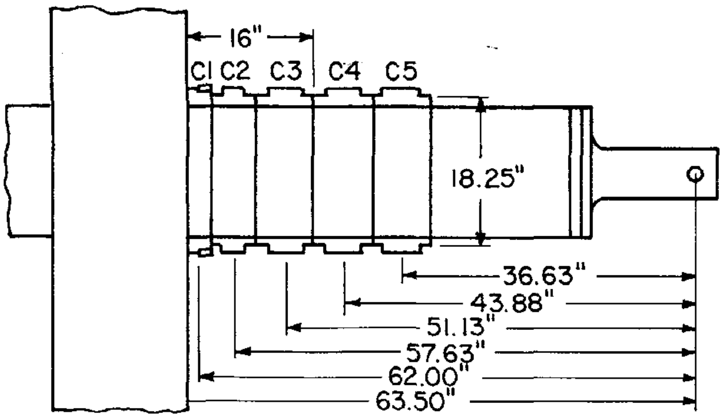

1 in. = 25.4 mm

TABLE 4a TIP DISPLACEMENTS FOR SPECIMEN BC5 - EAST BEAM

LOAD POINT	DISPLACEMENT COMPONENTS IN IN. DUE TO					TOTAL FLEXURAL DISP. (IN.)	ACTUAL (IN.)	% DIFF.
	C1	C2	C3	C4	C5			
9	.057	.069	.132	.092	.031	.380	.586	-35
10	.069	.078	.116	.125	.032	.420	.671	-37
11	.065	.072	.141	.092	.033	.403	.609	-34
12	.069	.076	.117	.129	.031	.422	.681	-38
13	.084	.095	.441	.258	.041	.919	1.162	-21
14	.088	.077	.390	.260	.032	.845	1.210	-30
15	.084	.096	.466	.261	.040	.947	1.150	-18
16	.092	.072	.400	.260	.030	.854	1.160	-26
17	.111	.213	.867	.470	.047	1.710	2.010	-15
18	.121	.137	.704	.545	.041	1.580	1.930	-18
19	.118	.197	.864	.520	.044	1.740	2.010	-13
20	.129	.131	.686	.551	.039	1.540	1.930	-20
21	.260	.250	1.146	.752	.047	2.455	2.910	-16
22	.268	.151	.962	.846	.060	2.290	2.910	-21
23	.306	.139	1.150	.806	.029	2.430	2.910	-16
24	.260	.189	.907	.832	.048	2.236	2.910	-23
25	.536	.340	1.650	.889	.017	3.430	4.110	-17
26	.230	.387	1.530	1.230	.033	3.410	3.910	-13

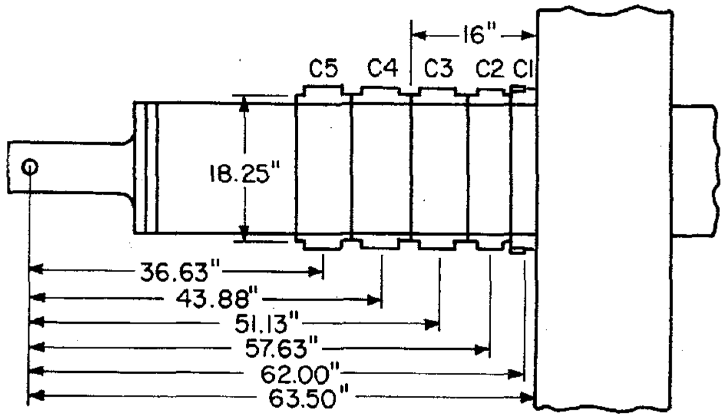

1 in. = 25.4 mm

TABLE 4b TIP DISPLACEMENTS FOR SPECIMEN BC5 - WEST BEAM

LOAD POINT	DISPLACEMENT COMPONENTS IN IN. DUE TO					TOTAL FLEXURAL DISP. (IN.)	ACTUAL (IN.)	% DIFF.
	C1	C2	C3	C4	C5			
9	.0612	.05596	.1202	.0952	.0291	.363	.586	-38
10	.0689	.08470	.1258	.1009	.0317	.412	.671	-39
11	.0612	.05330	.1222	.1093	.0266	.373	.609	-39
12	.0689	.08010	.1370	.1058	.0285	.420	.681	-38
13	.0804	.07610	.4188	.2576	.0377	.871	1.162	-25
14	.0850	.08880	.3881	.2699	.0355	.867	1.210	-28
15	.0804	.07320	.4443	.2633	.0342	.895	1.150	-22
16	.0854	.08356	.3993	.2751	.0344	.878	1.160	-24
17	.1684	.14700	.7767	.4419	.0484	1.580	2.010	-21
18	.0987	.14350	.7690	.5476	.0410	1.600	1.930	-17
19	.1607	.15390	.8093	.4748	.0451	1.640	2.010	-15
20	.0957	.14750	.7429	.5792	.0330	1.600	1.930	-17
21	.3138	.26570	1.0737	.6582	.0550	2.370	2.910	-19
22	.2832	.21150	.9674	.8680	.0297	2.360	2.910	-19
23	.2756	.23050	1.1356	.7319	.0531	2.430	2.910	-16
24	.3314	.11410	.9756	.7955	.0181	2.230	2.910	-16
25	.3092	.2080	1.9164	1.0900	.0575	3.670	4.110	-11
26	.4593	.2432	2.2480	.4150	.0020	3.370	3.910	-14

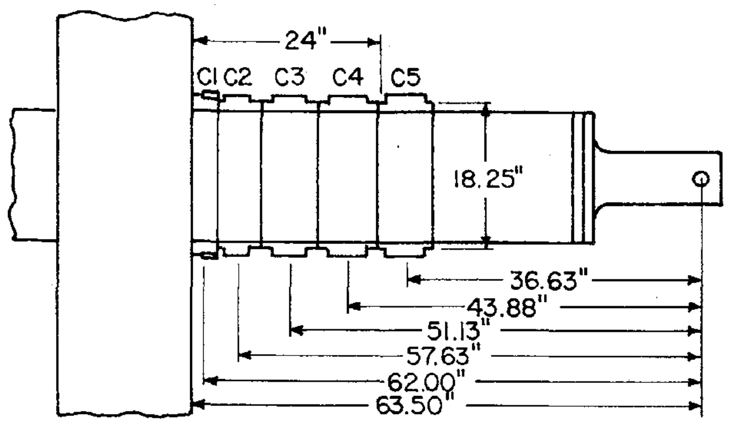

1 in. = 25.4 mm

TABLE 5a TIP DISPLACEMENTS FOR SPECIMEN BC6 - EAST BEAM

LOAD POINT	DISPLACEMENT COMPONENTS IN IN. DUE TO					TOTAL FLEXURAL DISP. (IN.)	SHEAR DISP. (IN.)	TOTAL MEASURED DISP. (IN.)	ACTUAL (IN.)	% DIFF.
	C1	C2	C3	C4	C5					
9	.057	.073	.037	.058	.114	.345	.043	.388	.59	-34
10	.061	.043	.065	.038	.124	.330	.051	.381	.63	-40
11	.057	.080	.036	.054	.115	.343	.056	.399	.59	-32
12	.061	.042	.065	.035	.130	.333	.056	.389	.64	-39
13	.064	.067	.077	.222	.362	.792	.243	1.035	1.17	-12
14	.073	.045	.083	.026	.501	.728	.219	.947	1.17	-19
15	.064	.088	.079	.332	.260	.823	.398	1.221	1.19	+ 3
16	.077	.044	.086	.277	.491	.975	.289	1.264	1.19	+ 6
17	.077	.099	.117	.696	.538	1.527	.702	2.229	1.95	+14
18	.080	.048	.115	.036	.815	1.092	.670	1.763	1.94	- 9
19	.080	.098	.145	.803	.315	1.441	.983	2.424	1.95	+24
20	.080	.047	.112	.332	.507	1.071	.836	1.913	1.95	- 2
21	.087	.110	.286	1.376	.332	2.191	1.301	3.492	2.90	+20
22	.084	.057	.151	.774	.705	1.771	1.479	3.250	3.03	+ 7
23	.092	.130	.388	1.377	.019	2.006	1.902	3.908	3.03	+29
24	.084	.059	.440	1.370	.197	2.150	1.928	4.078	3.03	+35

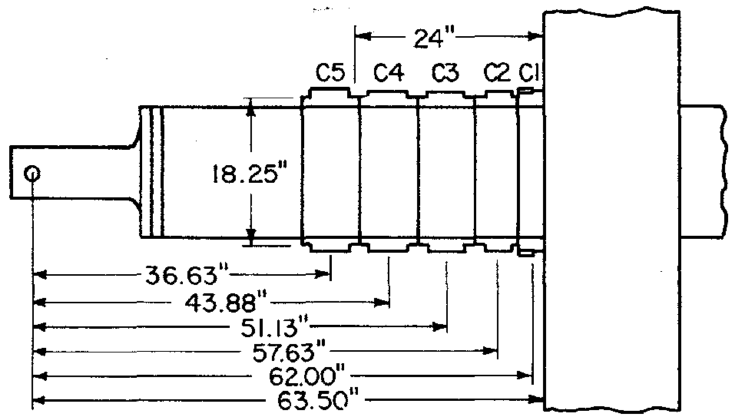

1 in. = 25.4 mm

TABLE 5b TIP DISPLACEMENTS FOR SPECIMEN BC6 - WEST BEAM

LOAD POINT	DISPLACEMENT COMPONENTS IN IN. DUE TO					TOTAL FLEXURAL DISP. (IN.)	SHEAR DISP. (IN.)	TOTAL MEASURED DISP. (IN.)	ACTUAL (IN.)	% DIFF.
	C1	C2	C3	C4	C5					
9	.048	.060	.072	.039	.105	.324	.040	.364	.59	-38
10	.061	.077	.041	.054	.117	.350	.036	.386	.63	-39
11	.048	.057	.065	.043	.107	.320	.044	.364	.59	-38
12	.063	.077	.045	.051	.117	.352	.046	.398	.64	-38
13	.057	.065	.101	.039	.522	.784	.195	.979	1.17	-16
14	.073	.086	.063	.094	.447	.763	.254	1.017	1.17	-13
15	.057	.064	.095	.034	.591	.841	.238	1.079	1.19	- 9
16	.073	.085	.064	.211	.343	.775	.336	1.111	1.19	- 7
17	.084	.070	.133	.260	.838	1.385	.444	1.829	1.95	- 6
18	.084	.099	.101	.735	.278	1.297	.286	1.583	1.94	-18
19	.061	.066	.128	.628	.458	1.342	.725	2.067	1.95	+ 6
20	.087	.100	.116	.691	.188	1.182	.284	1.466	1.95	-25
21	.087	.071	.158	1.177	.607	2.100	.930	3.030	2.90	+ 4
22	.100	.121	.168	1.093	.322	1.803	.293	2.096	3.03	-31
23	.068	.068	.126	1.302	.369	1.933	.495	3.428	3.03	+13
24	.100	.130	.206	1.082	.094	1.611	.923	2.534	3.03	-16

FIGURES

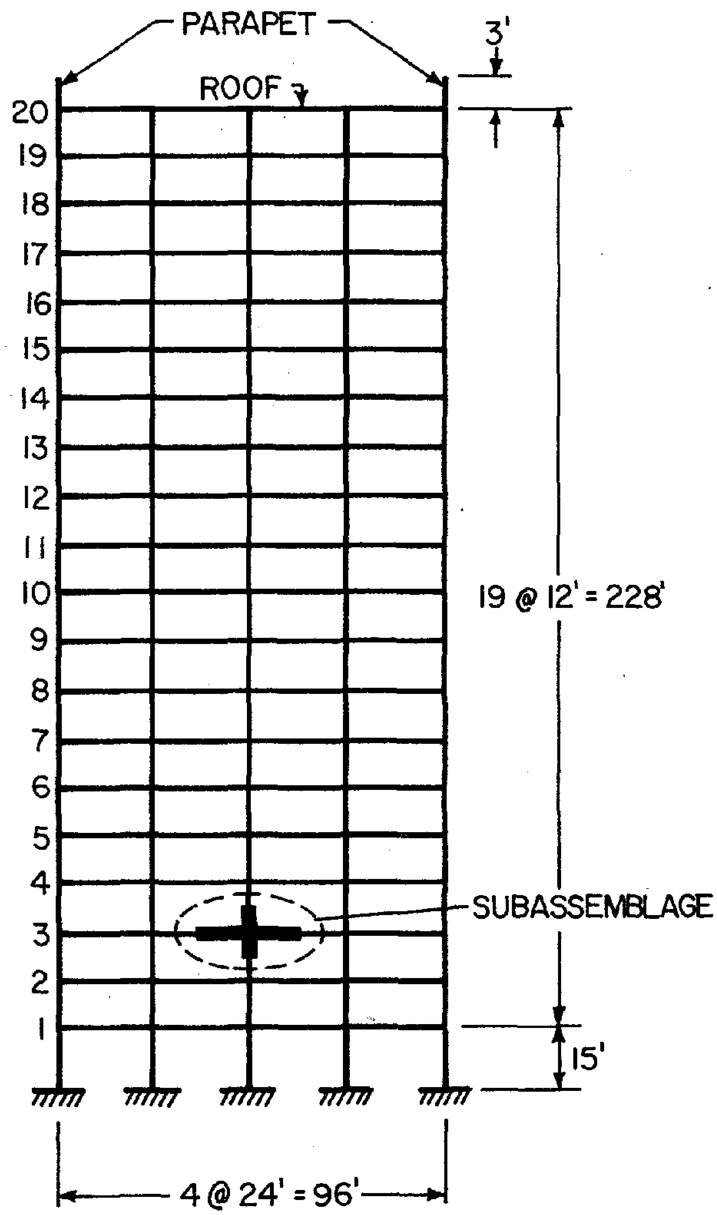

FIG. 1 TWENTY-STORY BUILDING

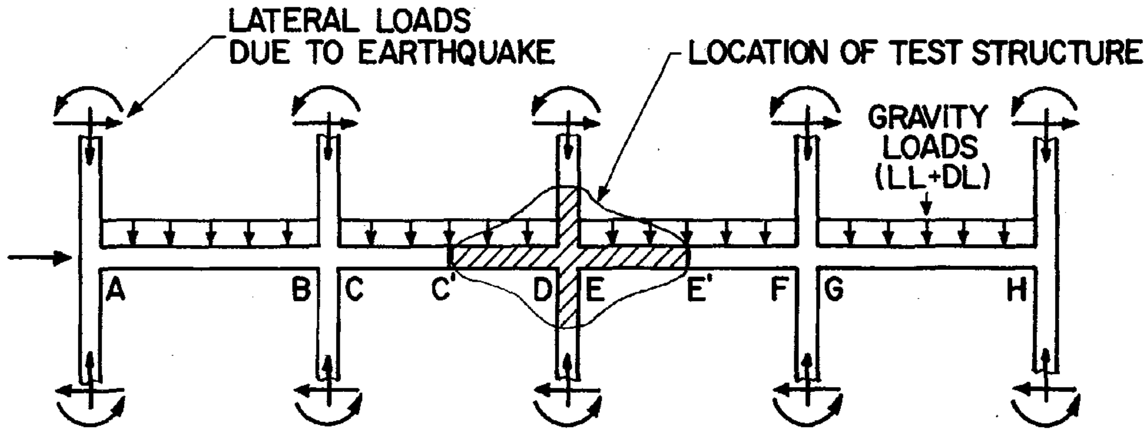

FIG. 2 SCHEMATIC OF THIRD FLOOR LEVEL OF BUILDING WITH APPLIED GRAVITY AND LATERAL LOADS

FIG. 3a MOMENTS DUE TO GRAVITY LOAD

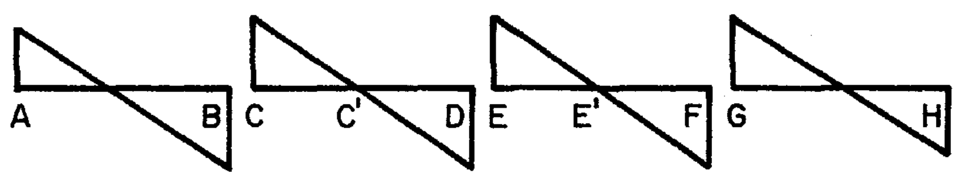

FIG. 3b MOMENTS DUE TO EARTHQUAKE LATERAL FORCES

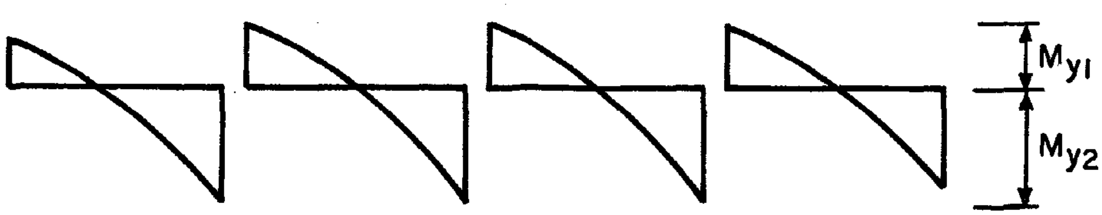

FIG. 4 SUPERPOSITION OF MOMENTS FROM GRAVITY AND LATERAL LOAD EFFECTS

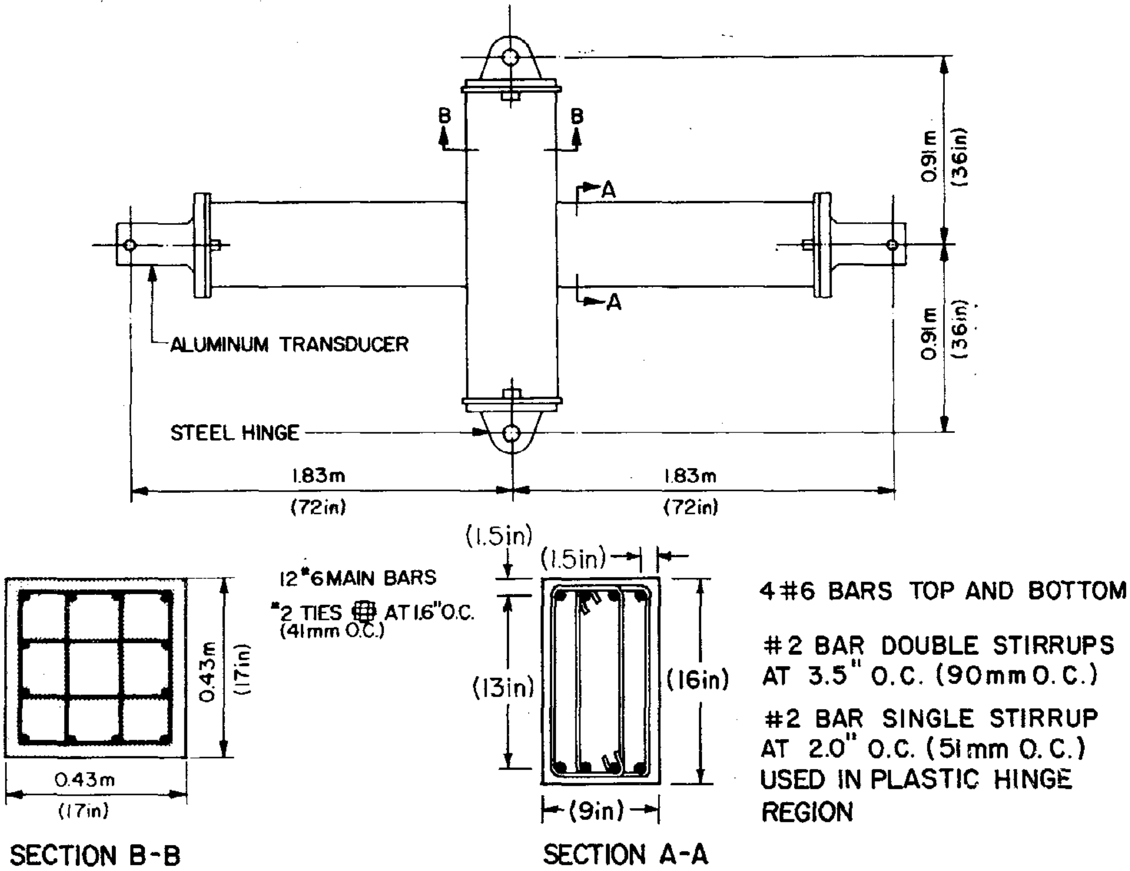

FIG. 5a SUBASSEMBLAGE WITH TYPICAL CROSS SECTIONS

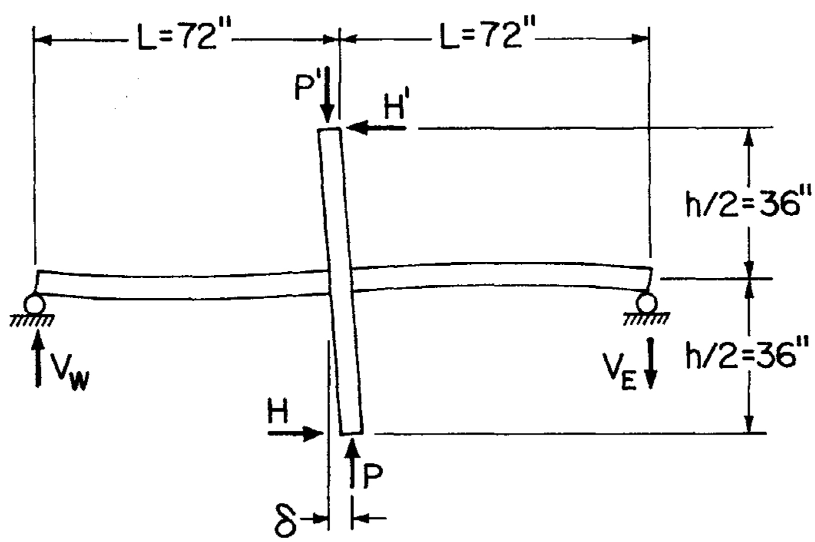

FIG. 5b DEFINITIONS OF FORCES AND DISPLACEMENTS
FOR A SUBASSEMBLAGE

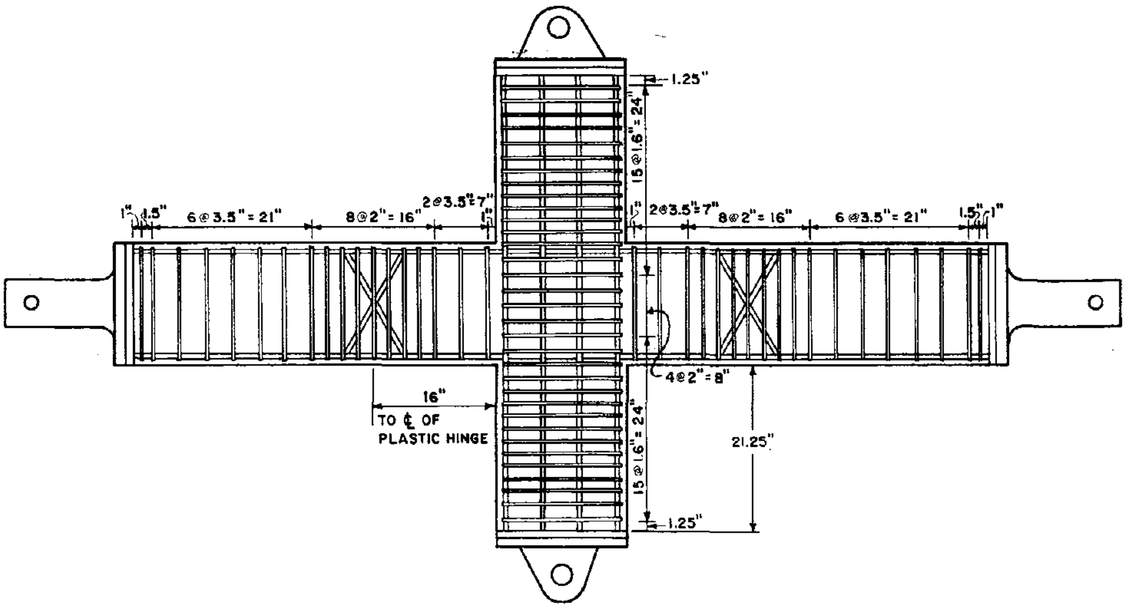

FIG. 6a REINFORCEMENT - BC5

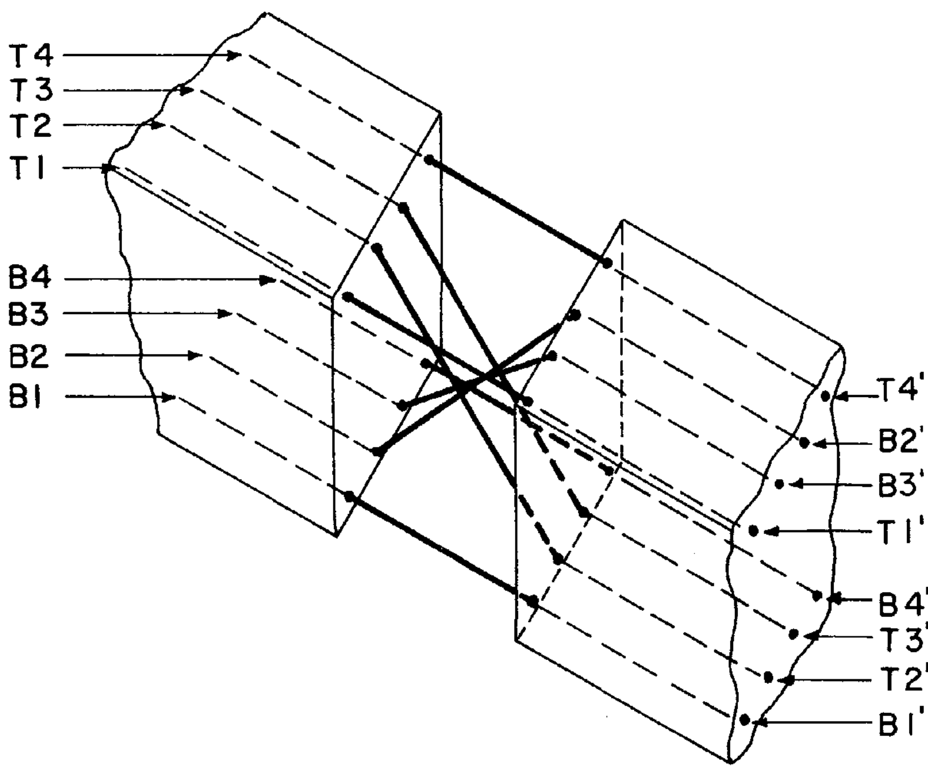

FIG. 6b ISOMETRIC VIEW OF PLASTIC HINGE - BC5

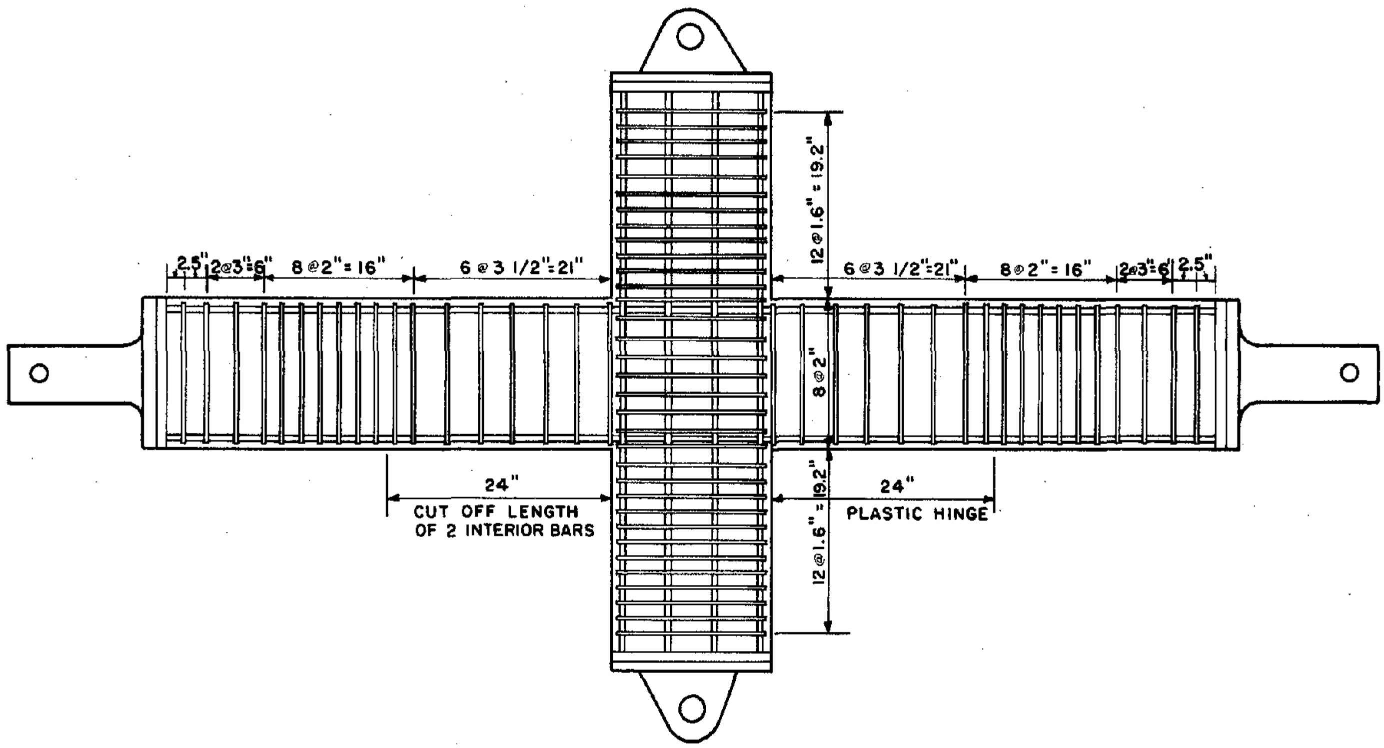

FIG. 7a REINFORCEMENT - BC6

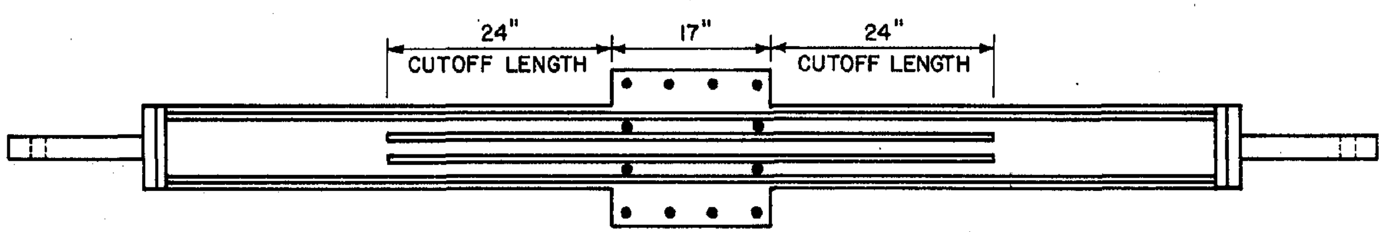

FIG. 7b TOP VIEW OF REINFORCEMENT - BC6

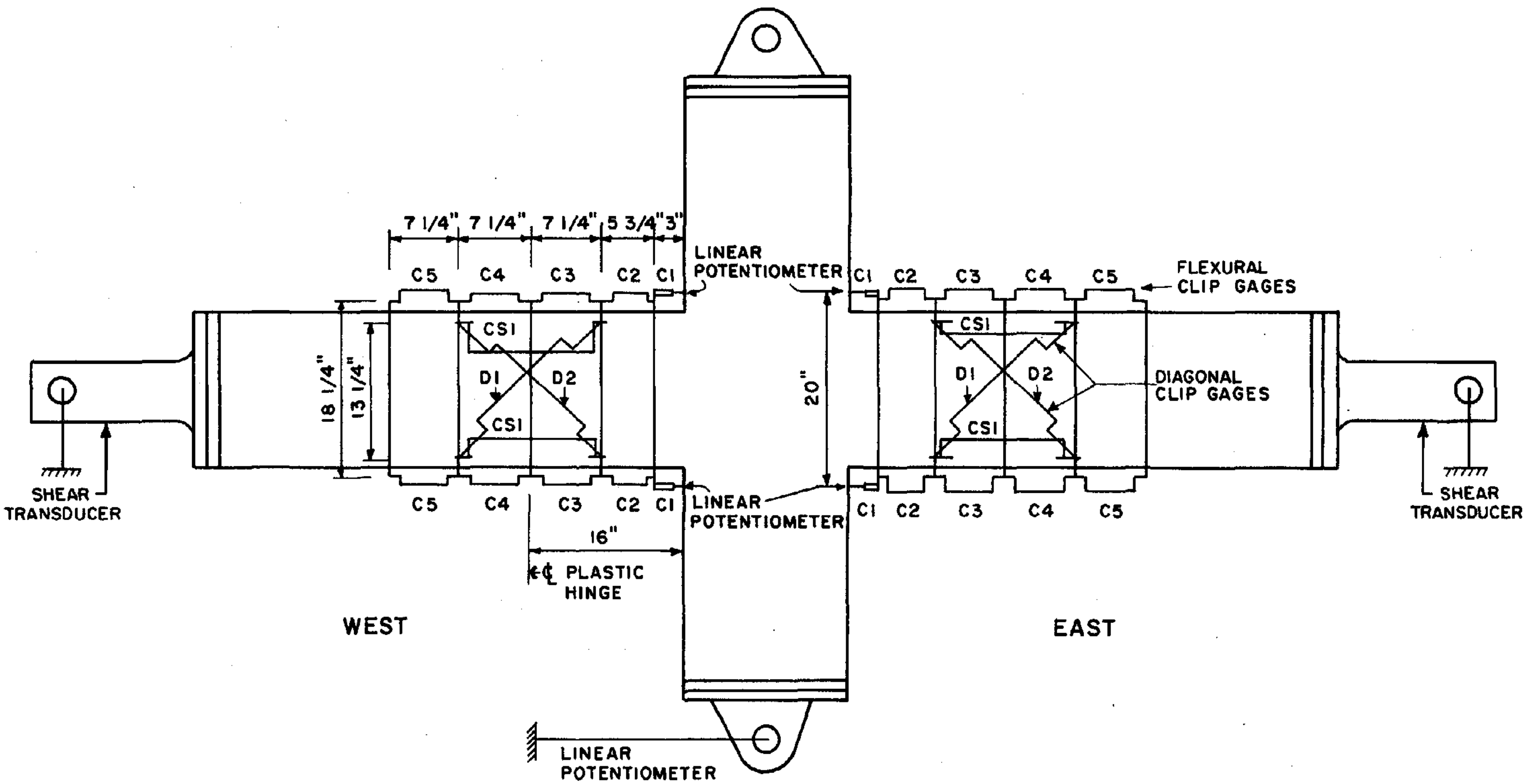

FIG. 8 CURVATURE AND SHEAR INSTRUMENTATION - BC5

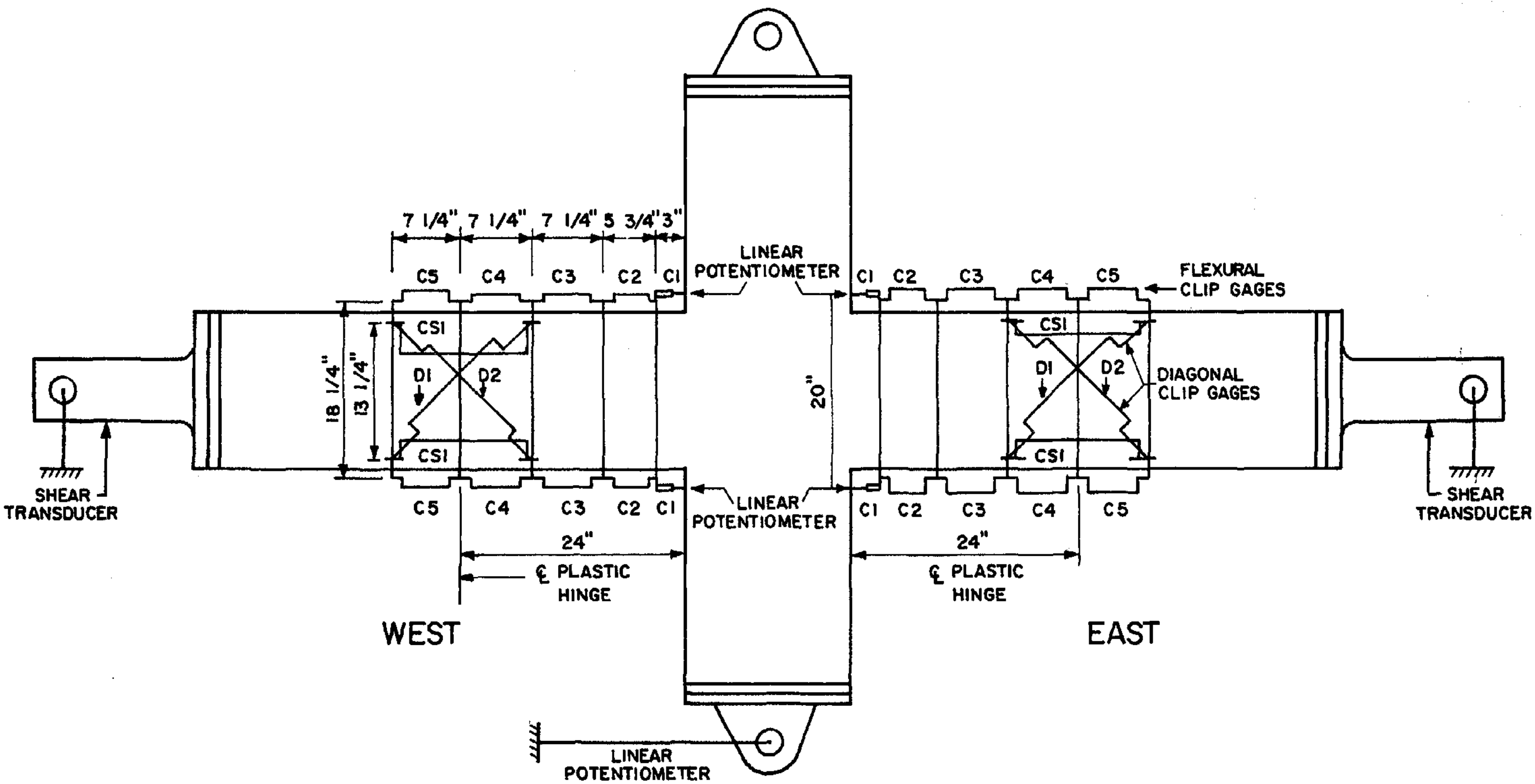

FIG. 9 CURVATURE AND SHEAR INSTRUMENTATION - BC6

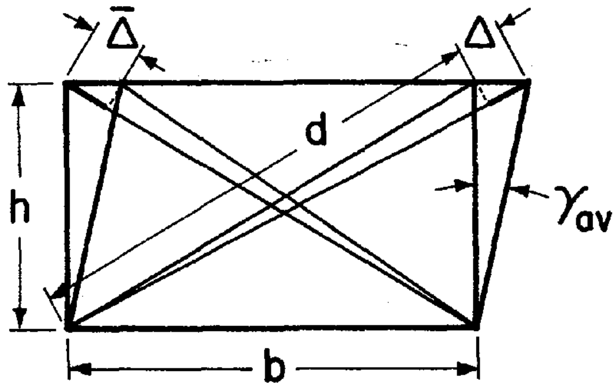

FIG. 10 MEASUREMENT OF SHEAR DISTORTION

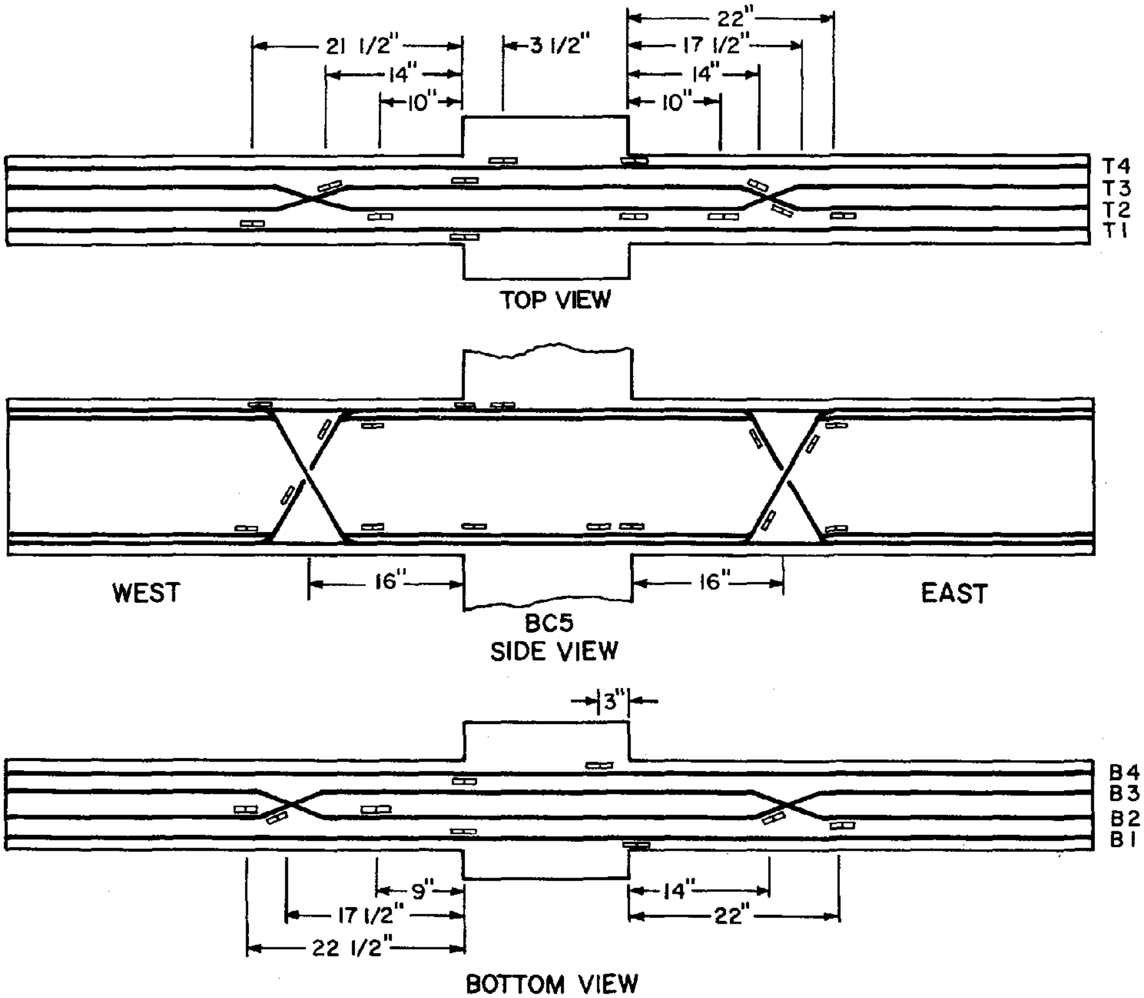

FIG. 11 STRAIN GAGE LOCATION - BC5

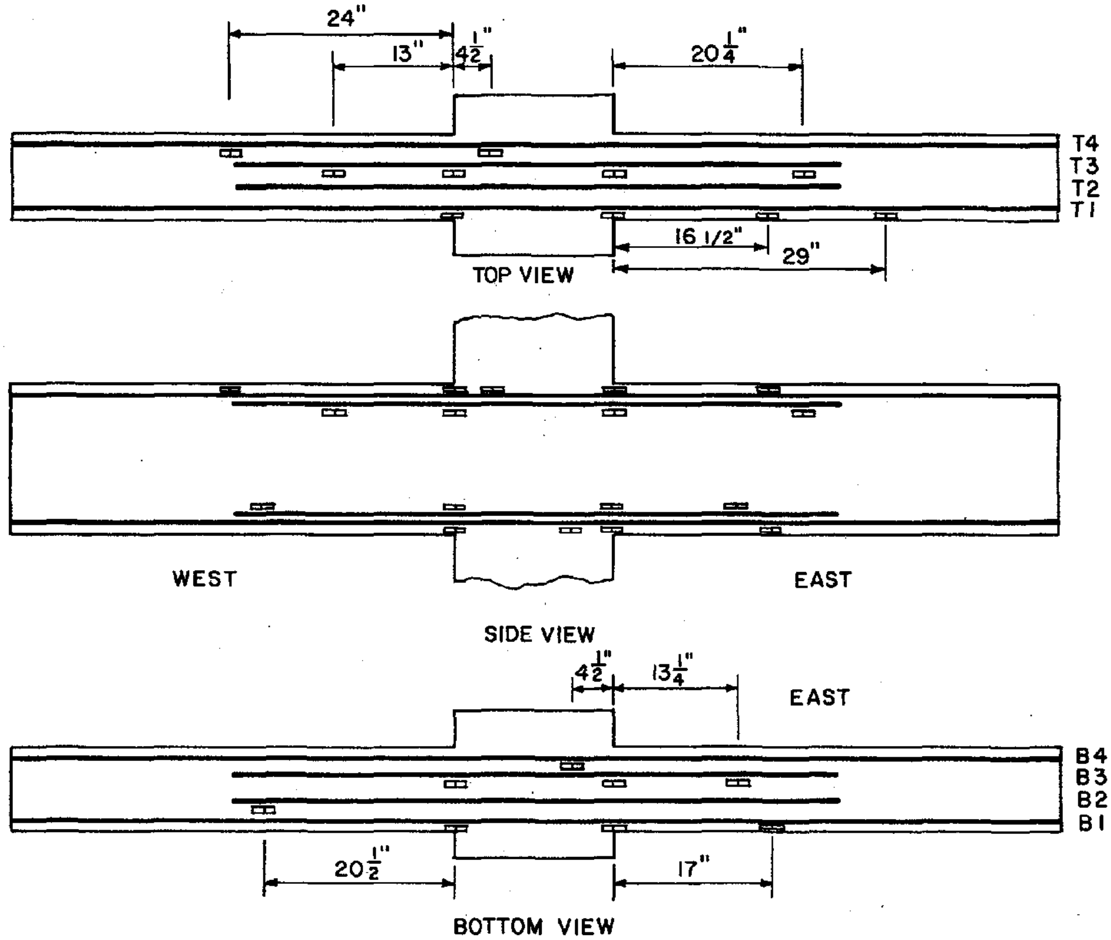

FIG. 12 STRAIN GAGE LOCATION - BC6

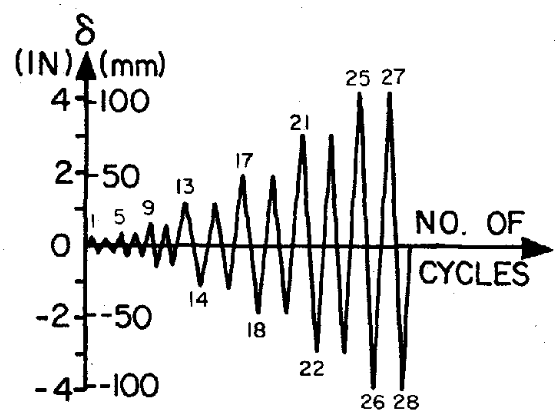

FIG. 13 LOADING PROGRAM FOR BC5 AND BC6

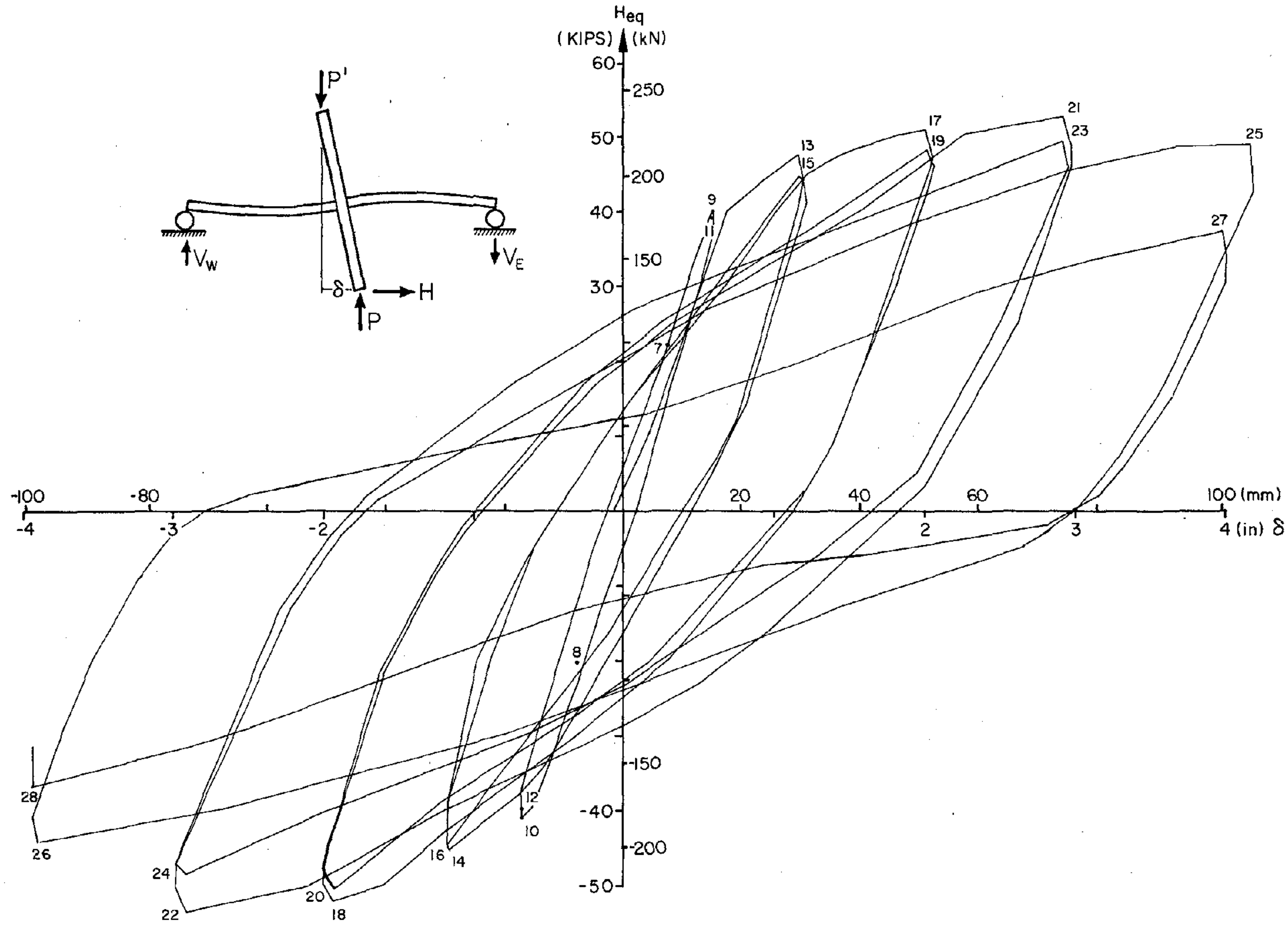

FIG. 14 H_{eq}-δ DIAGRAM - BC5

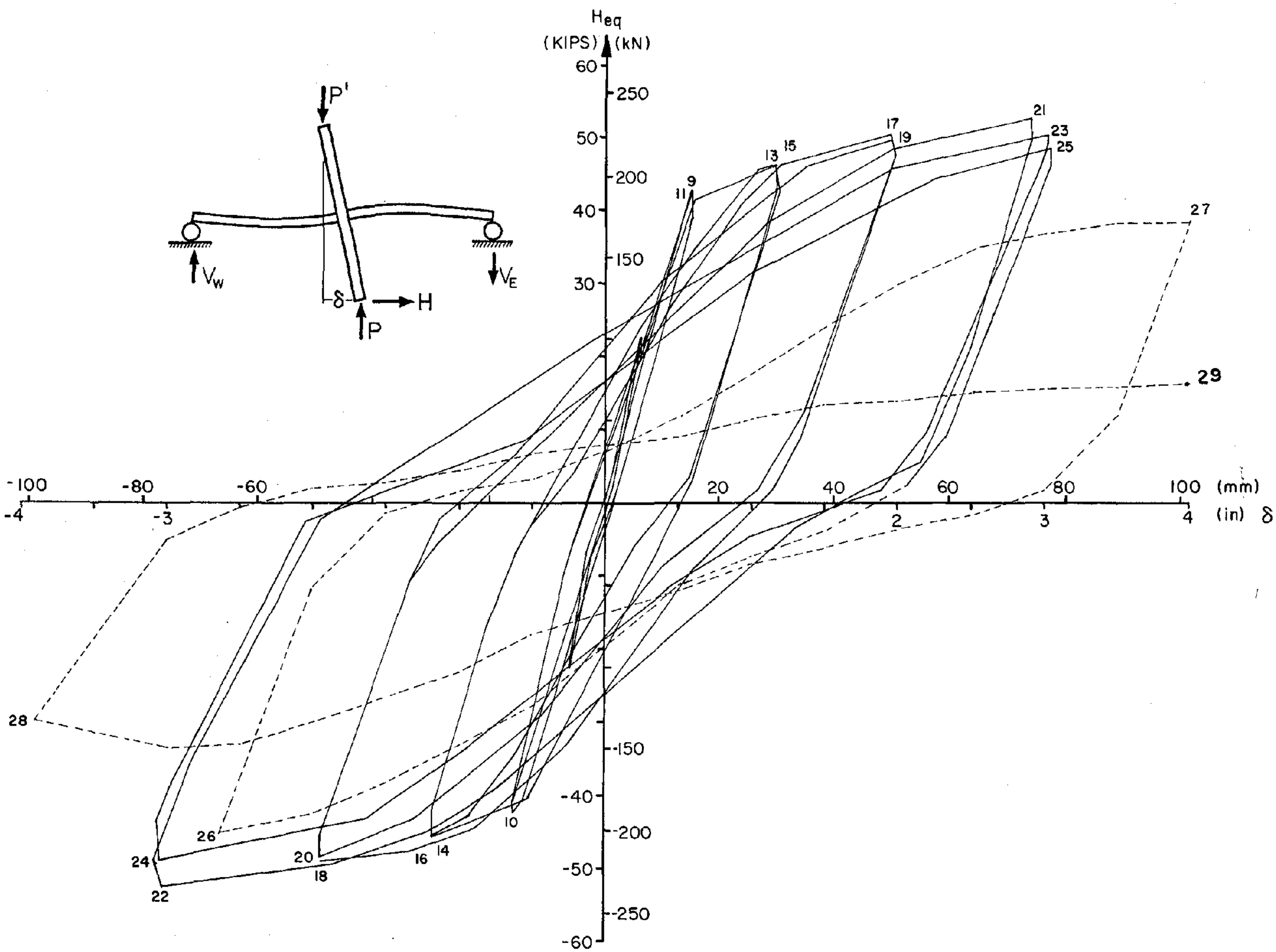

FIG. 15 H_{eq}-δ DIAGRAM - BC6

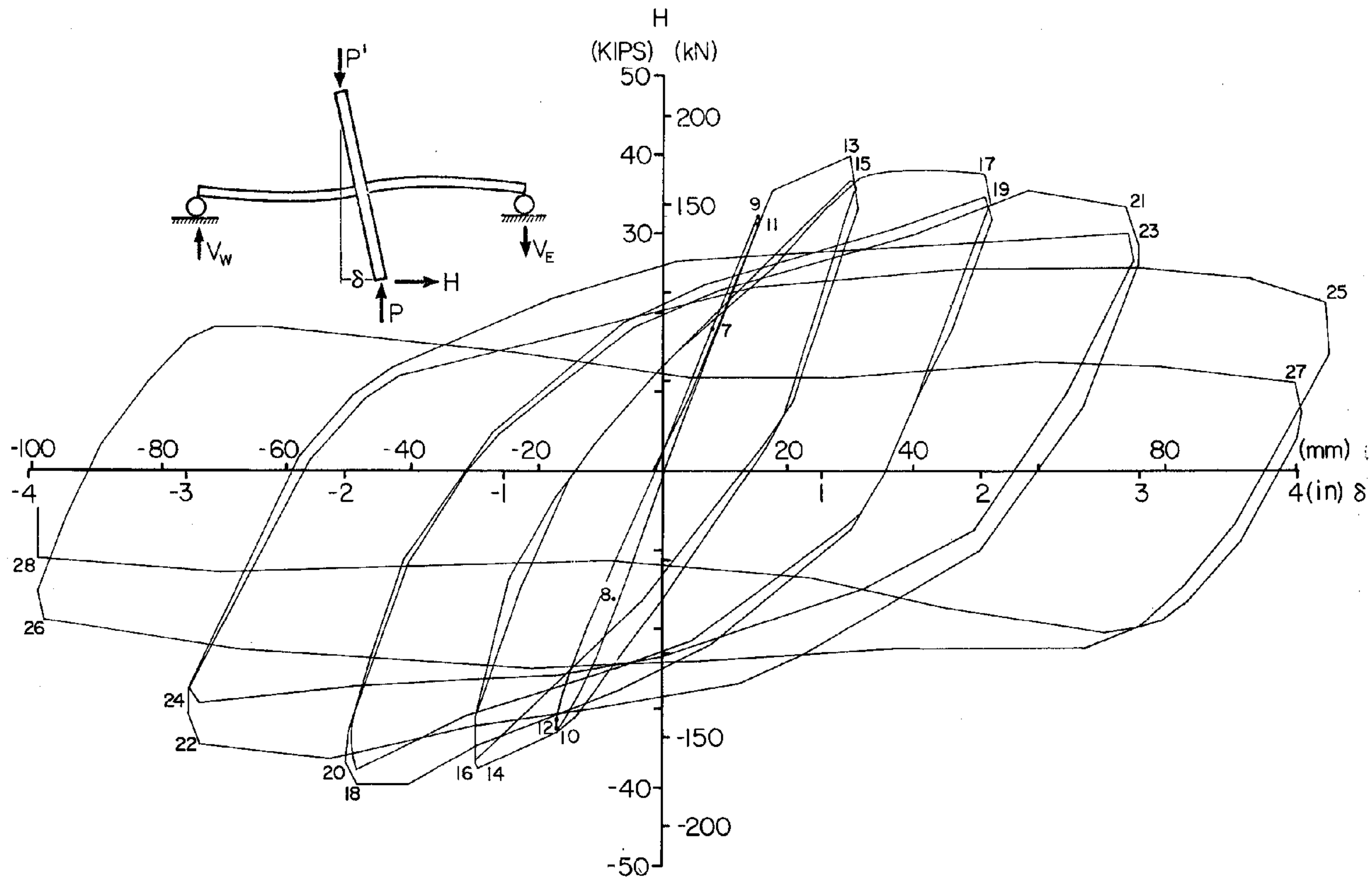

FIG. 16 H-δ DIAGRAM EXCLUDING FRICTION - BC5

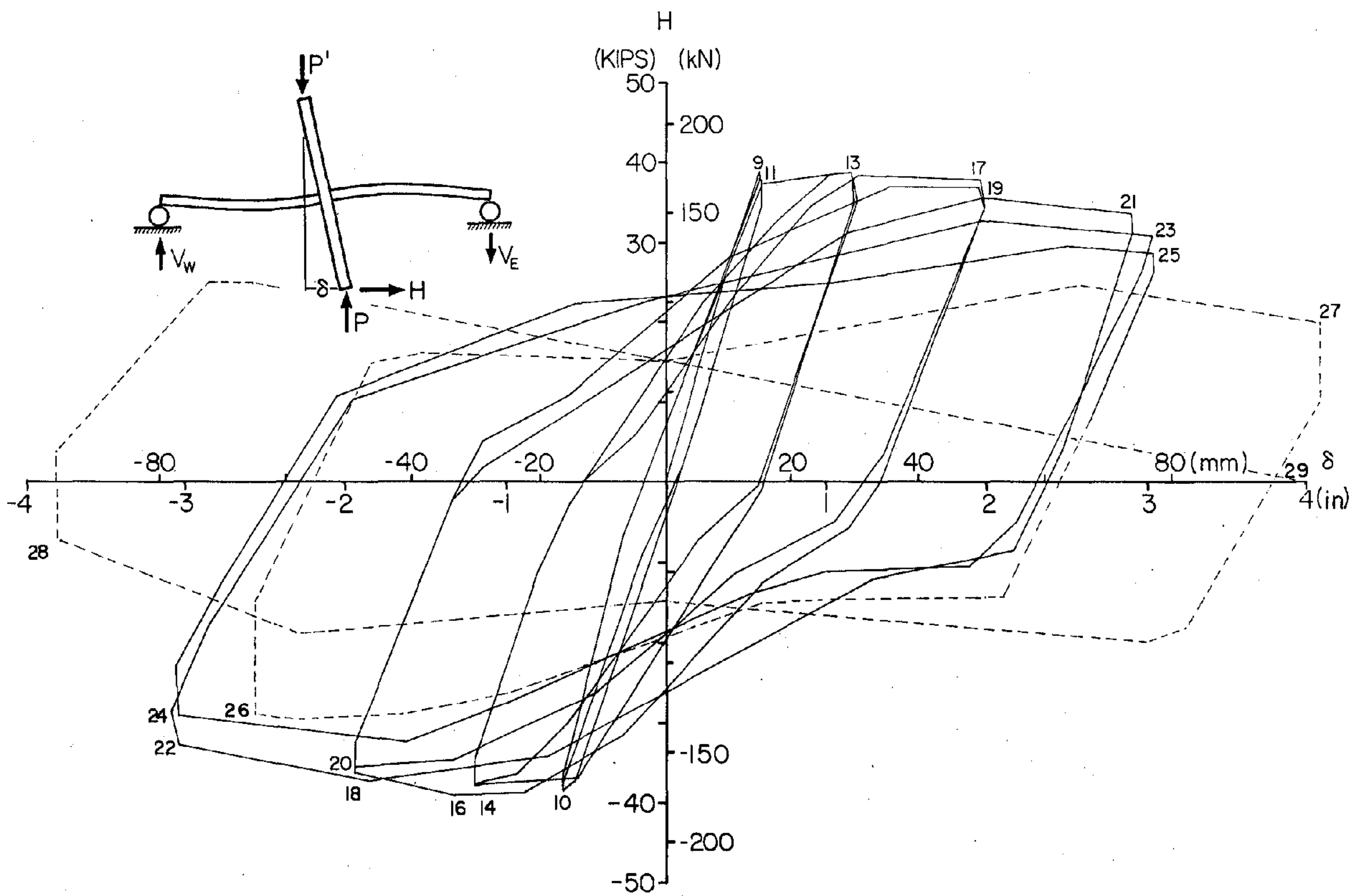

FIG. 17 H-δ DIAGRAM EXCLUDING FRICTION - BC6

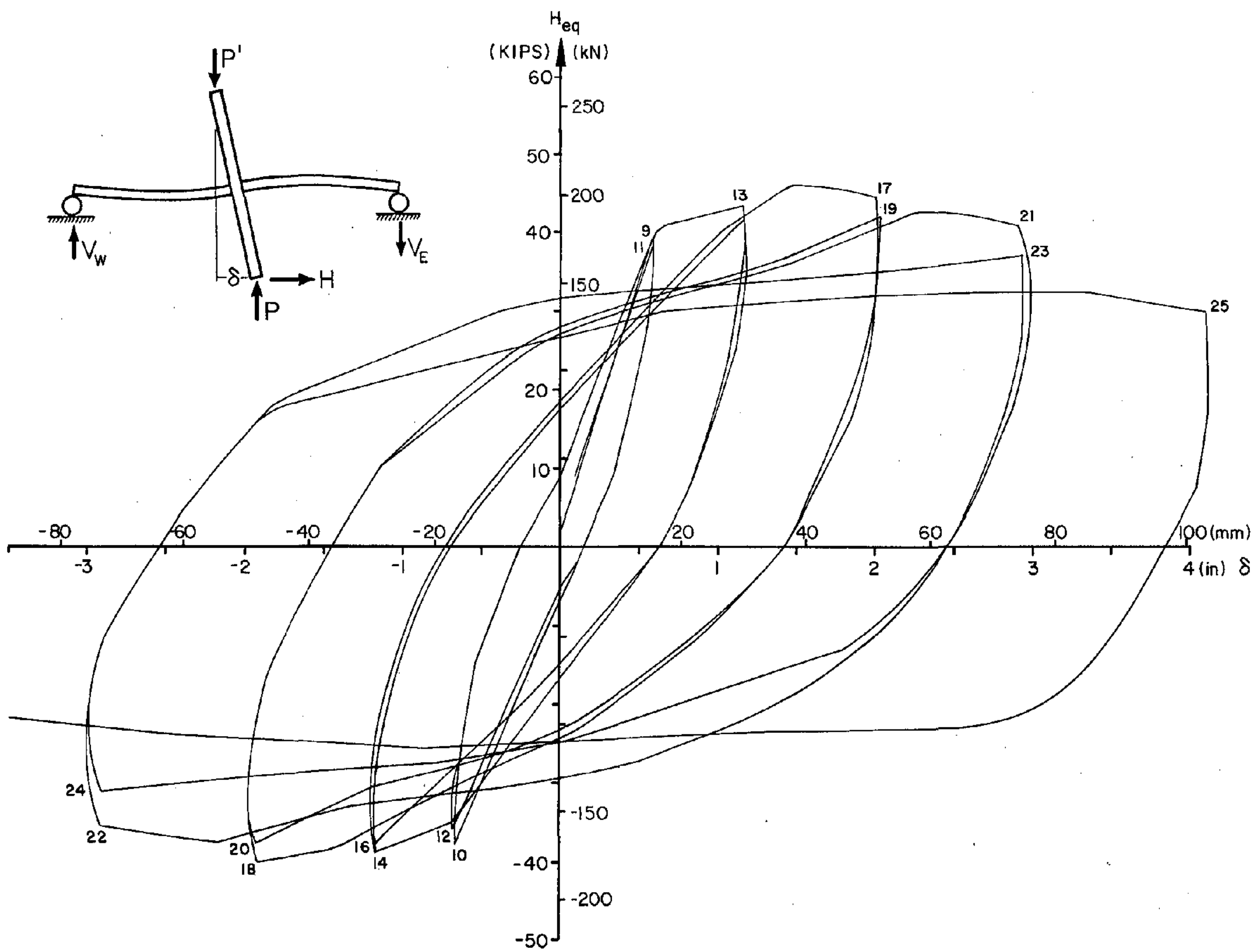

FIG. 18 H_{eq}-δ DIAGRAM INCLUDING FRICTION - BC5

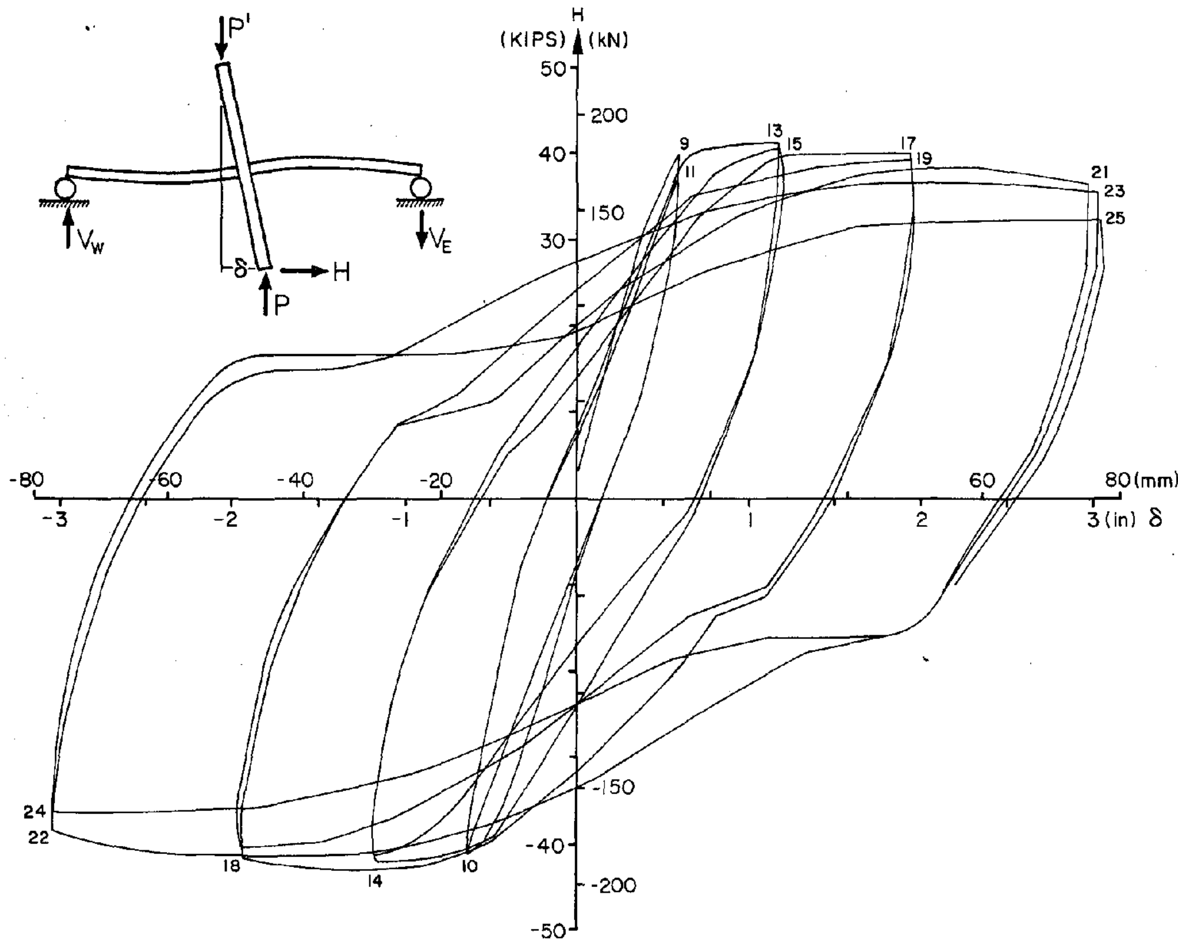

FIG. 19 H-δ DIAGRAM INCLUDING FRICTION - BC6

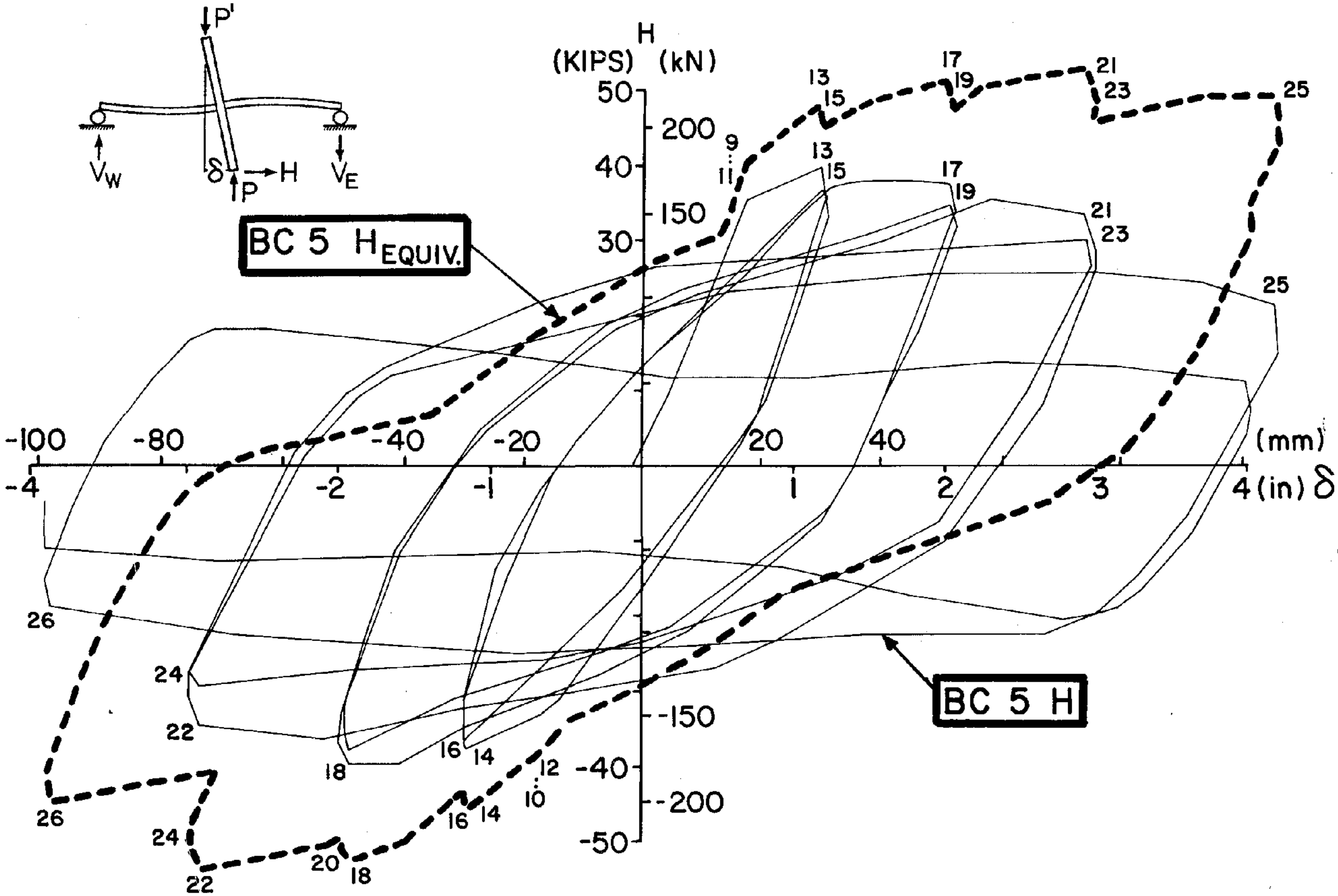

FIG. 20 COMPARISON OF H_{eq}-δ WITH H-δ - BC5

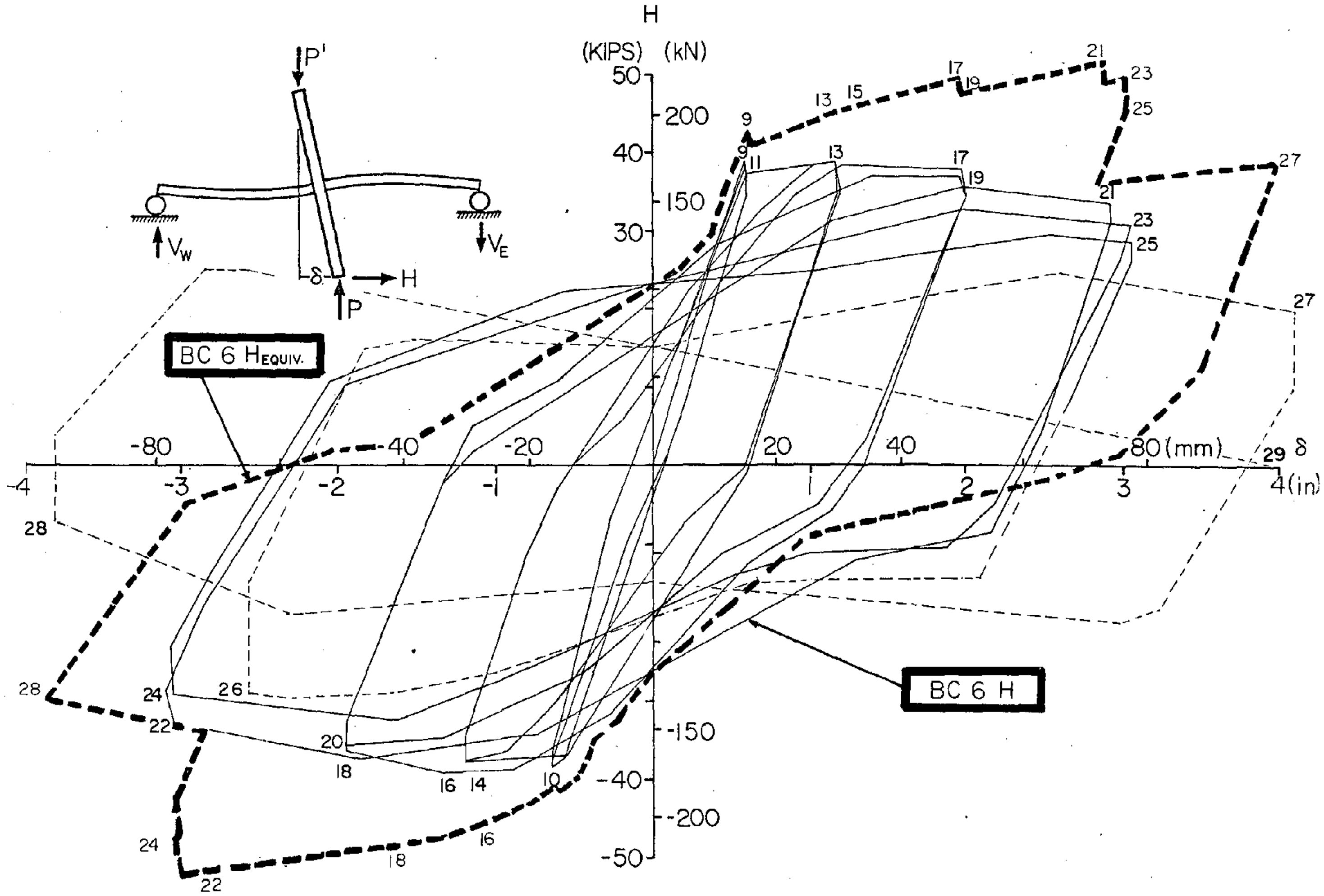

FIG. 21 COMPARISON OF H_{eq}-δ WITH H-δ - BC6

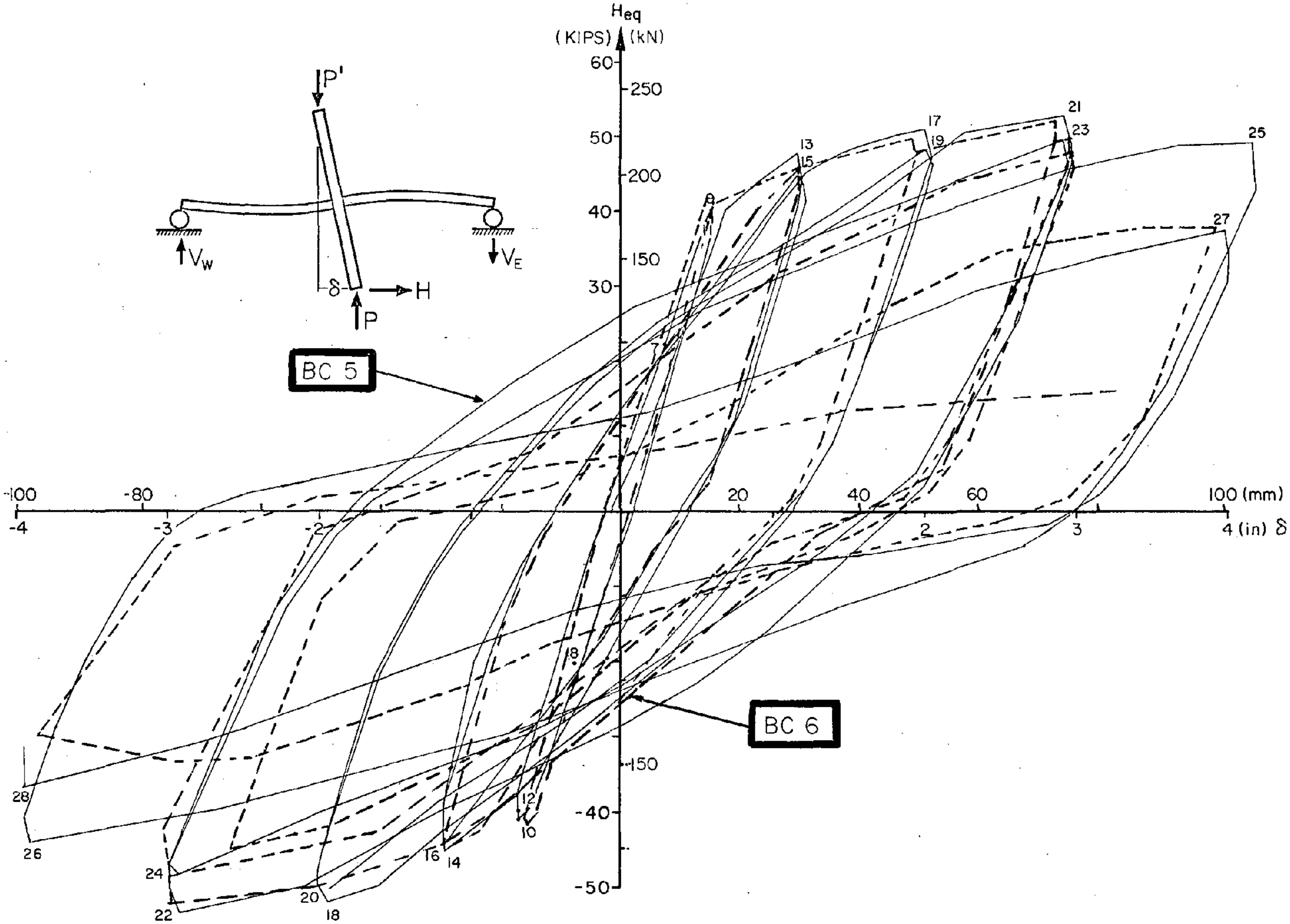

FIG. 22 COMPARISON OF H_{eq}-δ - BC5 AND BC6

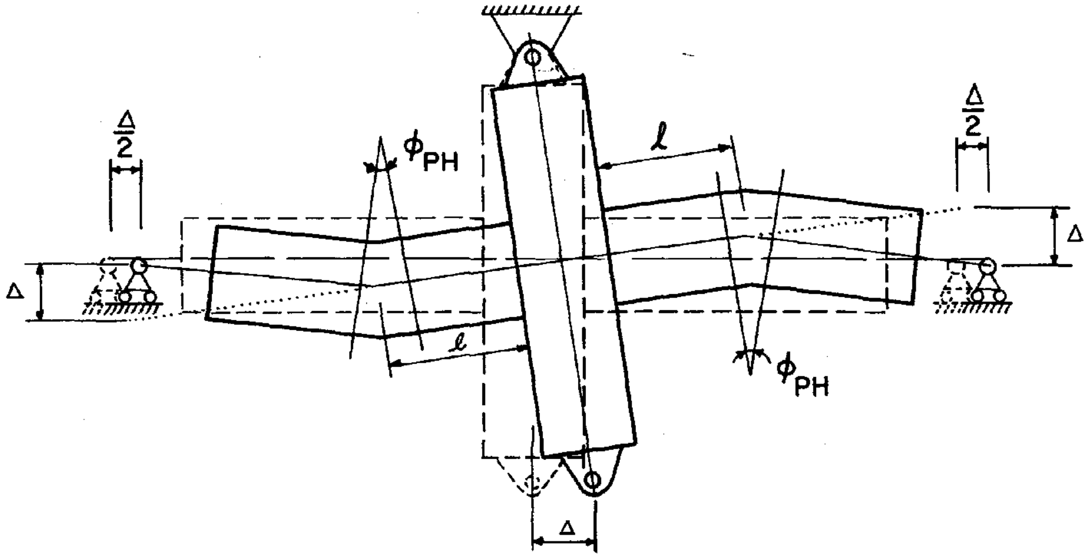

FIG. 23 LOCALIZED PLASTIC HINGE MECHANISM

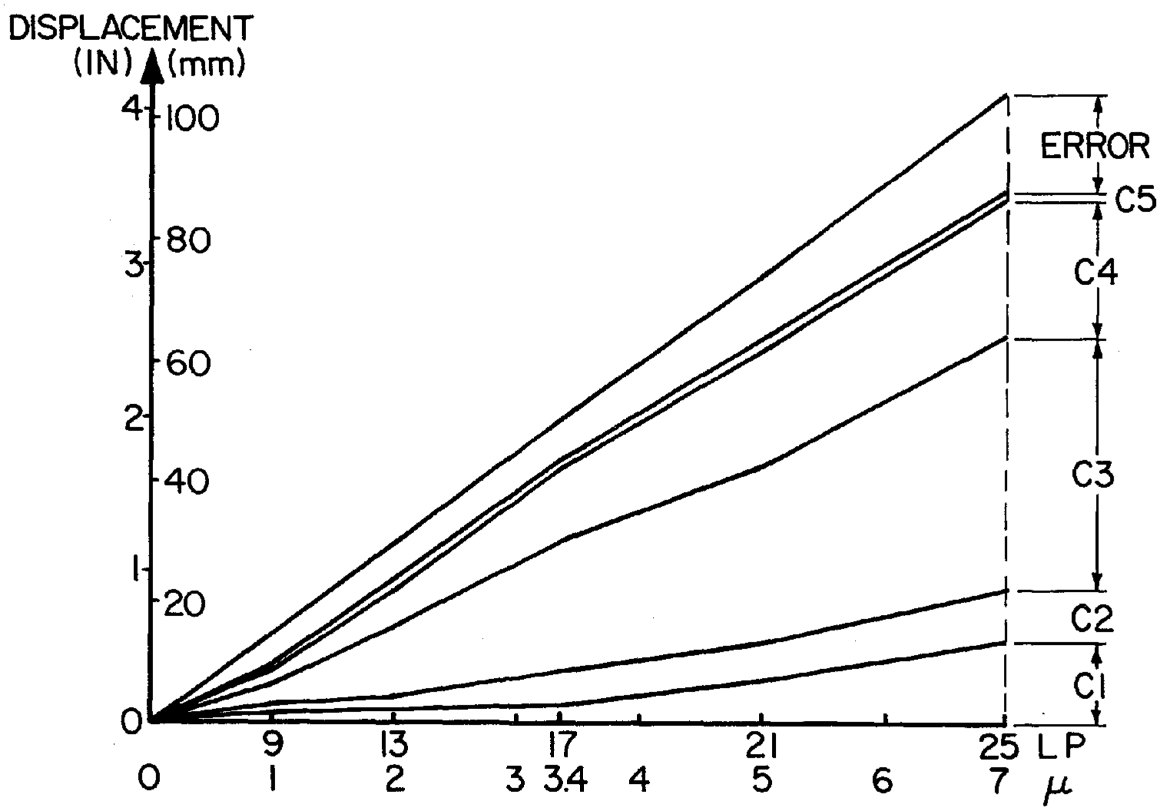

FIG. 24a DISPLACEMENT COMPONENTS - BC5

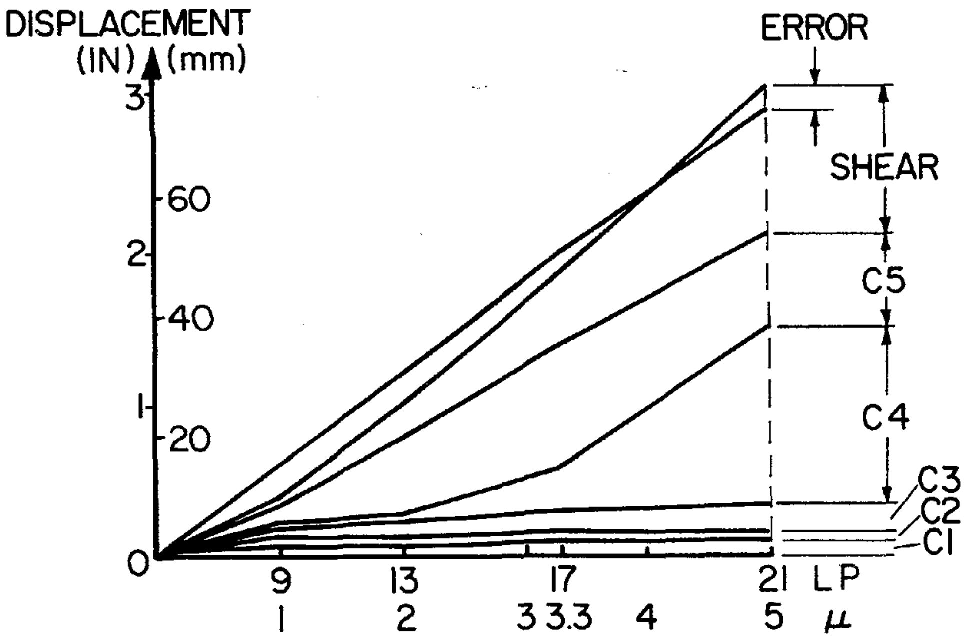

FIG. 24b DISPLACEMENT COMPONENTS - BC6

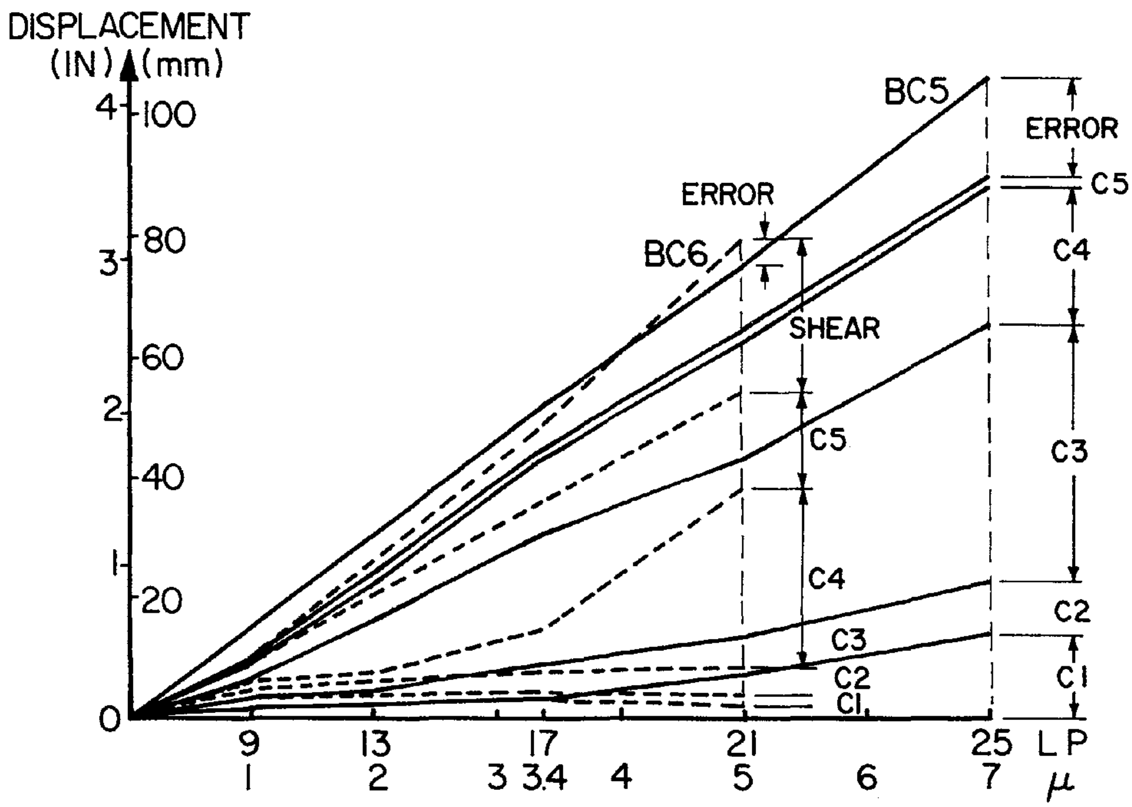

FIG. 25 COMPARISON OF DISPLACEMENT COMPONENTS - BC5 AND BC6

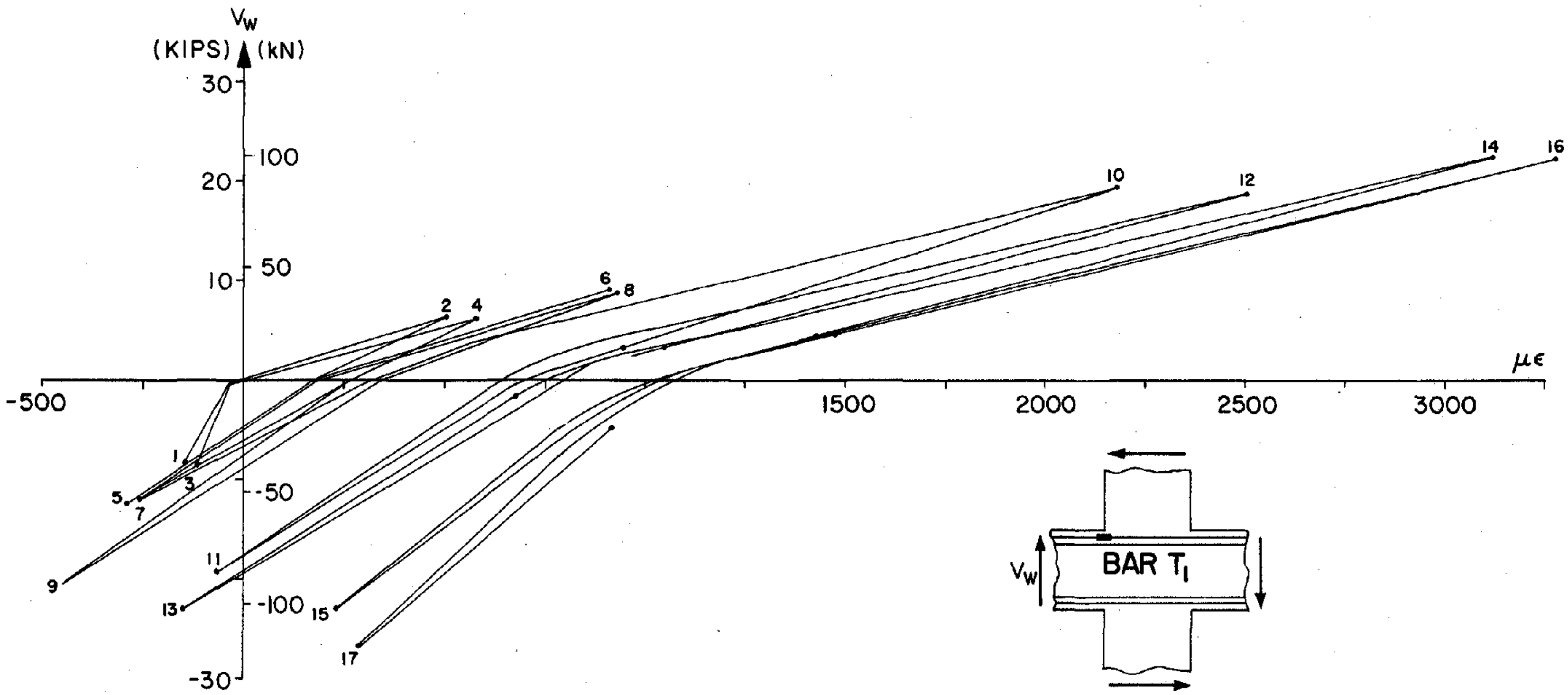

FIG. 26a STEEL STRAIN VS. SHEAR FORCE AT COLUMN FACE - BC5

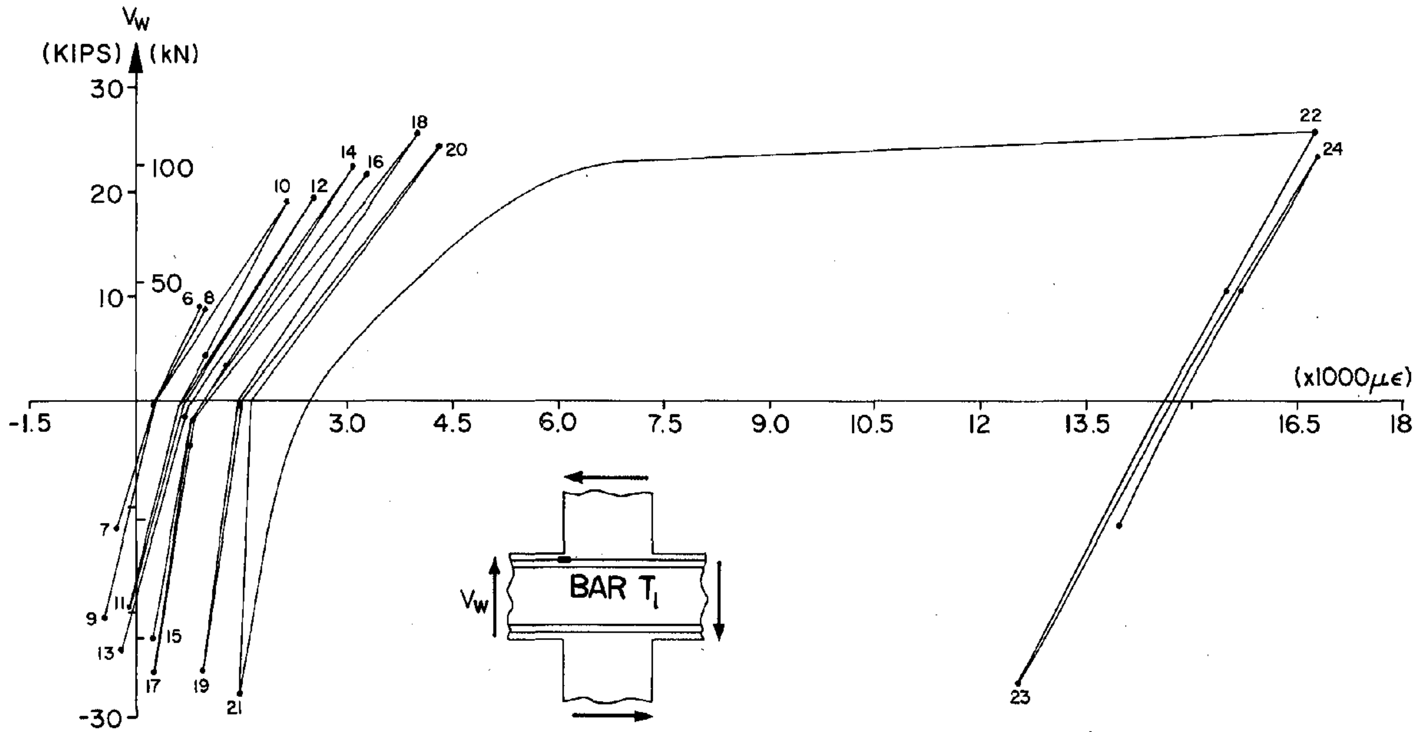

FIG. 26b STEEL STRAIN VS. SHEAR FORCE AT COLUMN FACE - BC5

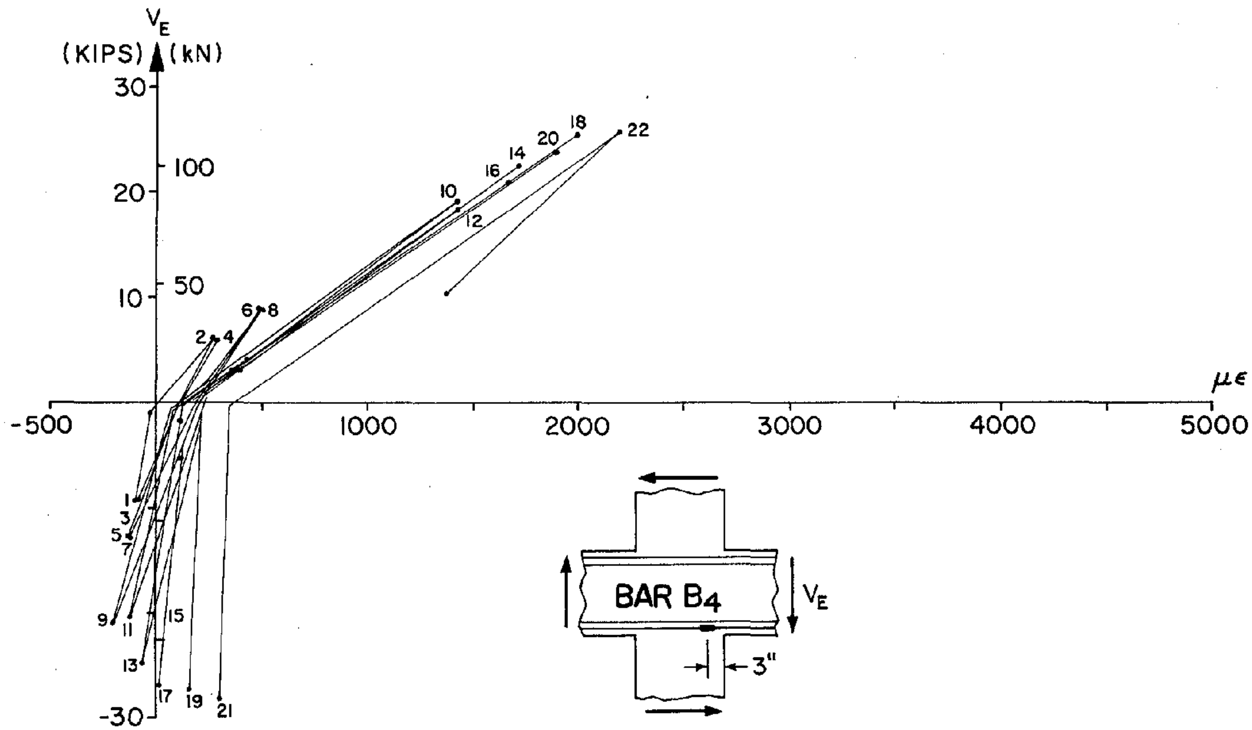

FIG. 27 STEEL STRAIN AT INSIDE JOINT 3 IN. FROM COLUMN FACE VS. SHEAR FORCE - BC5

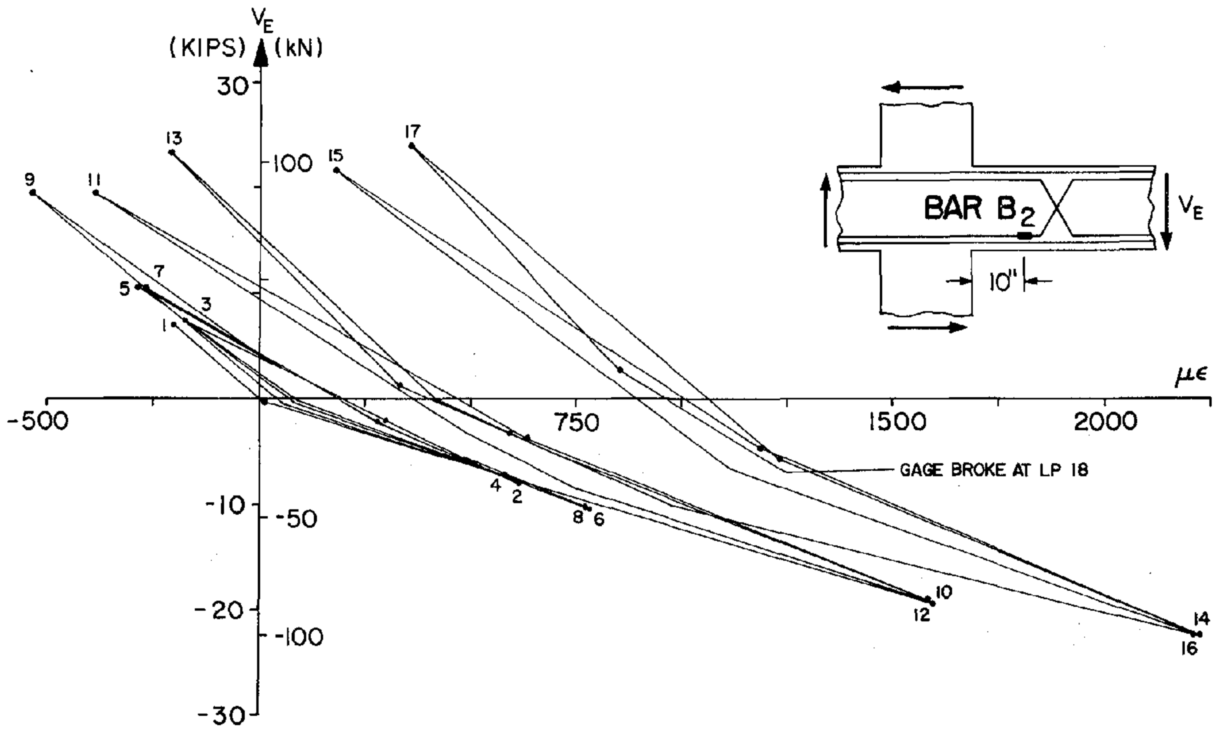

FIG. 28 STEEL STRAIN AT 10 IN. FROM COLUMN FACE VS. SHEAR FORCE - BC5

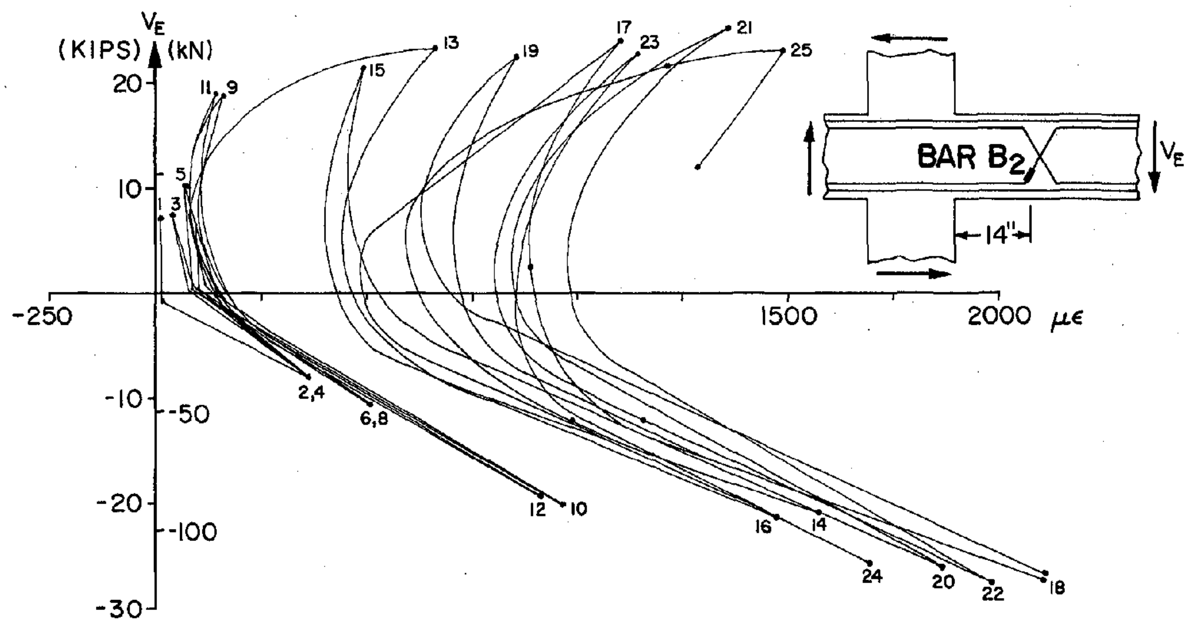

FIG. 29 STEEL STRAIN AT 14 IN. FROM COLUMN FACE VS. SHEAR FORCE - BC5

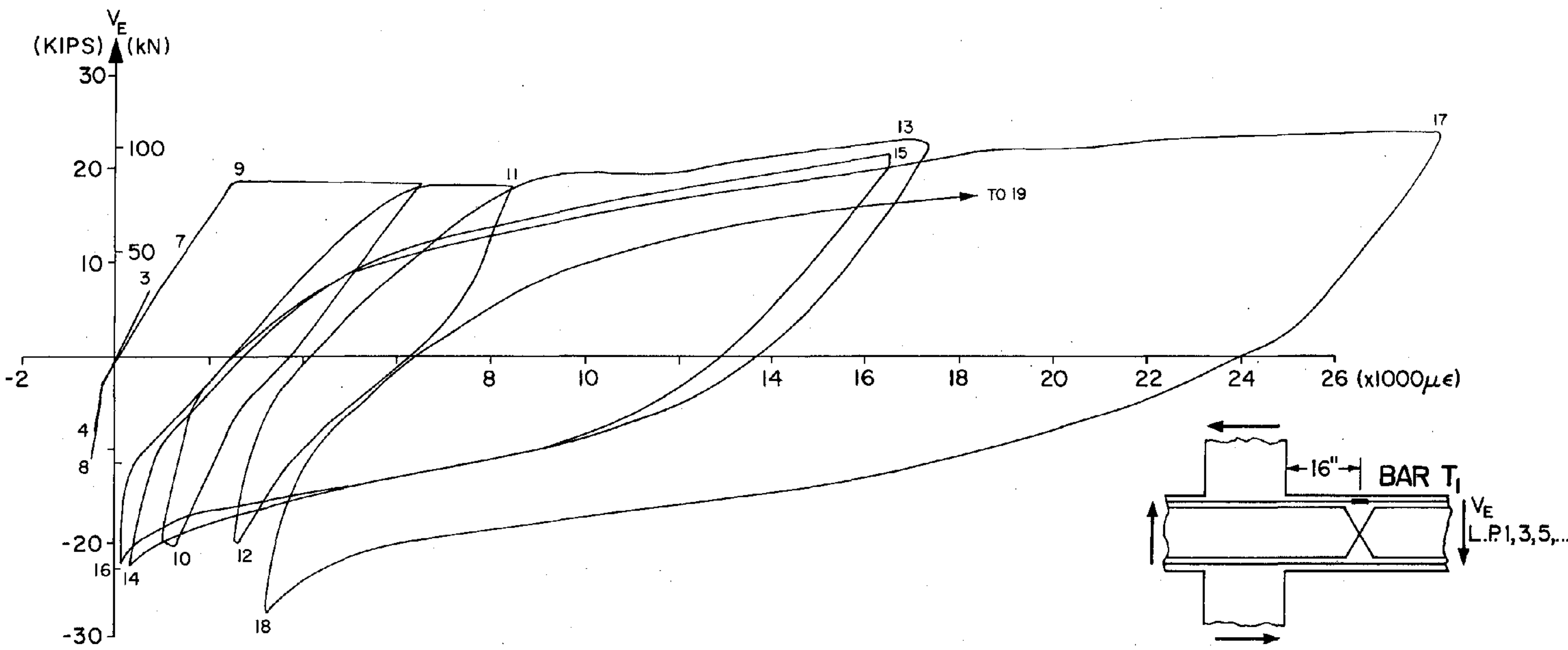

FIG. 30 STEEL STRAIN AT 16 IN. FROM COLUMN FACE (PLASTIC HINGE REGION) VS. SHEAR FORCE - BC5

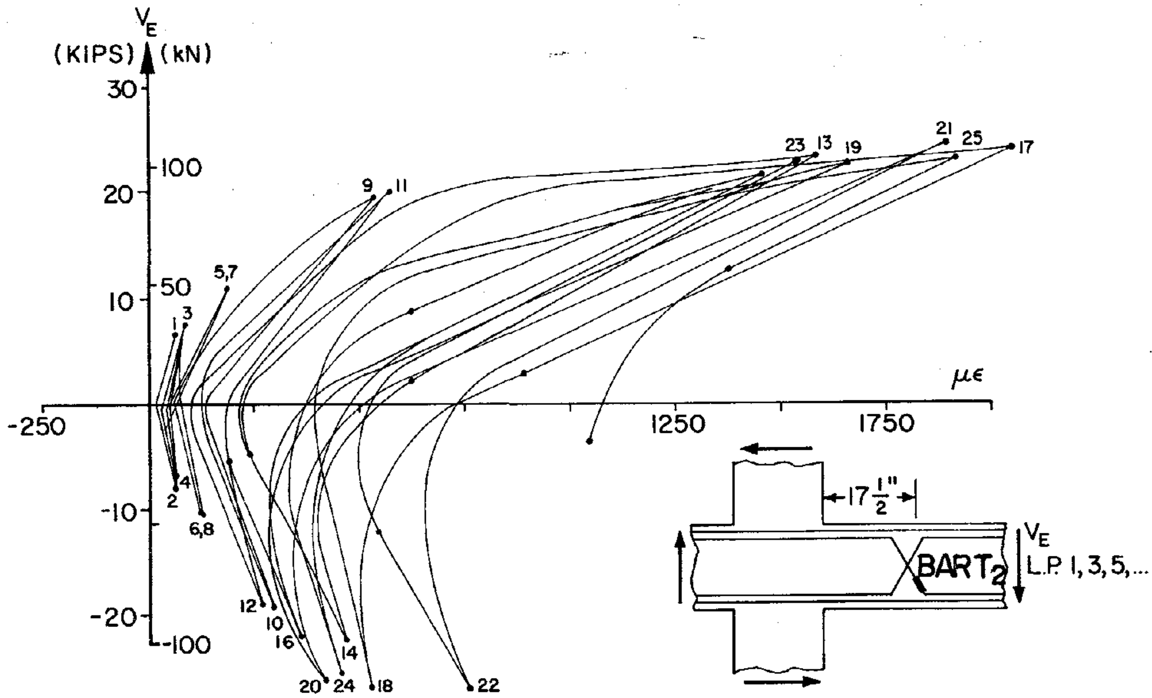

FIG. 31 STEEL STRAIN IN THE INCLINED BAR AT 17.5 IN. FROM COLUMN FACE VS. SHEAR FORCE - BC5

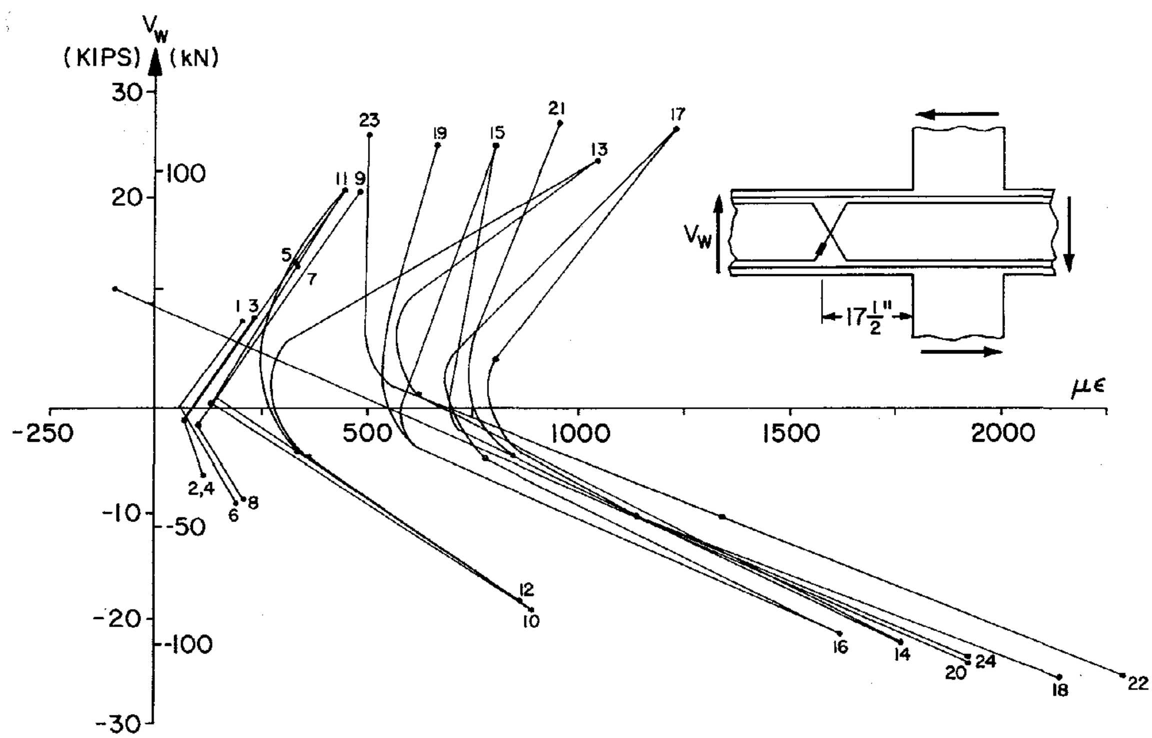

FIG. 32 STEEL STRAIN IN THE INCLINED BAR AT 17.5 IN. FROM COLUMN FACE VS. SHEAR FORCE - BC5

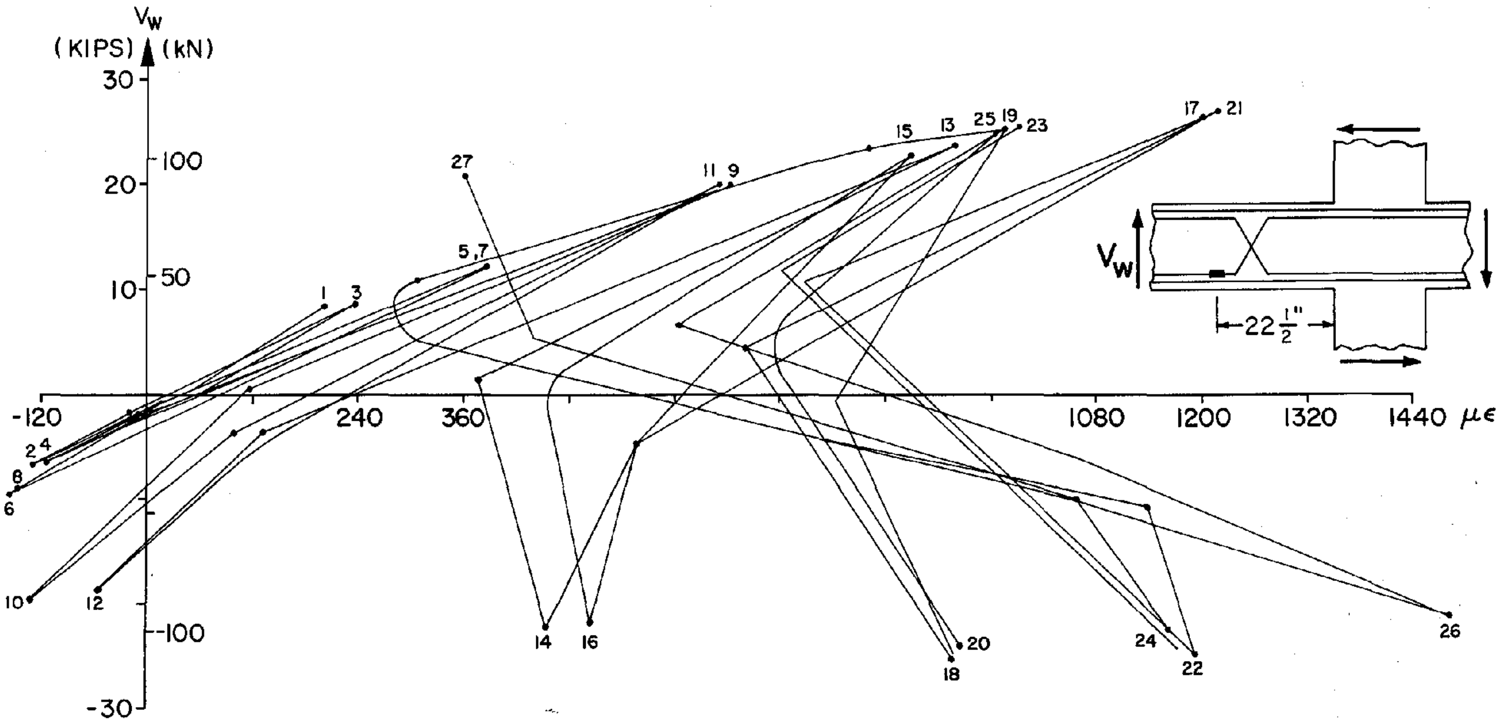

FIG. 33 STEEL STRAIN IN THE INCLINED BAR AT 17.5 IN. FROM COLUMN FACE VS. SHEAR FORCE - BC5

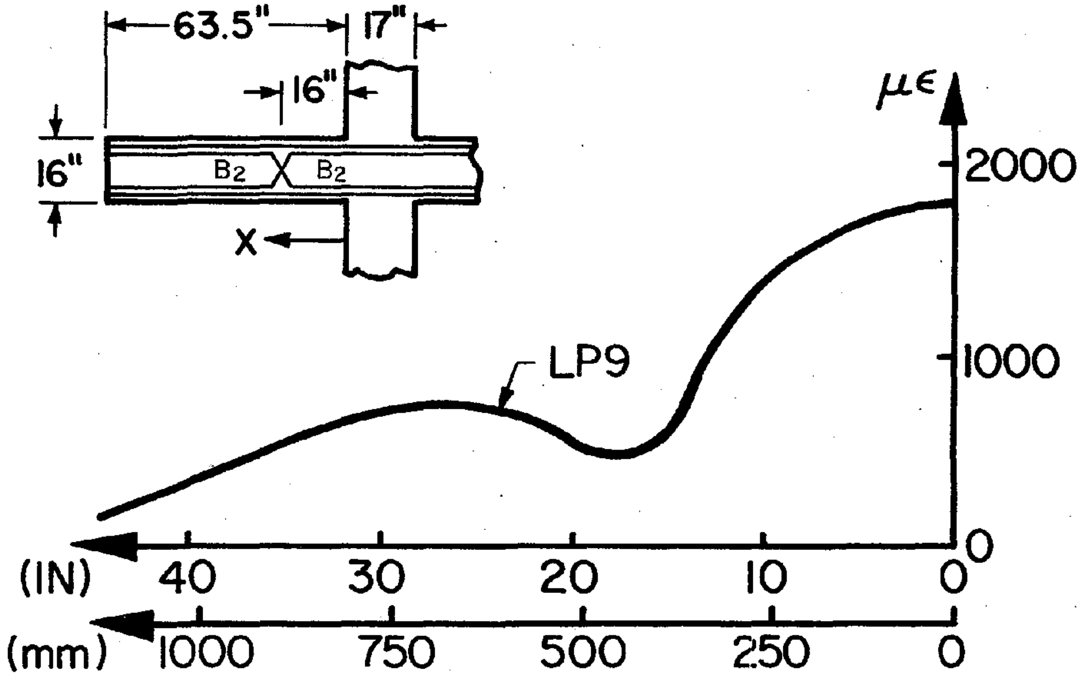

FIG. 34a LOAD POINT 9

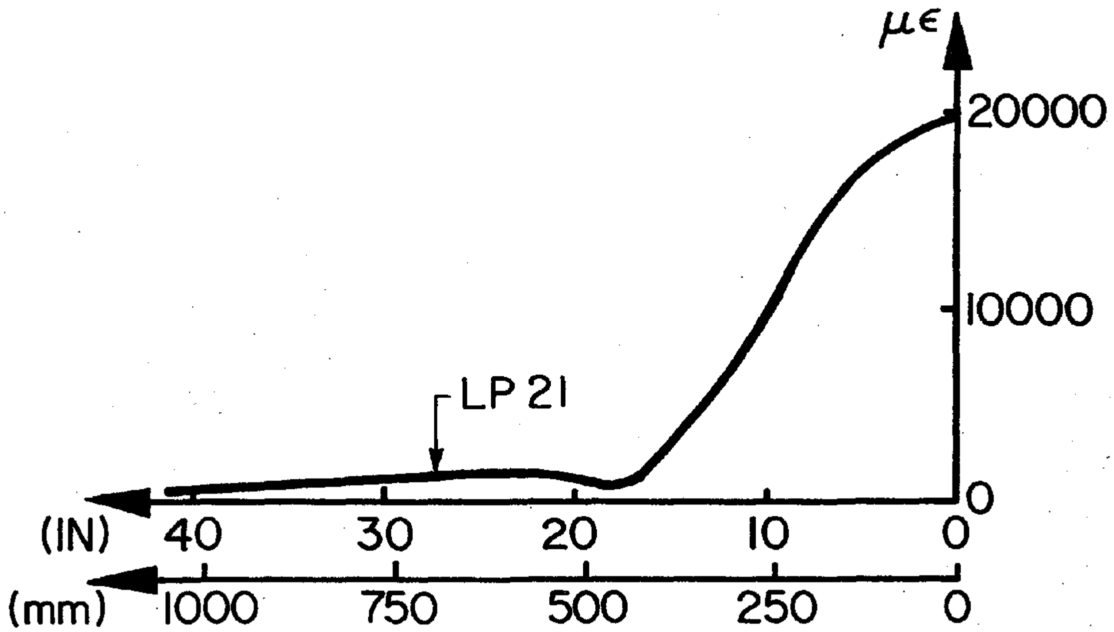

FIG. 34b LOAD POINT 21

FIG. 34 VARIATION OF STEEL STRAIN ALONG BAR B2, WEST BEAM - BC5

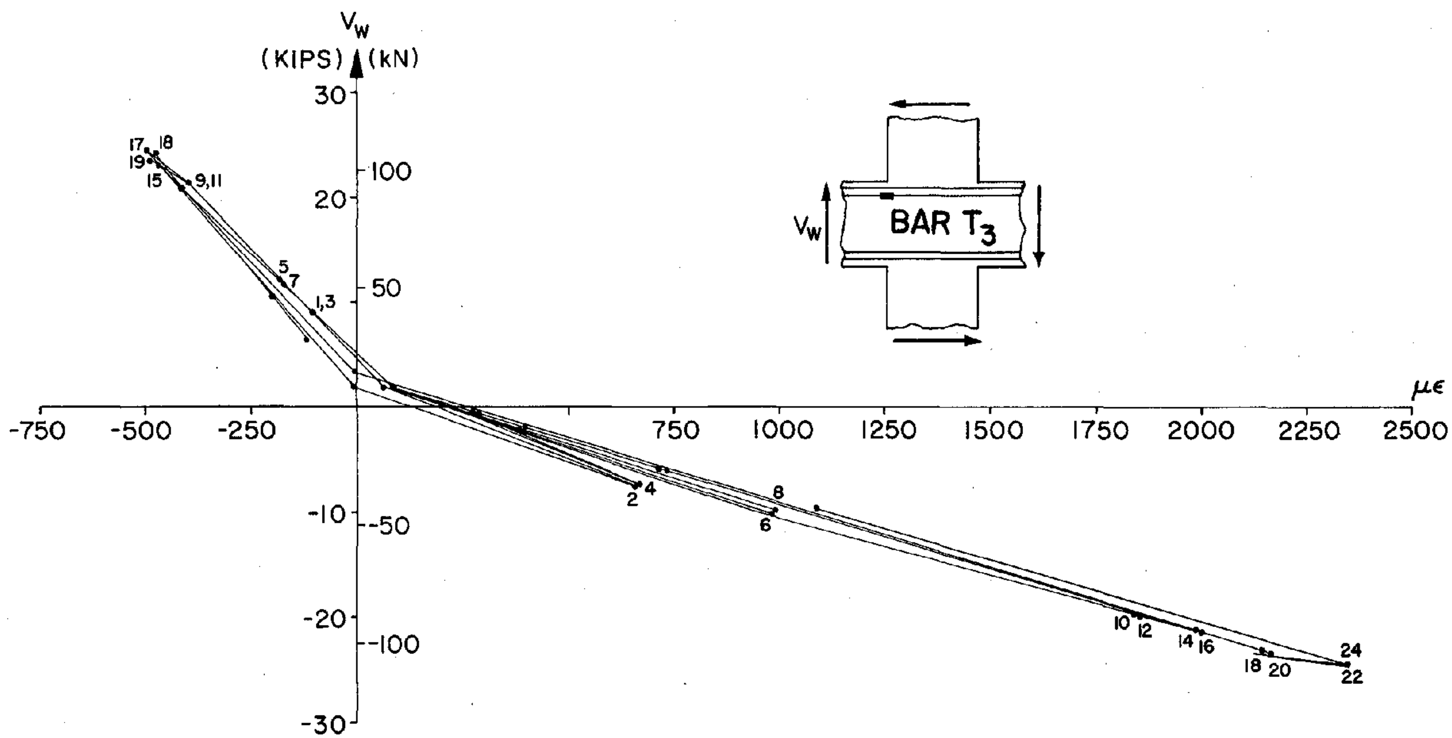

FIG. 35 STEEL STRAIN VS. SHEAR FORCE AT COLUMN FACE - BC6

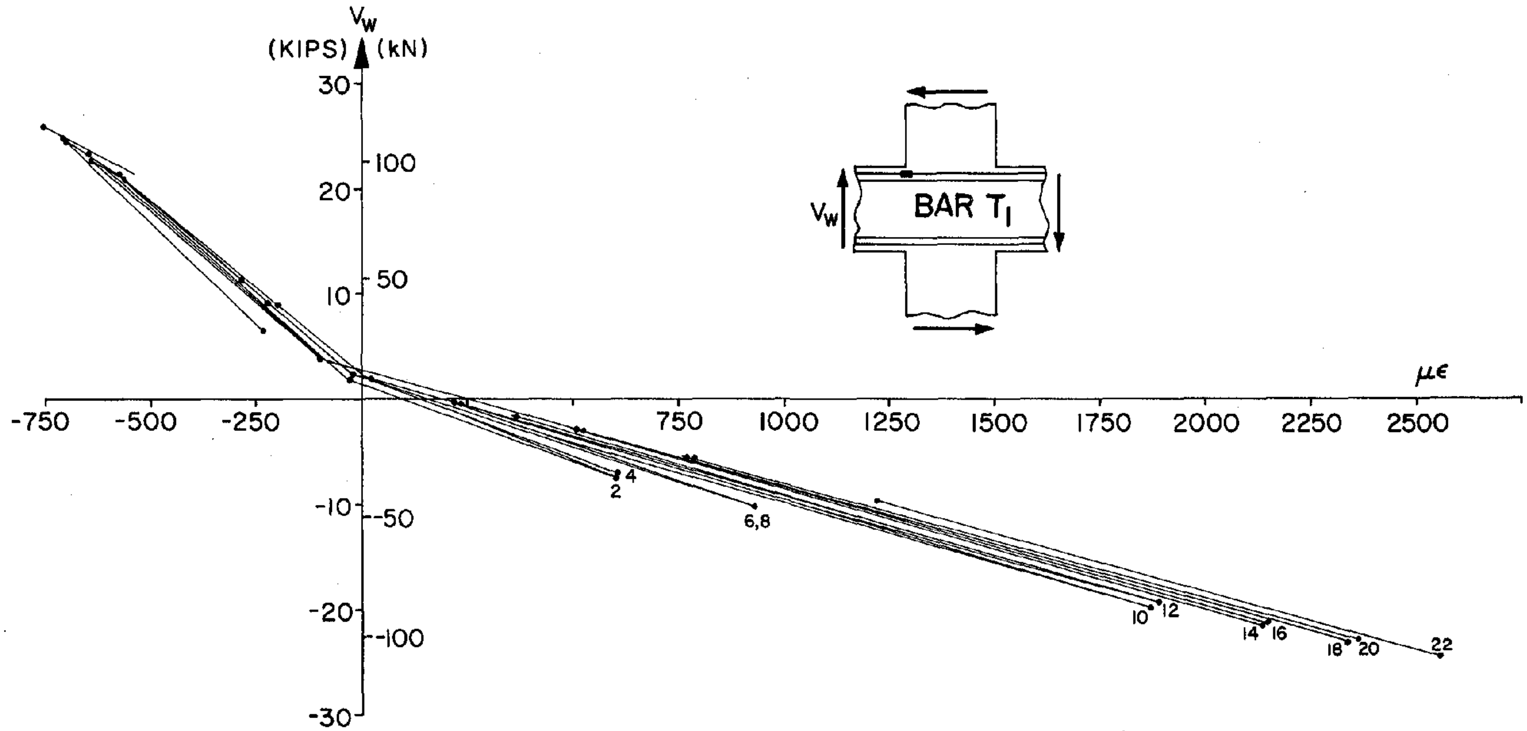

FIG. 36 STEEL STRAIN VS. SHEAR FORCE AT COLUMN FACE - BC6

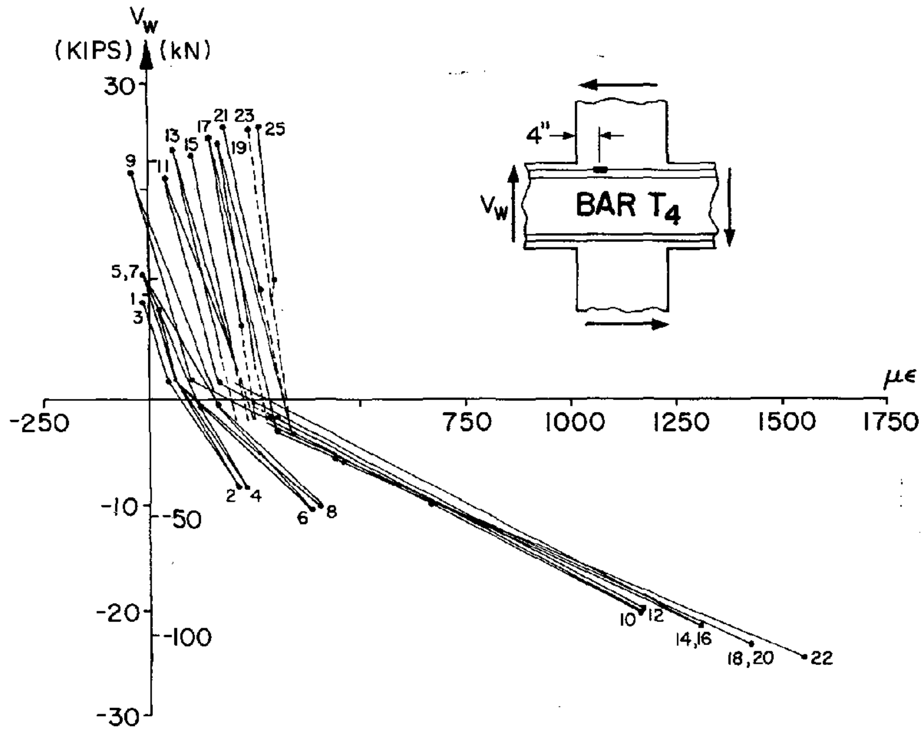

FIG. 37 STEEL STRAIN AT 4 IN. FROM COLUMN FACE, INSIDE THE JOINT, VS. SHEAR FORCE - BC6

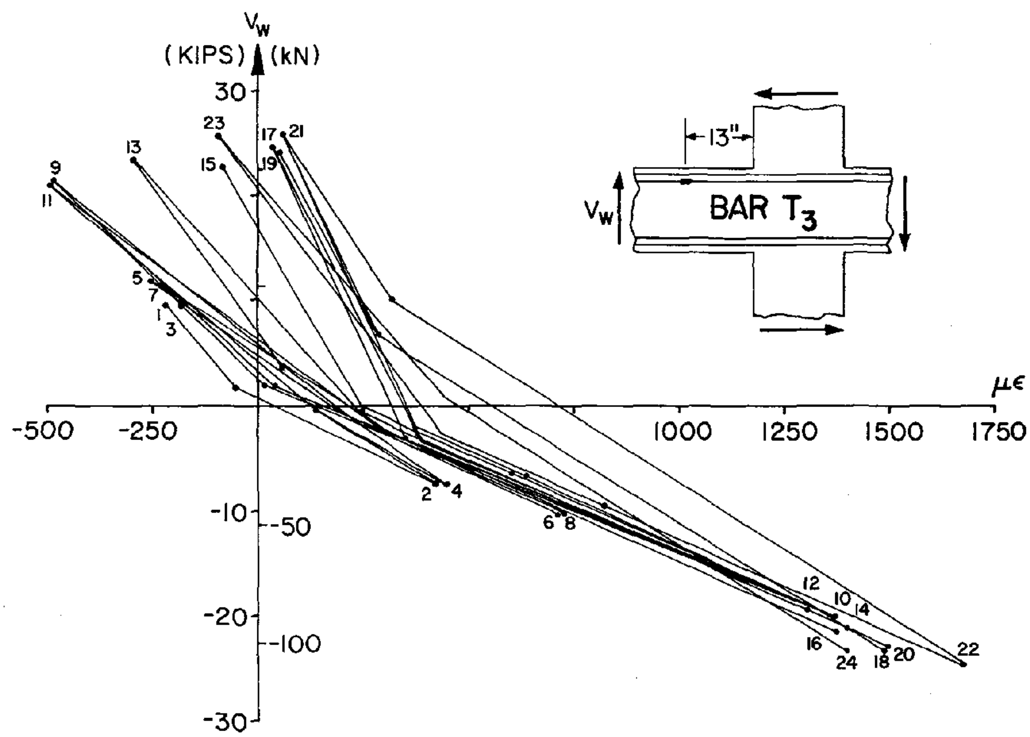

FIG. 38 STEEL STRAIN AT 13 IN. FROM COLUMN FACE VS. SHEAR FORCE - BC6

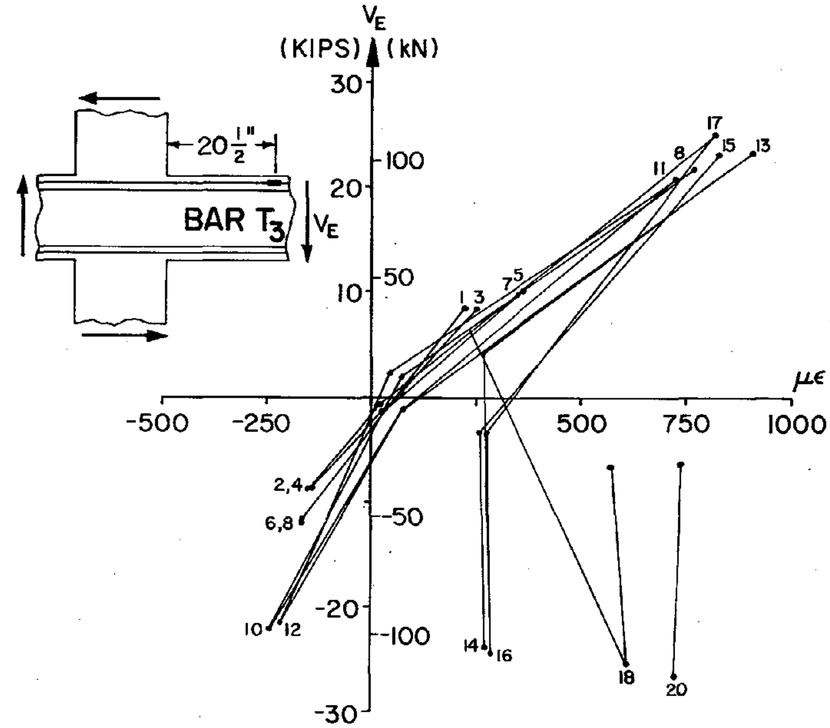

FIG. 39 STEEL STRAIN AT 20.5 IN. FROM COLUMN FACE - BC6

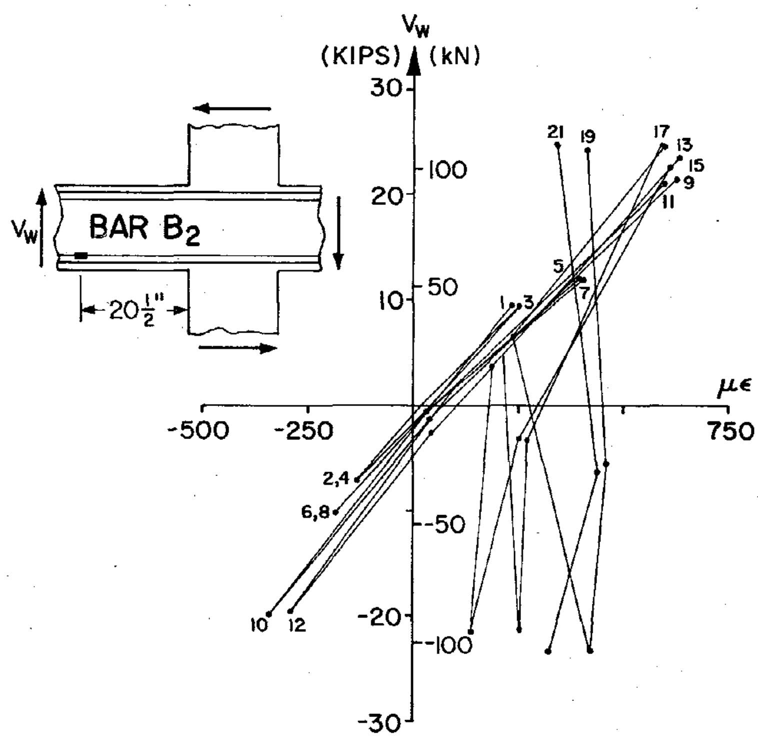

FIG. 40 STEEL STRAIN AT 20.5 IN. FROM COLUMN FACE - BC6

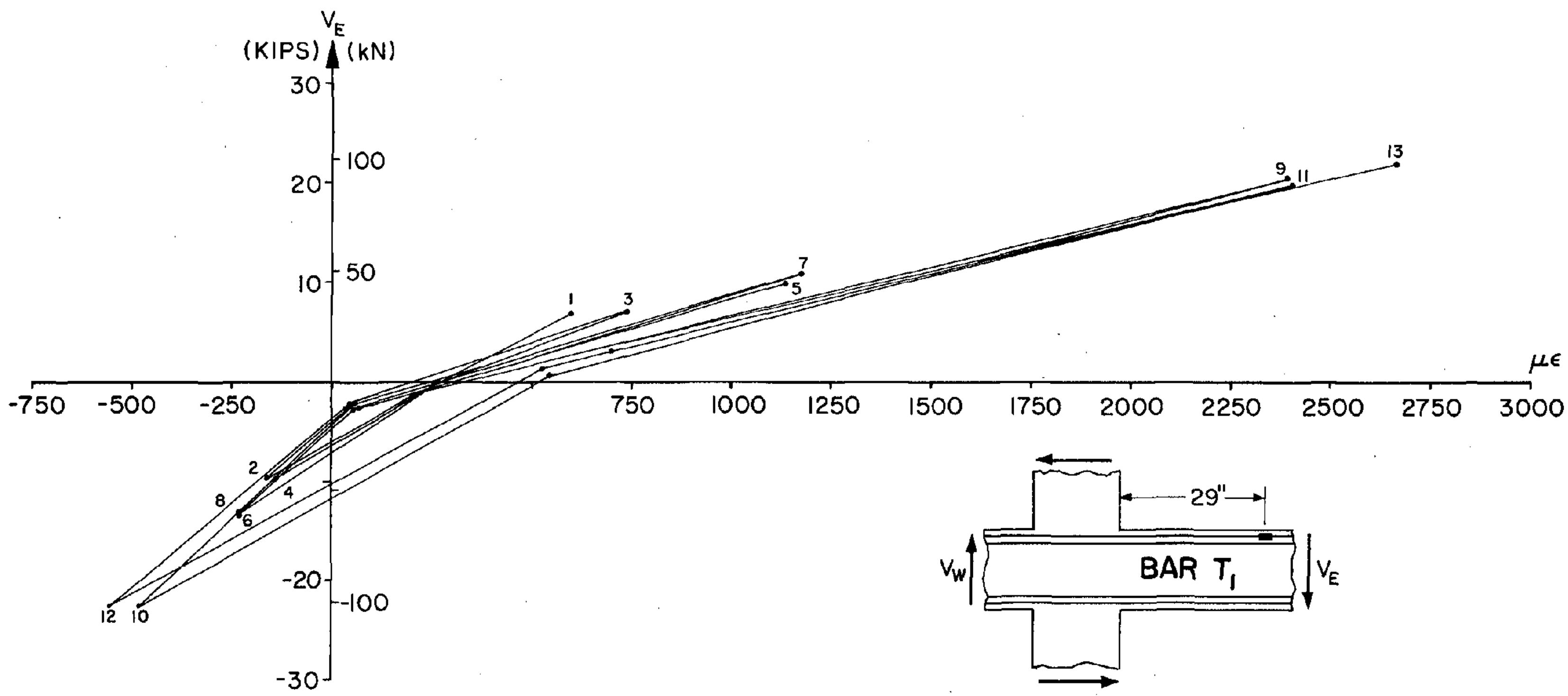

FIG. 41 STEEL STRAIN AT 29 IN. FROM COLUMN FACE VS. SHEAR FORCE - BC6

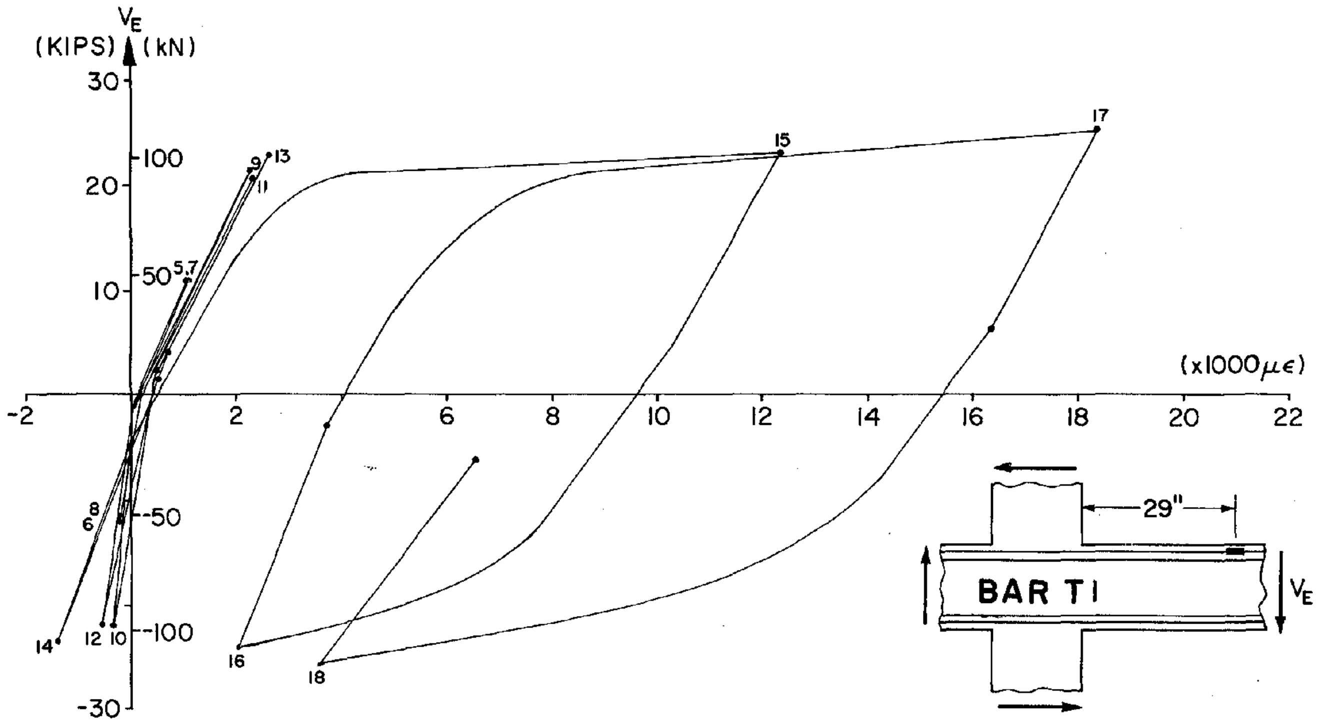

FIG. 42 STEEL STRAIN AT 29 IN. FROM COLUMN FACE VS. SHEAR FORCE - BC6

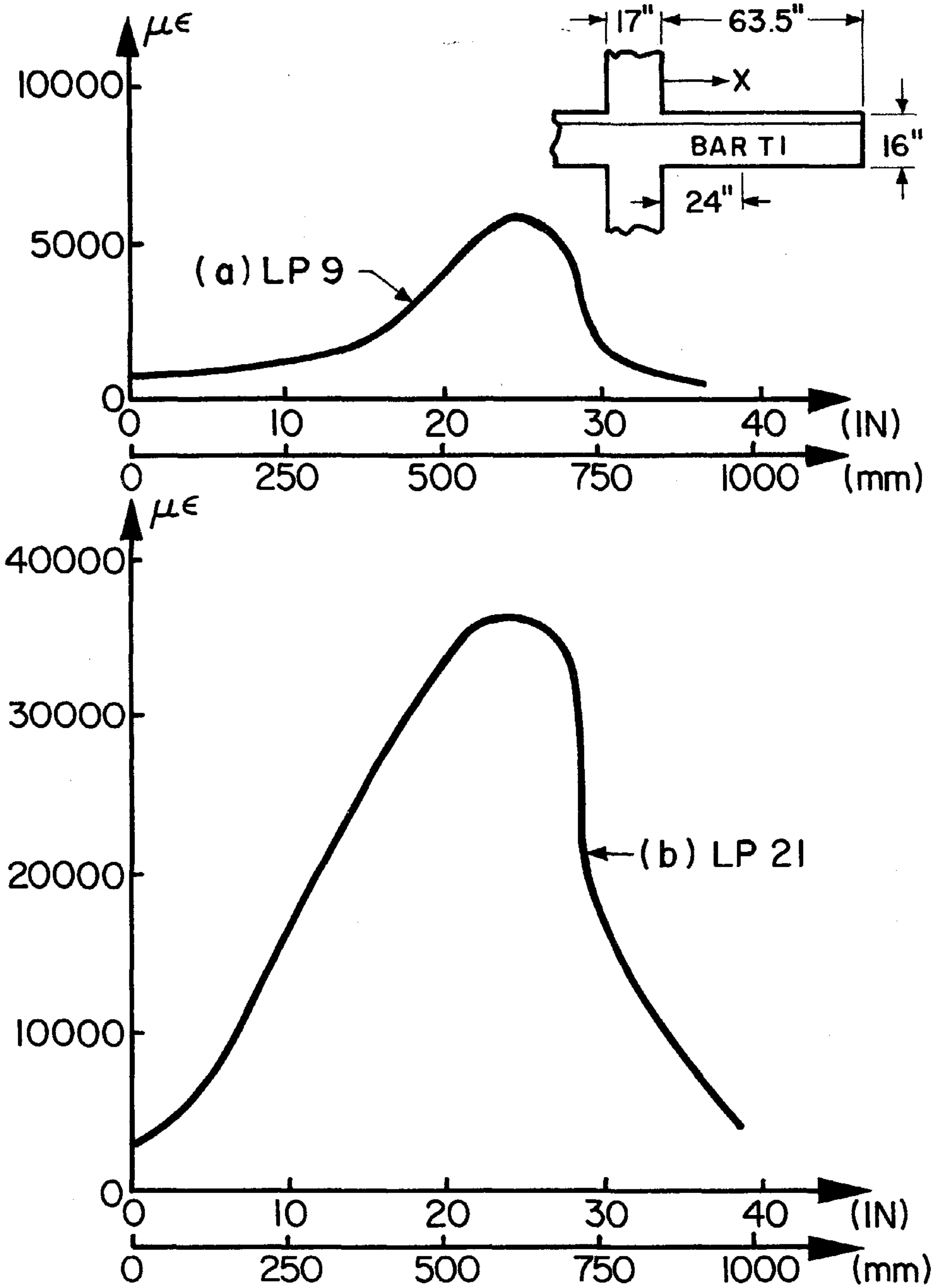

FIG. 43 VARIATION OF STEEL STRAIN ALONG BAR T_1 OF EAST BEAM - BC6

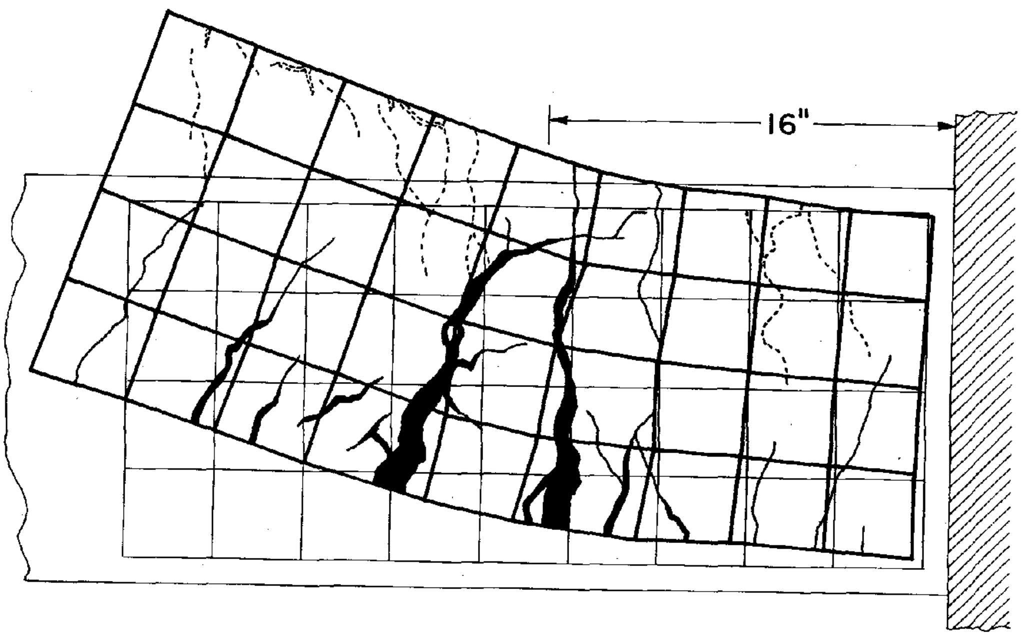

FIG. 44 CRACKING AT LP 17 - BC5

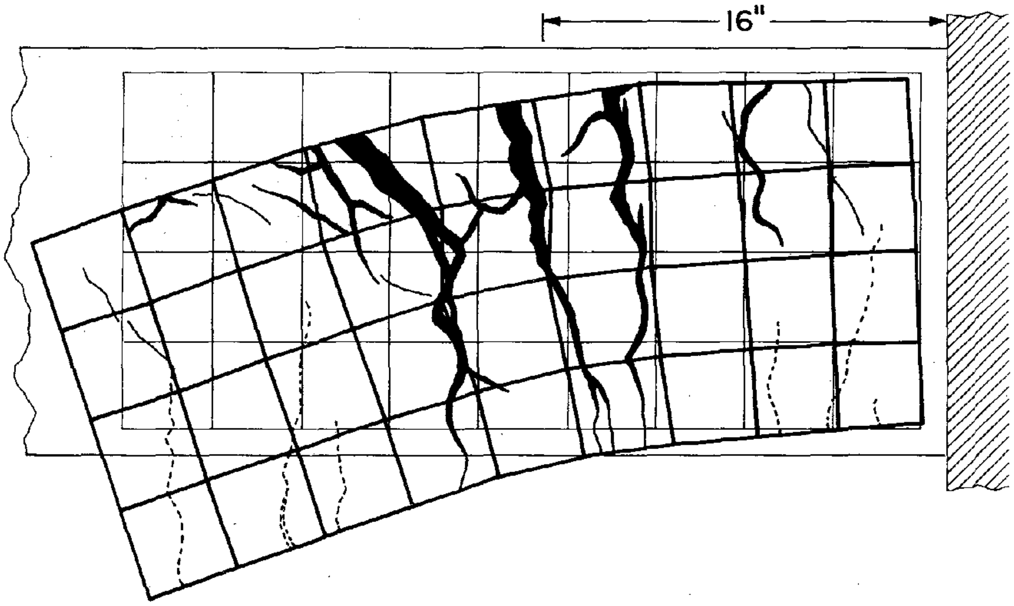

FIG. 45 CRACKING AT LP 18 - BC5

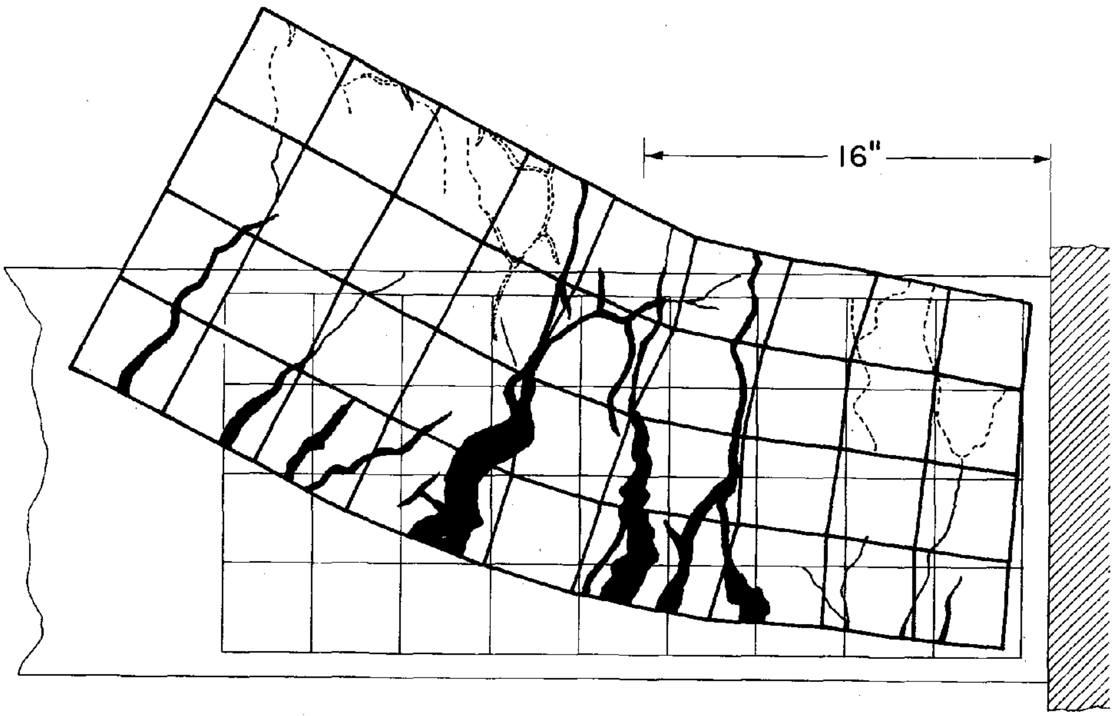

FIG. 46 CRACKING AT LP 21 - BC5

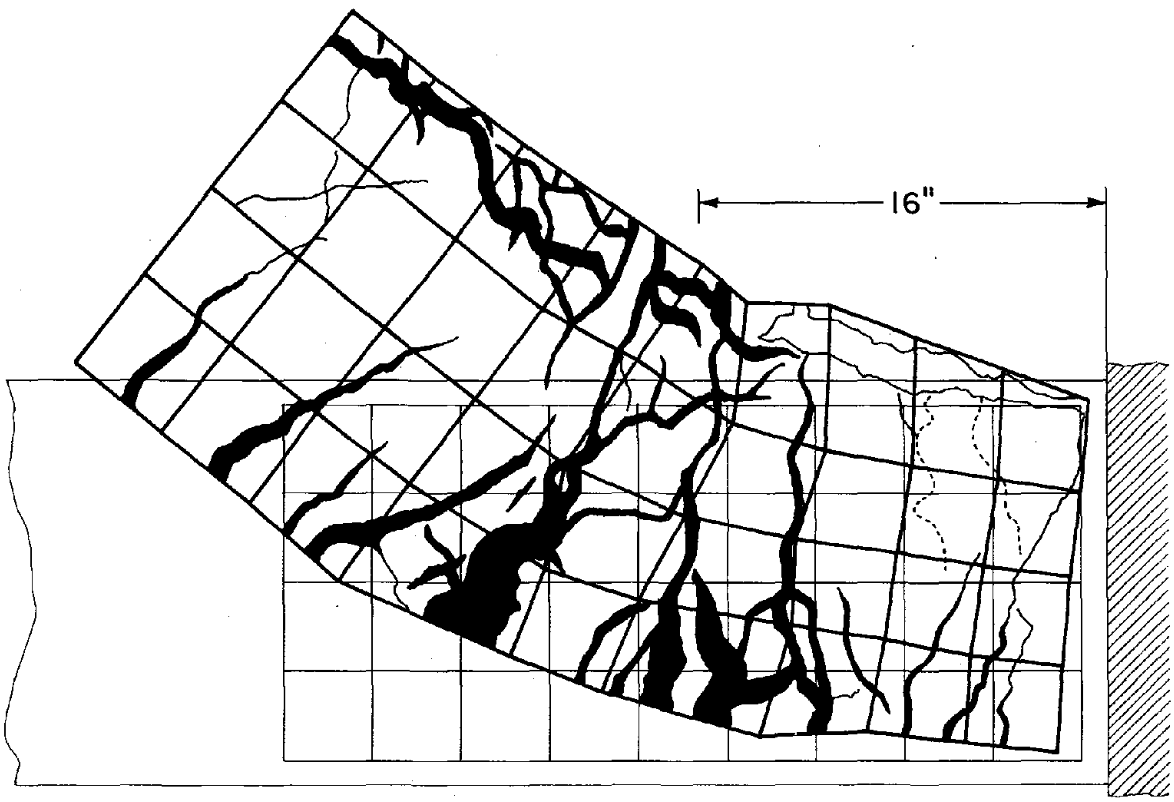

FIG. 47 CRACKING AT LP 25 - BC5

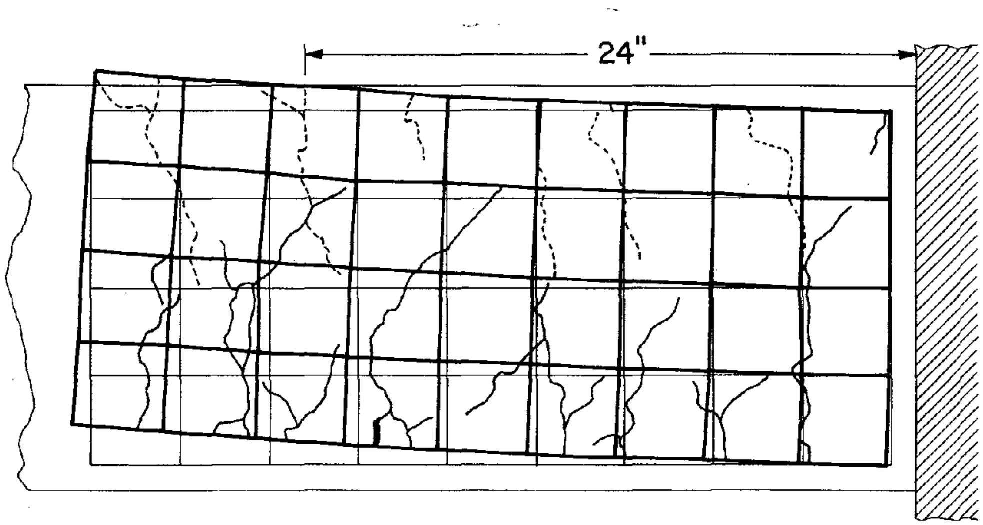

FIG. 48 CRACKING AT LP 9 - BC6

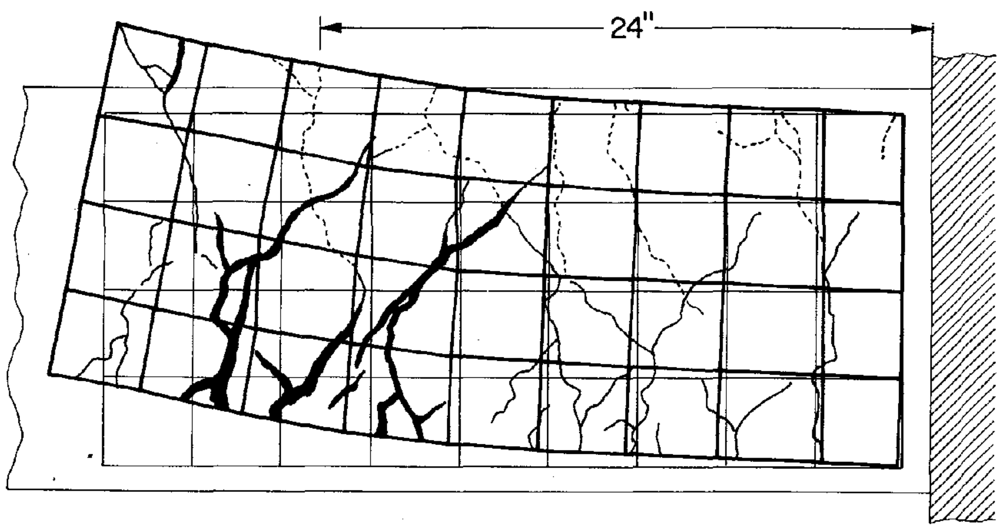

FIG. 49 CRACKING AT LP 13 - BC6

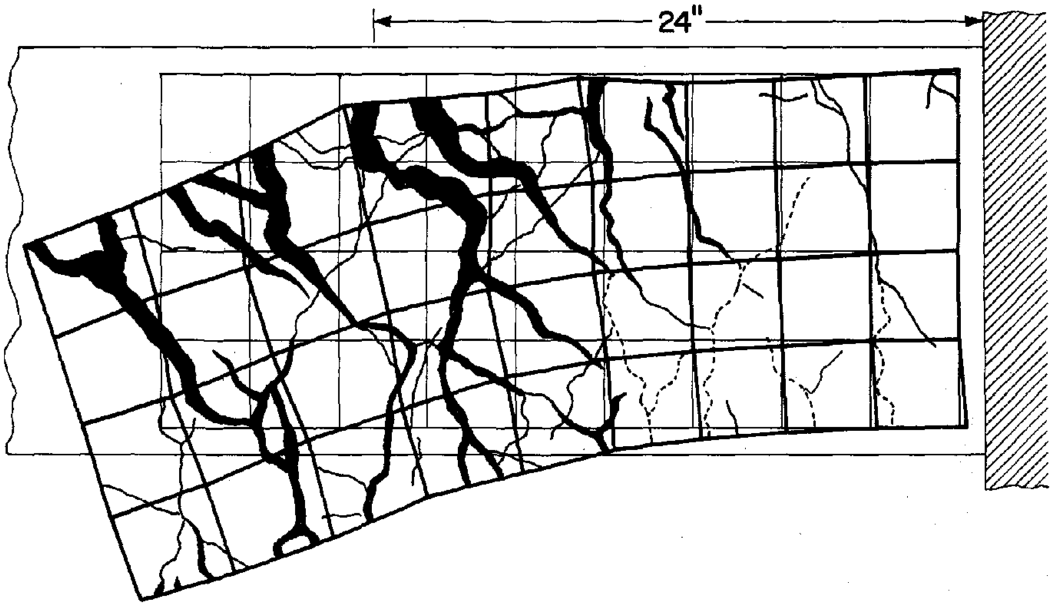

FIG. 50 CRACKING AT LP 18 - BC6

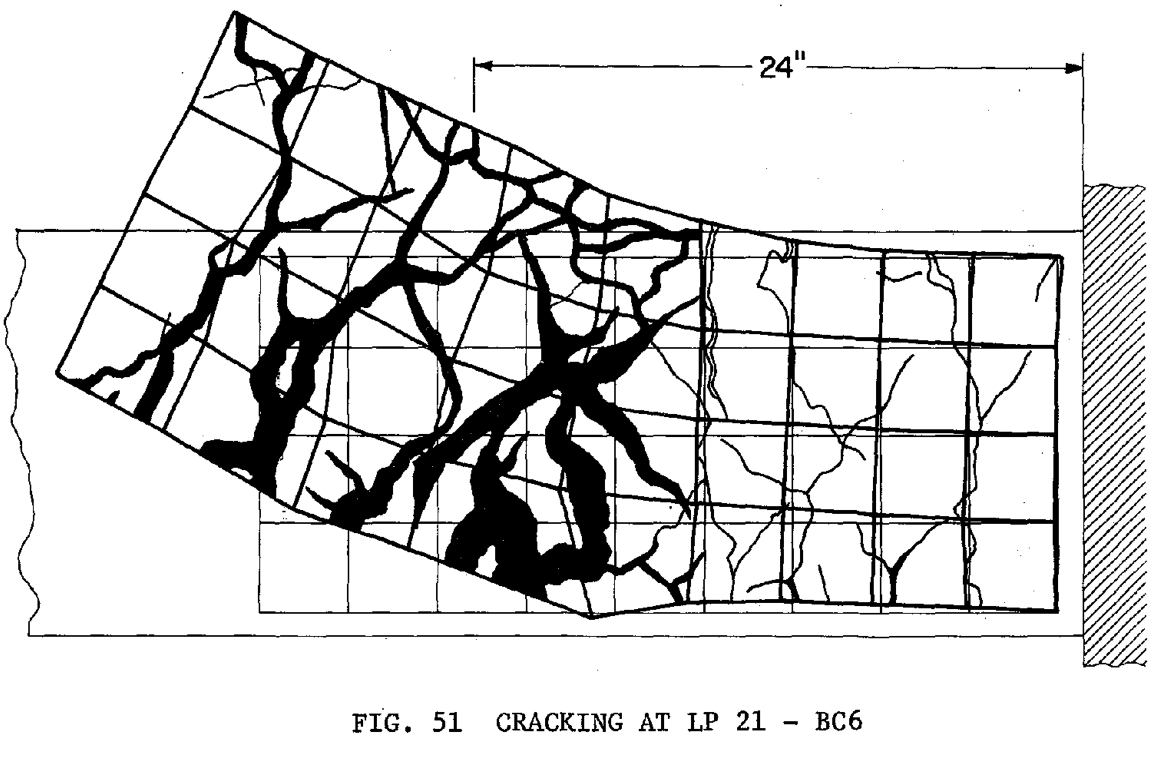

FIG. 51 CRACKING AT LP 21 - BC6

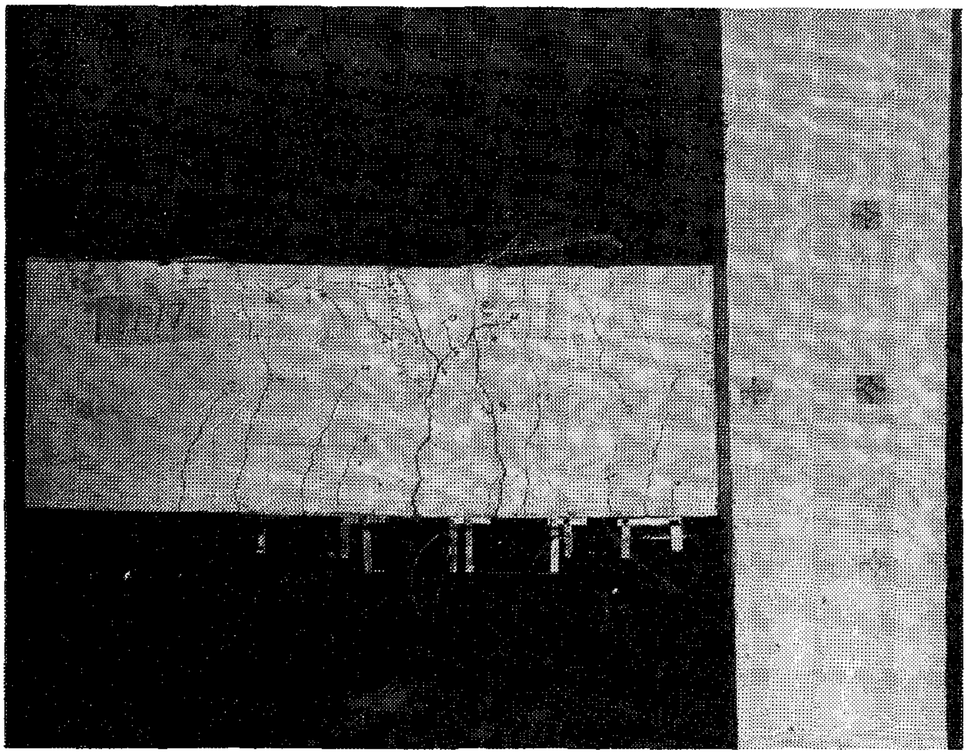

FIG. 52 BC5 AT LP 17

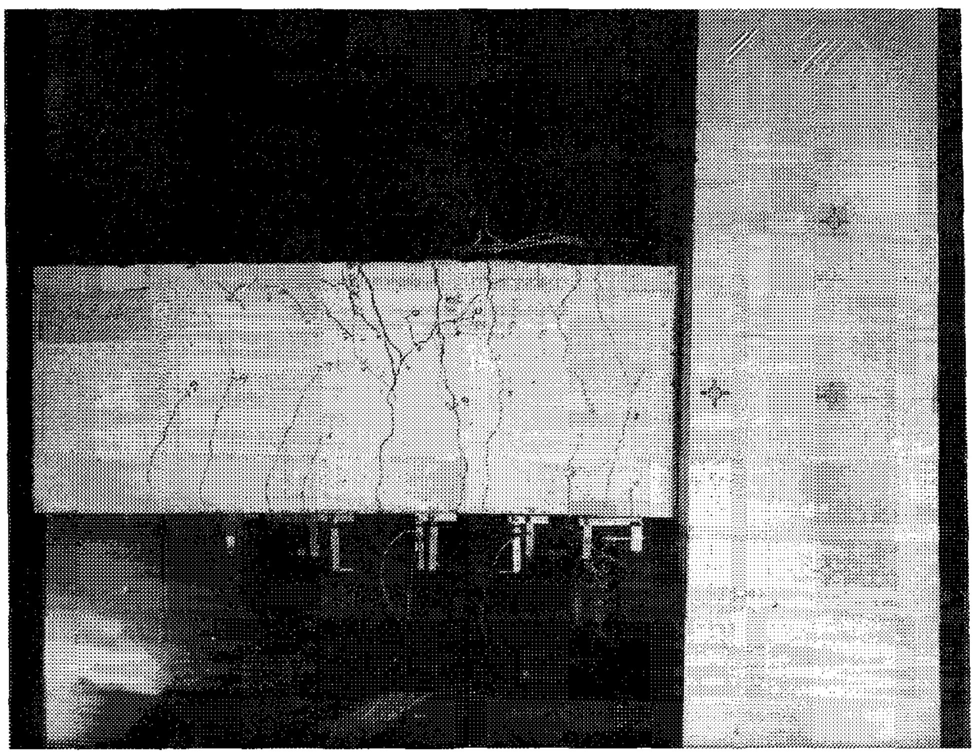

FIG. 53 BC5 AT LP 18

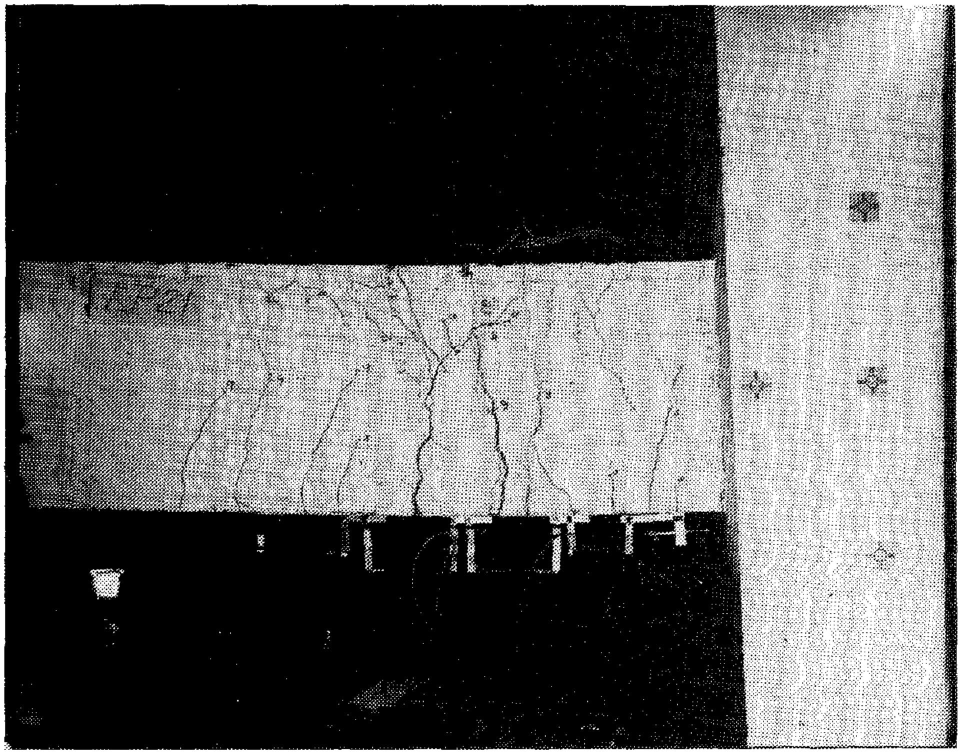

FIG. 54 BC5 AT LP 21

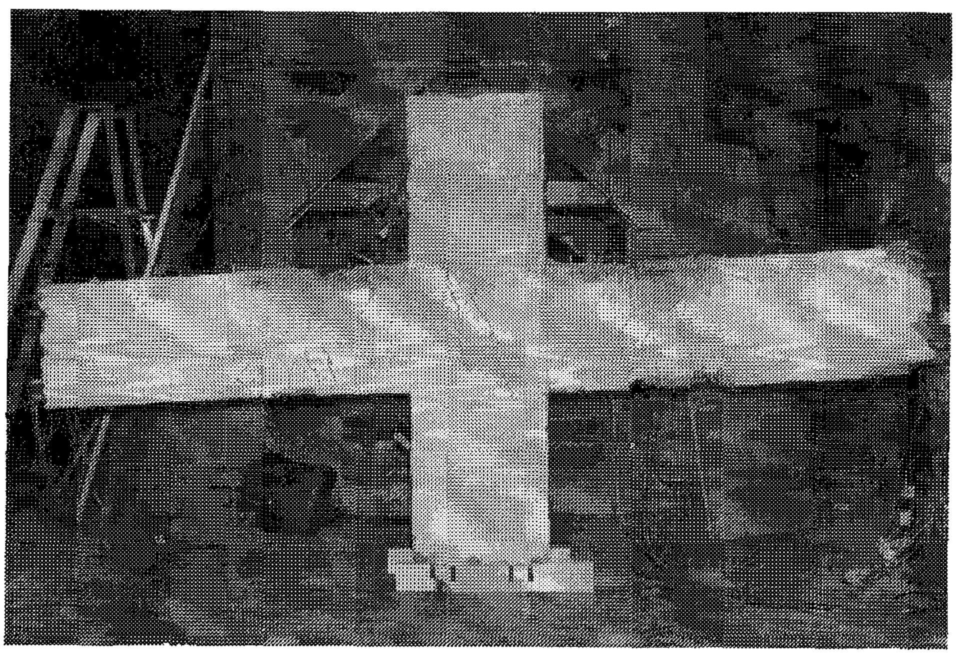

FIG. 55 BC5 UPON COMPLETION OF TEST

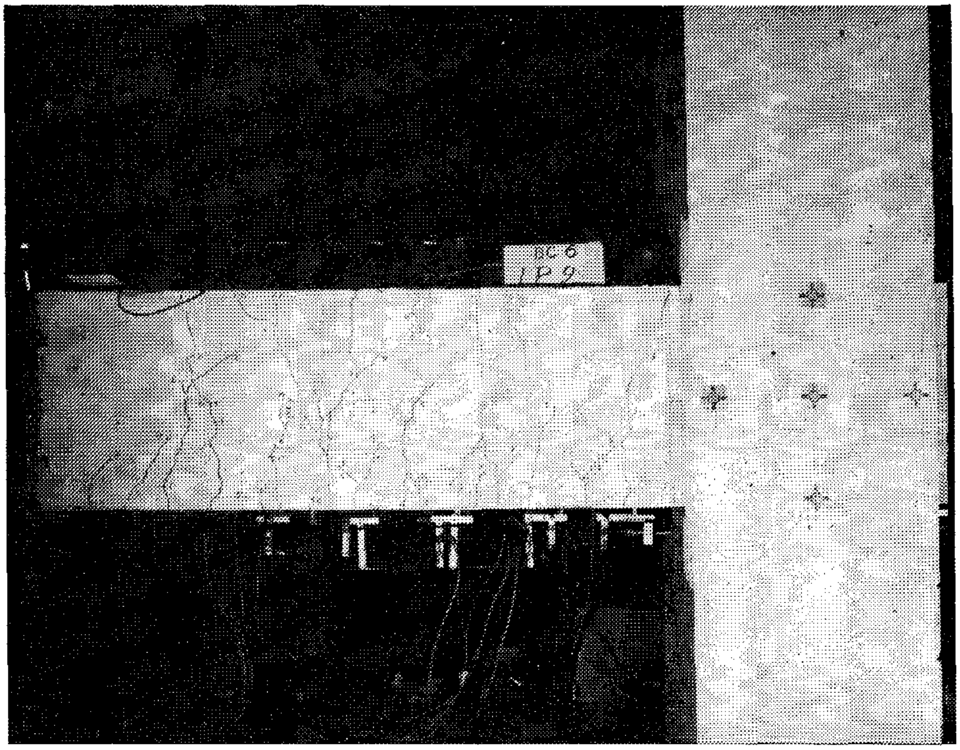

FIG. 56 BC6 AT LP 9

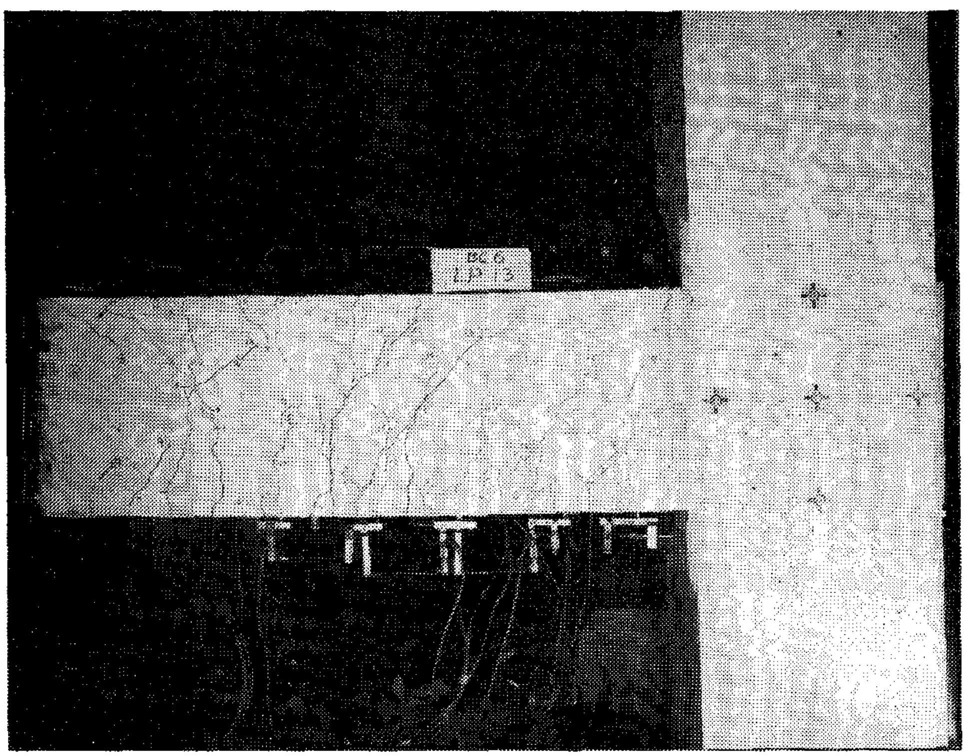

FIG. 57 BC6 AT LP 13

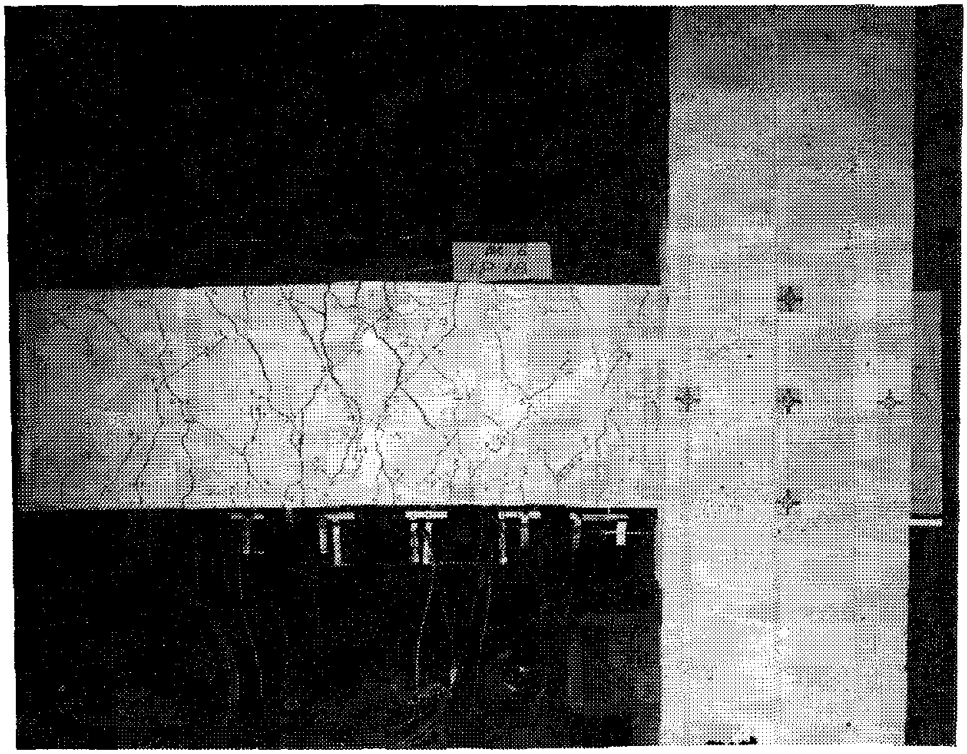

FIG. 58 BC6 AT LP 18

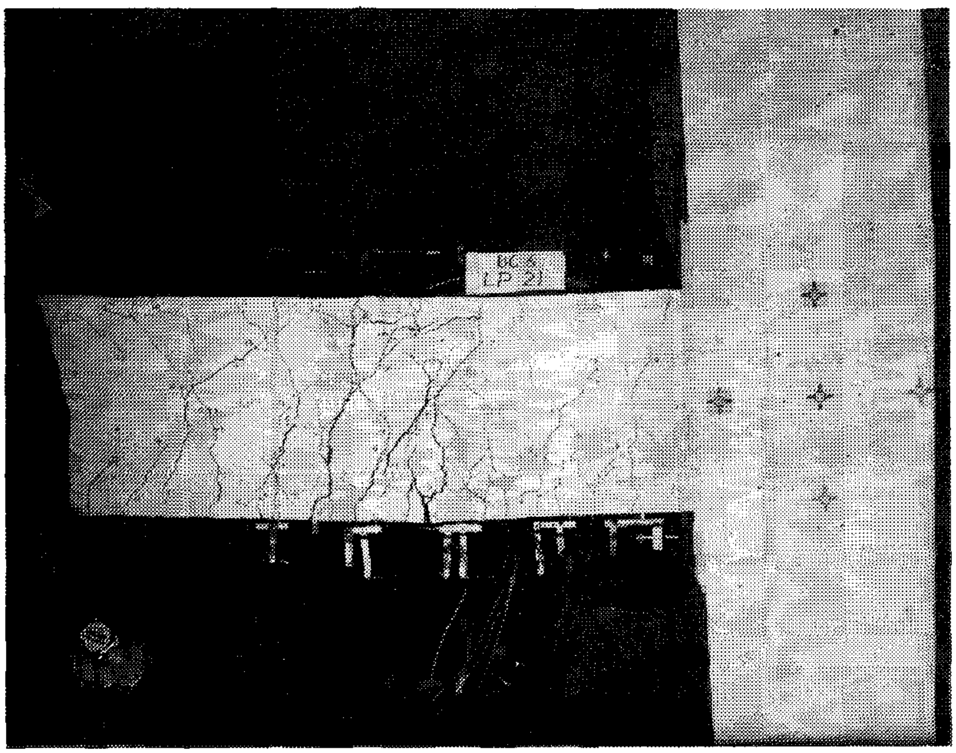

FIG. 59 BC6 AT LP 21

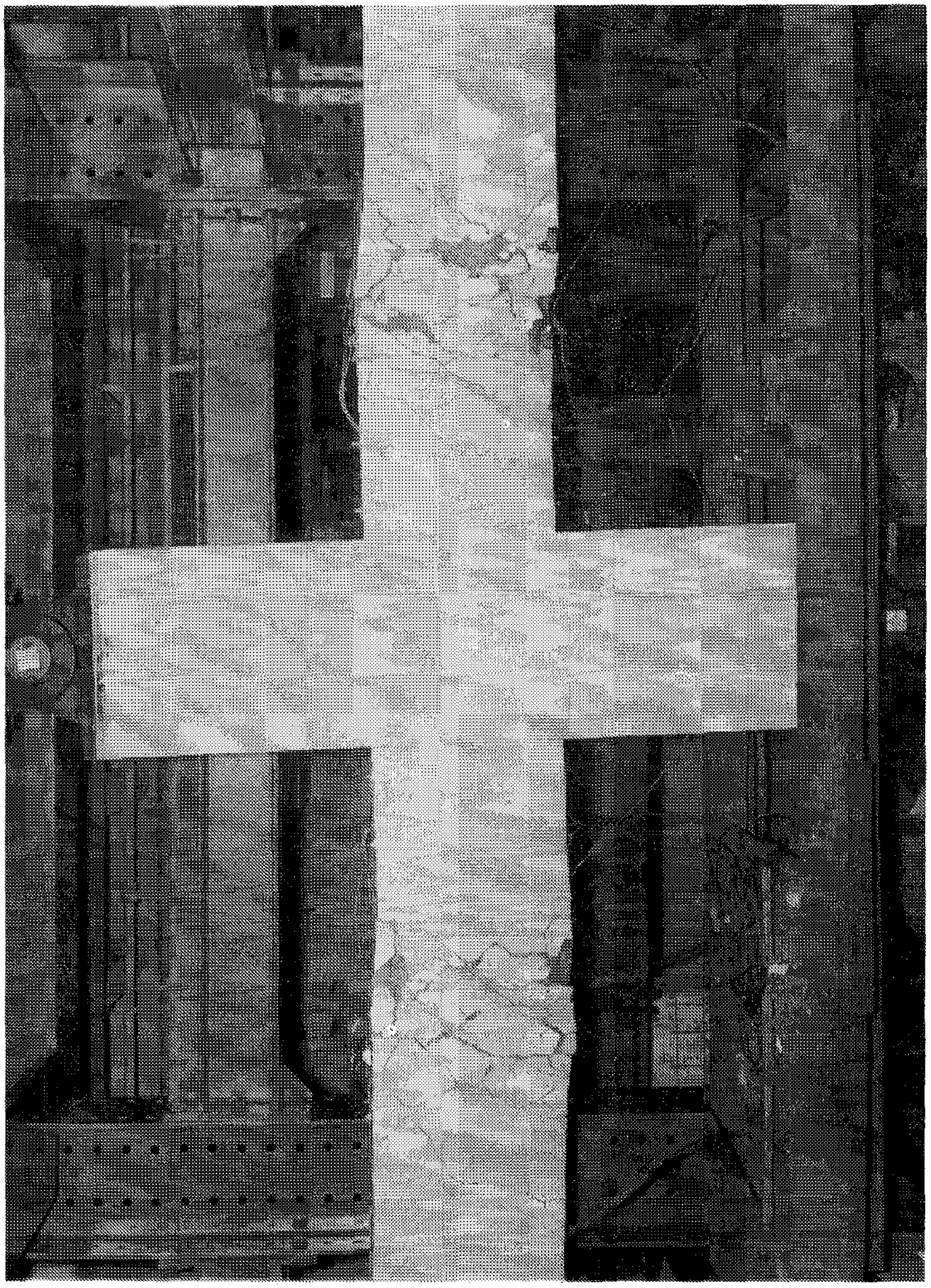

FIG. 60 SPECIMEN BC6 UPON COMPLETION OF TEST (LP25)

APPENDIX A

APPENDIX A -- LOCATION OF PLASTIC HINGE

The plastic hinges in the two specimens were located with the aid of a computer program that could determine the complete moment-curvature relationship of a particular cross section of a concrete beam. Both the nonlinear stress-strain characteristics of the concrete and the strain hardening properties of the steel were accounted for. Separate runs were made to determine the moment-curvature relationship of three different cross sections of the beam. These have been plotted in Figs. A.1, A.2, and A.3.

Figure A.1 gives the moment-curvature relationship of the beam for both specimens BC5 and BC6 with 4 #6 bars on the top and bottom. This figure describes the moment-curvature relationship of the beam at the column face. The onset of strain hardening of the reinforcing steel was at 189 kN-m (1670 k-in.).

Figure A.2 gives the moment-curvature relationship of the plastic hinge for member BC5. The cross section consisted of 2 #6 bars on the top and bottom, and 2 #6 bars crossing diagonally in the middle. Two cases were tried: (1) a 45-degree diagonal crossing and (2) a 60-degree diagonal crossing. The maximum moment for the 45-degree case was 3% larger than that for the 60-degree cases--156 kN-m (1380 k-in.) vs. 151 kN-m (1340 k-in.). The latter case was chosen because it required less total length to form the plastic hinge.

Figure A.3 gives the moment-curvature relationship of the plastic hinge for member BC6, which consisted of 2 #6 bars on the top and bottom. The maximum moment was 132 kN-m (1170 k-in.).

The ends of the beams were pinned so that the moment diagram is linear as shown in Fig. A.4. The equation for the moment M_x at a section x is

$$M_x = V(63.5 - x)\,k\text{-}in.$$

where V is the constant shear in the beam, 1.61 m (63.5 in.) is the length from the column face to the pin, and x is the distance from the column face to the beam cross section at which M_x is desired.

The center of plastic hinge region was located in such a way that the moment at the column face (4 #6 bars) would start strain hardening when the moment in the plastic hinge (2 #6 bars with diagonal crossing for BC5 or 2 #6 bars for BC6) reached maximum capacity. As already indicated the moment at the onset of strain hardening was 189 kN-m (1670 k-in.) (see Fig. A.1). The equation for M_x can be solved to determine the shear that causes the 189 kN-m (1670 k-in.) moment at the column face

$$V = \frac{1670}{63.5} = 26.3 kips (116 kN)$$

The maximum moments at the plastic hinge are known from Fig. A.2 for BC5 and Fig. A.3 for BC6. From the shear and moment, the location, x, of the latter can be calculated.

For BC5:

$$1340 k\text{-}in. = 26.3 \; kips \; (63.5 - x) \; in.$$

yields

$$x = 12.6 \; in. \; (320 \; mm)$$

For BC6:

$$1170 \; k\text{-}in. = 26.3 \; kips \; (63.5 - x) \; in.$$

yields

$$x = 19 \; in. \; (483 \; mm)$$

The actual location of the inclined bar intersection (or the center of plastic hinge region) for BC5 was 406 mm (16 in.) This larger distance was used because it was felt that the effectiveness of the diagonal bars after continuous yielding of the reinforcing bars at the plastic hinges would be less than that predicted, due in part to the deterioration of the concrete in the plastic hinge region. The experimental results show that such deterioration did not occur and that a location of 381 mm (15 in.) would have been preferable because the steel strain at the face of the column somewhat exceeded the strain-hardening value.

For BC6 the actual location of the cutoff of the bars was 610 mm (24 in.) from the column face. This was done because it was felt that after a few cycles of large rotations in the plastic hinge, the bond in the cutoff bars would be destroyed and the plastic hinge would tend to move toward the column face due to the moment gradient. The experiments proved that 610 mm (24 in.) was a good selection.

It is recommended that further studies be carried out on this topic in order to develop practical methods for establishing the correct locations of the plastic hinges.

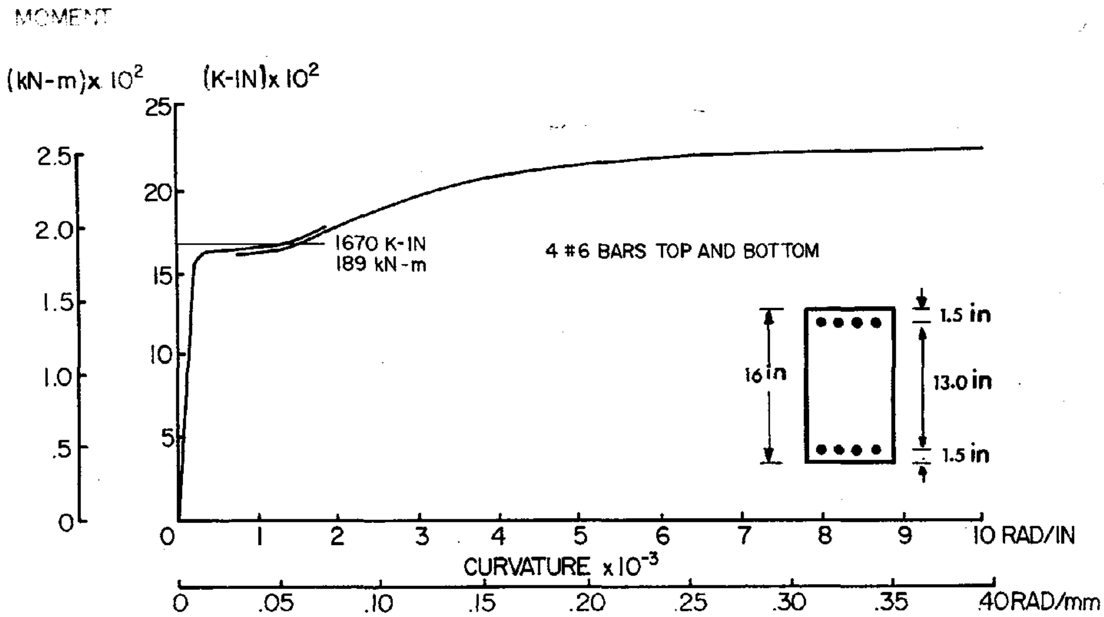

FIG. A.1 MOMENT-CURVATURE DIAGRAM FOR 4 #6 BARS TOP AND BOTTOM

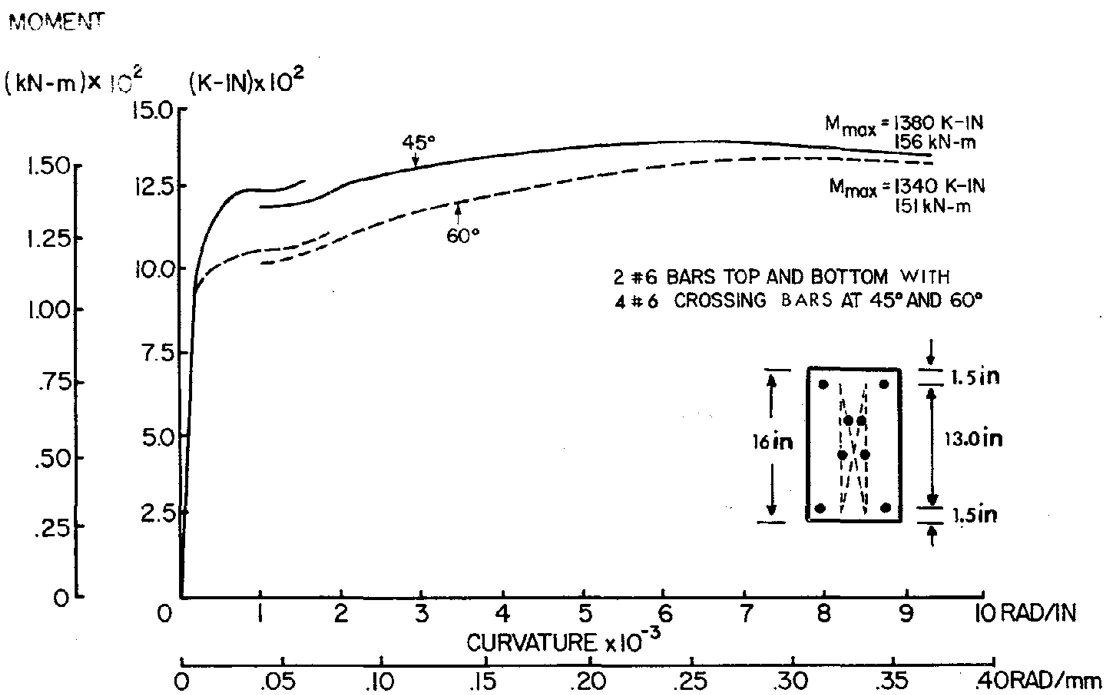

FIG. A.2 MOMENT-CURVATURE DIAGRAM FOR 2 #6 BARS TOP AND BOTTOM WITH CROSSING STEEL - BC5

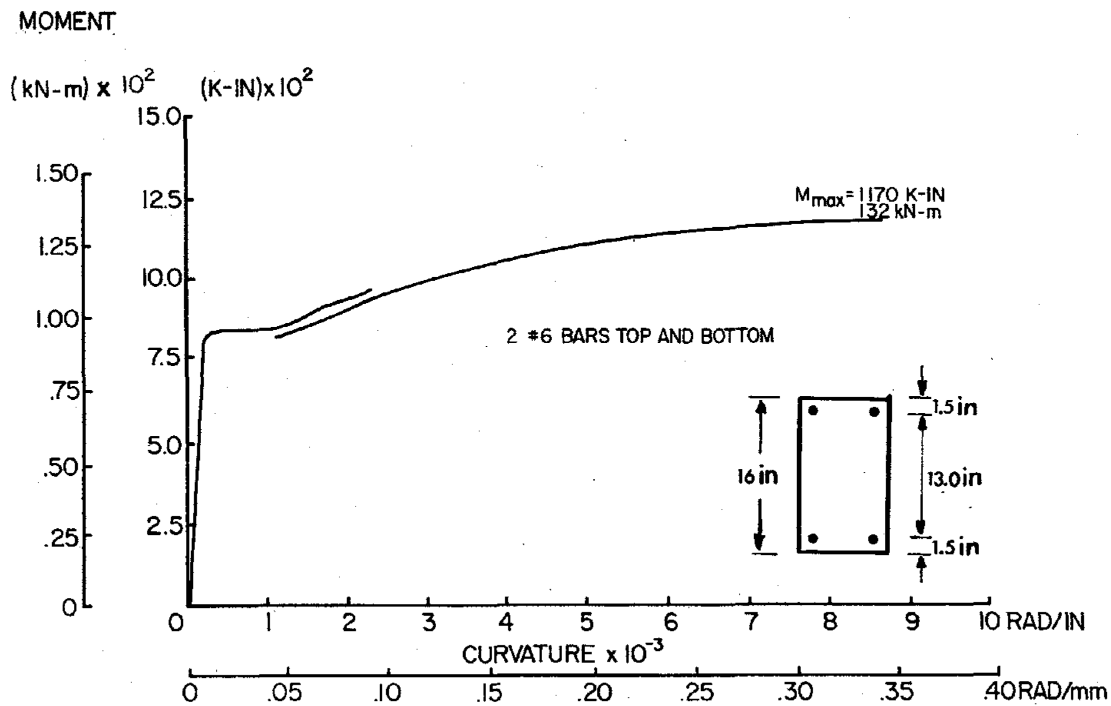

FIG. A.3 MOMENT-CURVATURE DIAGRAM FOR 2 #6 BARS TOP AND BOTTOM - BC6

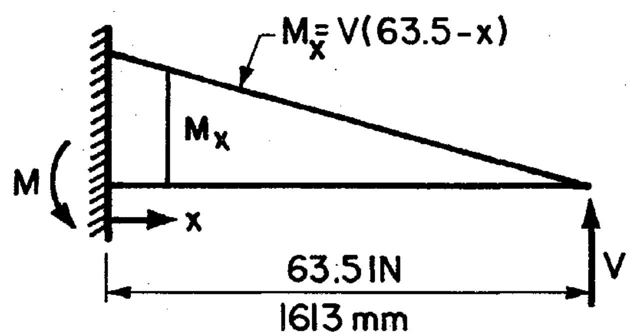

FIG. A.4 MOMENT DIAGRAM FOR TYPICAL BEAM

EARTHQUAKE ENGINEERING RESEARCH CENTER REPORTS

EARTHQUAKE ENGINEERING RESEARCH CENTER REPORTS

NOTE: Numbers in parentheses are Accession Numbers assigned by the National Technical Information Service; these are followed by a price code. Copies of the reports may be ordered from the National Technical Information Service, 5285 Port Royal Road, Springfield, Virginia, 22161. Accession Numbers should be quoted on orders for reports (PB--- ---) and remittance must accompany each order. Reports without this information were not available at time of printing. Upon request, EERC will mail inquirers this information when it becomes available.

EERC 67-1 "Feasibility Study of Large-Scale Earthquake Simulator Facility," by J. Penzien, J. G. Bouwkamp, R. W. Clough, and D. Rea - 1967 (PB 187 905)A07

EERC 68-1 Unassigned

EERC 68-2 "Inelastic Behavior of Beam-to-Column Subassemblages under Repeated Loading," by V. V. Bertero - 1968 (PB 184 888)A05

EERC 68-3 "A Graphical Method for Solving the Wave Reflection-Refraction Problem," by H. D. McNiven and Y. Mengi - 1968 (PB 187 943)A03

EERC 68-4 "Dynamic Properties of McKinley School Buildings," by D. Rea, J. G. Bouwkamp, and R. W. Clough - 1968 (PB 187 902)A07

EERC 68-5 "Characteristics of Rock Motions during Earthquakes," by H. B. Seed, I. M. Idriss, and F. W. Kiefer - 1968 (PB 188 338)A03

EERC 69-1 "Earthquake Engineering Research at Berkeley," - 1969 (PB 187 906)A11

EERC 69-2 "Nonlinear Seismic Response of Earth Structures," by M. Dibaj and J. Penzien - 1969 (PB 187 904)A08

EERC 69-3 "Probabilistic Study of the Behavior of Structures during Earthquakes," by R. Ruiz and J. Penzien - 1969 (PB 187 886)A06

EERC 69-4 "Numerical Solution of Boundary Value Problems in Structural Mechanics by Reduction to an Initial Value Formulation," by N. Distefano and J. Schujman - 1969 (PB 187 942)A02

EERC 69-5 "Dynamic Programming and the Solution of the Biharmonic Equation," by N. Distefano - 1969 (PB 187 941)A03

EERC 69-6 "Stochastic Analysis of Offshore Tower Structures," by A. K. Malhotra and J. Penzien - 1969 (PB 187 903)A09

EERC 69-7 "Rock Motion Accelerograms for High Magnitude Earthquakes," by H. B. Seed and I. M. Idriss - 1969 (PB 187 940)A02

EERC 69-8 "Structural Dynamics Testing Facilities at the University of California, Berkeley," by R. M. Stephen, J. G. Bouwkamp, R. W. Clough and J. Penzien - 1969 (PB 189 111)A04

EERC 69-9 "Seismic Response of Soil Deposits Underlain by Sloping Rock Boundaries," by H. Dezfulian and H. B. Seed - 1969 (PB 189 114)A03

EERC 69-10 "Dynamic Stress Analysis of Axisymmetric Structures under Arbitrary Loading," by S. Ghosh and E. L. Wilson - 1969 (PB 189 026)A10

EERC 69-11 "Seismic Behavior of Multistory Frames Designed by Different Philosophies," by J. C. Anderson and V. V. Bertero - 1969 (PB 190 662)A10

EERC 69-12 "Stiffness Degradation of Reinforcing Concrete Members Subjected to Cyclic Flexural Moments," by V. V. Bertero, B. Bresler, and H. Ming Liao - 1969 (PB 202 942)A07

EERC 69-13 "Response of Non-Uniform Soil Deposits to Travelling Seismic Waves," by H. Dezfulian and H. B. Seed - 1969 (PB 191 023)A03

EERC 69-14 "Damping Capacity of a Model Steel Structure," by D. Rea, R. W. Clough, and J. G. Bouwkamp - 1969 (PB 190 663)A06

EERC 69-15 "Influence of Local Soil Conditions on Building Damage Potential during Earthquakes," by H. B. Seed and I. M. Idriss - 1969 (PB 191 036)A03

EERC 69-16 "The Behavior of Sands under Seismic Loading Conditions," by M. L. Silver and H. B. Seed - 1969 (AD 714 982)A07

EERC 70-1 "Earthquake Response of Gravity Dams," by A. K. Chopra - 1970 (AD 709 640)A03

EERC 70-2 "Relationships between Soil Conditions and Building Damage in the Caracas Earthquake of July 29, 1967," by H. B. Seed, I. M. Idriss, and H. Dezfulian - 1970 (PB 195 762)A05

EERC 70-3 "Cyclic Loading of Full Size Steel Connections," by E. P. Popov and R. M. Stephen - 1970 (PB 213 545)A04

EERC 70-4 "Seismic Analysis of the Charaima Building, Caraballeda, Venezuela," by Subcommittee of the SEAONC Research Committee: V. V. Bertero, P. F. Fratessa, S. A. Mahin, J. H. Sexton, A. C. Scordelis, E. L. Wilson, L. A. Wyllie, H. B. Seed, and J. Penzien, Chairman - 1970 (PB 201 455)A06

EERC 70-5 "A Computer Program for Earthquake Analysis of Dams," by A. K. Chopra and P. Chakrabarti - 1970 (AD 723 994)A05

EERC 70-6 "The Propagation of Love Waves Across Non-Horizontally Layered Structures," by J. Lysmer and L. A. Drake - 1970 (PB 197 896)A03

EERC 70-7 "Influence of Base Rock Characteristics on Ground Response," by J. Lysmer, H. B. Seed, and P. B. Schnabel - 1970 (PB 197 897)A03

EERC 70-8 "Applicability of Laboratory Test Procedures for Measuring Soil Liquefaction Characteristics under Cyclic Loading," by H. B. Seed and W. H. Peacock - 1970 (PB 198 016)A03

EERC 70-9 "A Simplified Procedure for Evaluating Soil Liquefaction Potential," by H. B. Seed and I. M. Idriss - 1970 (PB 198 009)A03

EERC 70-10 "Soil Moduli and Damping Factors for Dynamic Response Analysis," by H. B. Seed and I. M. Idriss - 1970 (PB 197 869)A03

EERC 71-1 "Koyna Earthquake of December 11, 1967 and the Performance of Koyna Dam," by A. K. Chopra and P. Chakrabarti - 1971 (AD 731 496)A06

EERC 71-2 "Preliminary In-Situ Measurements of Anelastic Absorption in Soils using a Prototype Earthquake Simulator," by R. D. Borcherdt and P. W. Rodgers - 1971 (PB 201 454)A03

EERC 71-3 "Static and Dynamic Analysis of Inelastic Frame Structures," by F. L. Porter and G. H. Powell - 1971 (PB 210 135)A06

EERC 71-4 "Research Needs in Limit Design of Reinforced Concrete Structures," by V. V. Bertero - 1971 (PB 202 943)A04

EERC 71-5 "Dynamic Behavior of a High-Rise Diagonally Braced Steel Building," by D. Rea, A. A. Shah, and J. G. Bouwkamp - 1971 (PB 203 584)A06

EERC 71-6 "Dynamic Stress Analysis of Porous Elastic Solids Saturated with Compressible Fluids," by J. Ghaboussi and E. L. Wilson - 1971 (PB 211 396)A06

EERC 71-7 "Inelastic Behavior of Steel Beam-to-Column Subassemblages," by H. Krawinkler, V. V. Bertero, and E. P. Popov - 1971 (PB 211 355)A14

EERC 71-8 "Modification of Seismograph Records for Effects of Local Soil Conditions," by P. Schnabel, H. B. Seed, and J. Lysmer - 1971 (PB 214 450)A03

EERC 72-1 "Static and Earthquake Analysis of Three Dimensional Frame and Shear Wall Buildings," by E. L. Wilson and H. H. Dovey - 1972 (PB 212 904)A05

EERC 72-2 "Accelerations in Rock for Earthquakes in the Western United States," by P. B. Schnabel and H. B. Seed - 1972 (PB 213 100)A03

EERC 72-3 "Elastic-Plastic Earthquake Response of Soil-Building Systems," by T. Minami - 1972 (PB 214 868)A08

EERC 72-4 " Stochastic Inelastic Response of Offshore Towers to Strong Motion Earthquakes," by M. K. Kaul - 1972 (PB 215 713)A05

EERC 72-5 "Cyclic Behavior of Three Reinforced Concrete Flexural Members with High Shear," by E. P. Popov, V. V. Bertero, and H. Krawinkler - 1972 (PB 214 555)A05

EERC 72-6 "Earthquake Response of Gravity Dams Including Reservoir Interaction Effects," by P. Chakrabarti and A. K. Chopra - 1972 (AD 762 330)A08

EERC 72-7 "Dynamic Properties of Pine Flat Dam," by D. Rea, C. Y. Liaw, and A. K. Chopra - 1972 (AD 763 928)A05

EERC 72-8 "Three Dimensional Analysis of Building Systems," by E. L. Wilson and H. H. Dovey - 1972 (PB 222 438)A06

EERC 72-9 "Rate of Loading Effects on Uncracked and Repaired Reinforced Concrete Members," by S. Mahin, V. V. Bertero, D. Rea and M. Atalay - 1972 (PB 224 520)A08

EERC 72-10 "Computer Program for Static and Dynamic Analysis of Linear Structural Systems," by E. L. Wilson, K.-J. Bathe, J. E. Peterson and H. H. Dovey - 1972 (PB 220 437)A04

EERC 72-11 "Literature Survey - Seismic Effects on Highway Bridges," by T. Iwasaki, J. Penzien, and R. W. Clough - 1972 (PB 215 613)A19

EERC 72-12 "SHAKE - A Computer Program for Earthquake Response Analysis of Horizontally Layered Sites," by P. B. Schnabel and J. Lysmer - 1972 (PB 220 207)A06

EERC 73-1 "Optimal Seismic Design of Multistory Frames," by V. V. Bertero and H. Kamil - 1973

EERC 73-2 "Analysis of the Slides in the San Fernando Dams during the Earthquake of February 9, 1971," by H. B. Seed, K. L. Lee, I. M. Idriss, and F. Makdisi - 1973 (PB 223 402)A14

EERC 73-3 "Computer Aided Ultimate Load Design of Unbraced Multistory Steel Frames," by M. B. El-Hafez and G. H. Powell - 1973 (PB 248 315)A09

EERC 73-4 "Experimental Investigation into the Seismic Behavior of Critical Regions of Reinforced Concrete Components as Influenced by Moment and Shear," by M. Celebi and J. Penzien - 1973 (PB 215 884)A09

EERC 73-5 "Hysteretic Behavior of Epoxy-Repaired Reinforced Concrete Beams," by M. Celebi and J. Penzien - 1973 (PB 239 568)A03

EERC 73-6 "General Purpose Computer Program for Inelastic Dynamic Response of Plane Structures," by A. Kanaan and G. H. Powell - 1973 (PB 221 260)A08

EERC 73-7 "A Computer Program for Earthquake Analysis of Gravity Dams Including Reservoir Interaction," by P. Chakrabarti and A. K. Chopra - 1973 (AD 766 271)A04

EERC 73-8 "Behavior of Reinforced Concrete Deep Beam-Column Subassemblages under Cyclic Loads," by O. Küstü and J. G. Bouwkamp - 1973 (PB 246 117)A12

EERC 73-9 "Earthquake Analysis of Structure-Founation Systems," by A. K. Vaish and A. K. Chopra - 1973 (AD 766 272)A07

EERC 73-10 "Deconvolution of Seismic Response for Linear Systems," by R. B. Reimer - 1973 (PB 227 179)A08

EERC 73-11 "SAP IV: A Structural Analysis Program for Static and Dynamic Response of Linear Systems," by K.-J. Bathe, E. L. Wilson, and F. E. Peterson - 1973 (PB 221 967)A09

EERC 73-12 "Analytical Investigations of the Seismic Response of Long, Multiple Span Highway Bridges," by W. S. Tseng and J. Penzien - 1973 (PB 227 816)A10

EERC 73-13 "Earthquake Analysis of Multi-Story Buildings Including Foundation Interaction," by A. K. Chopra and J. A. Gutierrez - 1973 (PB 222 970)A03

EERC 73-14 "ADAP: A Computer Program for Static and Dynamic Analysis of Arch Dams," by R. W. Clough, J. M. Raphael, and S. Mojtahedi - 1973 (PB 223 763)A09

EERC 73-15 "Cyclic Plastic Analysis of Structural Steel Joints," by R. B. Pinkney and R. W. Clough - 1973 (PB 226 843)A08

EERC 73-16 "QUAD-4: A Computer Program for Evaluating the Seismic Response of Soil Structures by Variable Damping Finite Element Procedures," by I. M. Idriss, J. Lysmer, R. Hwang, and H. B. Seed - 1973 (PB 229 424)A05

EERC 73-17 "Dynamic Behavior of a Multi-Story Pyramid Shaped Building," by R. M. Stephen, J. P. Hollings, and J. G. Bouwkamp - 1973 (PB 240 718)A06

EERC 73-18 "Effect of Different Types of Reinforcing on Seismic Behavior of Short Concrete Columns," by V. V. Bertero, J. Hollings, O. Küstü, R. M. Stephen, and J. G. Bouwkamp - 1973

EERC 73-19 "Olive View Medical Center Materials Studies, Phase I," by B. Bresler and V. V. Bertero - 1973 (PB 235 986)A06

EERC 73-20 "Linear and Nonlinear Sesismic Analysis Computer Programs for Long Multiple-Span Highway Bridges," by W. S. Tseng and J. Penzien - 1973

EERC 73-21 "Constitutive Models for Cyclic Plastic Deformation of Engineering Materials," by J. M. Kelly and P. P. Gillis - 1973 (PB 226 024)A03

EERC 73-22 "DRAIN-2D User's Guide," by G. H. Powell - 1973 (PB 227 016)A05

EERC 73-23 "Earthquake Engineering at Berkeley - 1973 " 1973 (PB 226 033)A11

EERC 73-24 Unassigned

EERC 73-25 "Earthquake Response of Axisymmetric Tower Structures Surrounded by Water," by C. Y. Liaw and A. K. Chopra - 1973 (AD 773 052)A09

EERC 73-26 "Investigation of the Failures of the Olive View Stairtowers during the San Fernando Earthquake and Their Implications on Seismic Design," by V. V. Bertero and R. G. Collins - 1973 (PB 235 106)A13

EERC 73-27 "Further Studies on Seismis Behavior of Steel Beam-Column Subassemblages," by V. V. Bertero, H. Krawinkler, and E. P. Popcv - 1973 (PB 234 172)A06

EERC 74-1 "Seismic Risk Analysis," by C. S. Oliveira - 1974 (PB 235 920)A06

EERC 74-2 "Settlement and Liquefaction of Sands under Multi-Directional Shaking," by R. Pyke, C. K. Chan, and H. B. Seed - 1974

EERC 74-3 "Optimum Design of Earthquake Resistant Shear Buildings," by D. Ray, K. S. Pister, and A. K. Chopra - 1974 (PB 231 172)A06

EERC 74-4 "LUSH - A Computer Program for Complex Response Analysis of Soil-Structure Systems," by J. Lysmer, T. Udaka, H. B. Seed, and R. Hwang - 1974 (PB 236 796)A05

EERC 74-5 "Sensitivity Analysis for Hysteretic Dynamic Systems: Applications to Earthquake Engineering," by D. Ray - 1974 (PB 233 213)A06

EERC 74-6 "Soil Structure Interaction Analyses for Evaluating Seismic Response," by H. B. Seed, J. Lysmer, and R. Hwang - 1974 (PB 236 519)A04

EERC 74-7 Unassigned

EERC 74-8 "Shaking Table Tests of a Steel Frame - A Progress Report," by R. W. Clough and D. Tang - 1974 (PB 240 869)A03

EERC 74-9 "Hysteretic Behavior of Reinforced Concrete Flexural Members with Special Web Reinforcement," by V. V. Bertero, E. P. Popov, and T. Y. Wang - 1974 (PB 236 797)A07

EERC 74-10 "Applications of Realiability-Based, Global Cost Optimization to Design of Earthquake Resistant Structures," by E. Vitiello and K. S. Pister - 1974 (PB 237 231)A06

EERC 74-11 "Liquefaction of Gravelly Soils under Cyclic Loading Conditions," by R. T. Wong, H. B. Seed, and C. K. Chan - 1974 (PB 242 042)A03

EERC 74-12 "Site-Dependent Spectra for Earthquake-Resistant Design," by H. B. Seed, C. Ugas, and J. Lysmer - 1974 (PB 240 953)A03

EERC 74-13 "Earthquake Simulator Study of a Reinforced Concrete Frame," by P. Hidalgo and R. W. Clough - 1974 (PB 241 944)A13

EERC 74-14 "Nonlinear Earthquake Response of Concrete Gravity Dams," by N. Pal - 1974 (AD/A 006 583)A06

EERC 74-15 "Modeling and Identification in Nonlinear Structural Dynamics - I. One Degree of Freedom Models," by N. Distefano and A. Rath - 1974 (PB 241 548)A06

EERC 75-1 "Determination of Seismic Design Criteria for the Dumbarton Bridge Replacement Structure, Vol. I: Description, Theory and Analytical Modeling of Bridge and Parameters," by F. Baron and S.-H. Pang - 1975 (PB 259 407)A15

EERC 75-2 "Determination of Seismic Design Criteria for the Dumbarton Bridge Replacement Structure, Vol. II: Numerical Studies and Establishment of Seismic Design Criteria," by F. Baron and S.-H. Pang - 1975 (PB 259 408)A11 [For set of EERC 75-1 and 75-2 (PB 241 454)A09]

EERC 75-3 "Seismic Risk Analysis for a Site and a Metropolitan Area," by C. S. Oliveira - 1975 (PB 248 134)A09

EERC 75-4 "Analytical Investigations of Seismic Response of Short, Single or Multiple-Span Highway Bridges," by M.-C. Chen and J. Penzien - 1975 (PB 241 454)A09

EERC 75-5 "An Evaluation of Some Methods for Predicting Seismic Behavior of Reinforced Concrete Buildings," by S. A. Mahin and V. V. Bertero - 1975 (PB 246 306)A16

EERC 75-6 "Earthquake Simulator Story of a Steel Frame Structure, Vol. I: Experimental Results," by R. W. Clough and D. T. Tang - 1975 (PB 243 981)A13

EERC 75-7 "Dynamic Properties of San Bernardino Intake Tower," by D. Rea, C.-Y Liaw and A. K. Chopra - 1975 (AD/A 008 406)A05

EERC 75-8 "Seismic Studies of the Articulation for the Dumbarton Bridge Replacement Structure, Vol. 1: Description, Theory and Analytical Modeling of Bridge Components," by F. Baron and R. E. Hamati - 1975 (PB 251 539)A07

EERC 75-9 "Seismic Studies of the Articulation for the Dumbarton Bridge Replacement Structure, Vol. 2: Numerical Studies of Steel and Concrete Girder Alternates," by F. Baron and R. E. Hamati - 1975 (PB 251 540)A10

EERC 75-10 "Static and Dynamic Analysis of Nonlinear Structures," by D. P. Mondkar and G. H. Powell - 1975 (PB 242 434)A08

EERC 75-11 "Hysteretic Behavior of Steel Columns," by E. P. Popov, V. V. Bertero, and S. Chandramouli - 1975 (PB 252 365)A11

EERC 75-12 "Earthquake Engineering Research Center Library Printed Catalog " - 1975 (PB 243 711)A26

EERC 75-13 "Three Dimensional Analysis of Building Systems (Extended Version)," by E. L. Wilson, J. P. Hollings, and H. H. Dovey - 1975 (PB 243 989)A07

EERC 75-14 "Determination of Soil Liquefaction Characteristics by Large-Scale Laboratory Tests," by P. De Alba, C. K. Chan, and H. B. Seed - 1975 (NUREG 0027)A08

EERC 75-15 "A Literature Survey - Compressive, Tensile, Bond and Shear Strength of Masonry," by R. L. Mayes and R. W. Clough - 1975 (PB 246 292)A10

EERC 75-16 "Hysteretic Behavior of Ductile Moment-Resisting Reinforced Concrete Frame Components," by V. V. Bertero and E. P. Popov - 1975 (PB 246 388)A05

EERC 75-17 "Relationships Between Maximum Acceleration, Maximum Velocity, Distance from Source, Local Site Conditions for Moderately Strong Earthquakes," by H. B. Seed, R. Murarka, J. Lysmer, and I. M. Idriss - 1975 (PB 248 172)A03

EERC 75-18 "The Effects of Method of Sample Preparation on the Cyclic Stress-Strain Behavior of Sands," by J. Mulilis, C. K. Chan, and H. B. Seed - 1975 (Summarized in EERC 75-28)

EERC 75-19 "The Seismic Behavior of Critical Regions of Reinforced Concrete Components as Influenced by Moment, Shear and Axial Force," by M. B. Atalay and J. Penzien - 1975 (PB 258 842)A11

EERC 75-20 "Dynamic Properties of an Eleven Story Masonry Building," by R. M. Stephen, J. P. Hollings, J. G. Bouwkamp, and D. Jurukovski - 1975 (PB 246 945)A04

EERC 75-21 "State-of-the-Art in Seismic Strength of Masonry - An Evaluation and Review," by R. L. Mayes and R. W. Clough - 1975 (PB 249 040)A07

EERC 75-22 "Frequency Dependent Stiffness Matrices for Viscoelastic Half-Plane Foundations," by A. K. Chopra, P. Chakrabarti, and G. Dasgupta - 1975 (PB 248 121)A07

EERC 75-23 "Hysteretic Behavior of Reinforced Concrete Framed Walls," by T. Y. Wang, V. V. Bertero, and E. P. Popov - 1975

EERC 75-24 "Testing Facility for Subassemblages of Frame-Wall Structural Systems," by V. V. Bertero, E. P. Popov, and T. Endo - 1975

EERC 75-25 "Influence of Seismic History on the Liquefaction Characteristics of Sands," by H. B. Seed, K. Mori, and C. K. Chan - 1975 (Summarized in EERC 75-28)

EERC 75-26 "The Generation and Dissipation of Pore Water Pressures during Soil Liquefaction," by H. B. Seed, P. P. Martin, and J. Lysmer - 1975 (PB 252 648)A03

EERC 75-27 "Identification of Research Needs for Improving Aseismic Design of Building Structures," by V. V. Bertero - 1975 (PB 248 136)A05

EERC 75-28 "Evaluation of Soil Liquefaction Potential during Earthquakes," by H. B. Seed, I. Arango, and C. K. Chan - 1975 (NUREG 0026)A13

EERC 75-29 "Representation of Irregular Stress Time Histories by Equivalent Uniform Stress Series in Liquefaction Analyses," by H. B. Seed, I. M. Idriss, F. Makdisi, and N. Banerjee - 1975 (PB 252 635)A03

EERC 75-30 "FLUSH - A Computer Program for Approximate 3-D Analysis of Soil-Structure Interaction Problems," by J. Lysmer, T. Udaka, C.-F. Tsai, and H. B. Seed - 1975 (PB 259 332)A07

EERC 75-31 "ALUSH - A Computer Program for Seismic Response Analysis of Axisymmetric Soil-Structure Systems," by E. Berger, J. Lysmer, and H. B. Seed - 1975

EERC 75-32 "TRIP and TRAVEL - Computer Programs for Soil-Structure Interaction Analysis with Horizontally Travelling Waves," by T. Udaka, J. Lysmer, and H. B. Seed - 1975

EERC 75-33 "Predicting the Performance of Structures in Regions of High Seismicity," by J. Penzien - 1975 (PB 248 130)A03

EERC 75-34 "Efficient Finite Element Analysis of Seismic Structure-Soil-Direction," by J. Lysmer, H. B. Seed, T. Udaka, R. N. Hwang, and C.-F. Tsai - 1975 (PB 253 570)A03

EERC 75-35 "The Dynamic Behavior of a First Story Girder of a Three-Story Steel Frame Subjected to Earthquake Loading," by R. W. Clough and L.-Y. Li - 1975 (PB 248 841)A05

EERC 75-36 "Earthquake Simulator Story of a Steel Frame Structure, Volume II - Analytical Results," by D. T. Tang - 1975 (PB 252 926)A10

EERC 75-37 "ANSR-I General Purpose Computer Program for Analysis of Non-Linear Structural Response," by D. P. Mondkar and G. H. Powell - 1975 (PB 252 386)A08

EERC 75-38 "Nonlinear Response Spectra for Probabilistic Seismic Design and Damage Assessment of Reinforced Concrete Structures," by M. Murakami and J. Penzien - 1975 (PB 259 530)A05

EERC 75-39 "Study of a Method of Feasible Directions for Optimal Elastic Design of Frame Structures Subjected to Earthquake Loading," by N. D. Walker and K. S. Pister - 1975 (PB 247 781)A06

EERC 75-40 "An Alternative Representation of the Elastic-Viscoelastic Analogy," by G. Dasgupta and J. L. Sackman - 1975 (PB 252 173)A03

EERC 75-41 "Effect of Multi-Directional Shaking on Liquefaction of Sands," by H. B. Seed, R. Pyke, and G. R. Martin - 1975 (PB 258 781)A03

EERC 76-1 "Strength and Ductility Evaluation of Existing Low-Rise Reinforced Concrete Buildings - Screening Method," by T. Okada and B. Bresler - 1976 (PB 257 906)A11

EERC 76-2 "Experimental and Analytical Studies on the Hysteretic Behavior of Reinforced Concrete Rectangular and T-Beams," by S.-Y. M. Ma, E. P. Popov, and V. V. Bertero - 1976 (PB 260 843)A12

EERC 76-3 "Dynamic Behavior of a Multistory Triangular-Shaped Building," by J. Petrovski, R. M. Stephen, E. Gartenbaum, and J. G. Bouwkamp - 1976

EERC 76-4 "Earthquake Induced Deformations of Earth Dams," by N. Serff and H. B. Seed - 1976

EERC 76-5 "Analysis and Design of Tube-Type Tall Building Structures," by H. de Clercq and G. H. Powell - 1976 (PB 252 220)A10

EERC 76-6 "Time and Frequency Domain Analysis of Three-Dimensional Ground Motions,San Fernando Earthquake," by T. Kubo and J. Penzien - 1976 (PB 260 556)A11

EERC 76-7 "Expected Performance of Uniform Building Code Design Masonry Structures," by R. L. Mayes, Y. Omote, S. W. Chen, and R. W. Clough - 1976

EERC 76-8 "Cyclic Shear Tests on Concrete Masonry Piers, Part I - Test Results," by R. L. Mayes, Y. Omote, and R. W. Clough - 1976 (PB 264 424)A06

EERC 76-9 "A Substructure Method for Earthquake Analysis of Structure-Soil Interaction," by J. A. Gutierrez and A. K. Chopra - 1976 (PB 247 783)A08

EERC 76-10 "Stabilization of Potentially Liquefiable San Deposits using Gravel Drain Systems," by H. B. Seed and J. R. Booker - 1976 (PB 248 820)A04

EERC 76-11 "Influence of Design and Analysis Assumptions on Computed Inelastic Response of Moderately Tall Frames," by G. H. Powell and D. G. Row - 1976

EERC 76-12 "Sensitivity Analysis for Hysteretic Dynamic Systems: Theory and Applications," by D. Ray, K. S. Pister, and E. Polak - 1976 (PB 262 859)A04

EERC 76-13 "Coupled Lateral Torsional Response of Buildings to Ground Shaking," by C. L. Kan and A. K. Chopra - 1976 (PB 257 907)A09

EERC 76-14 "Seismic Analyses of the Banco de America," by V. V. Bertero, S. A. Mahin, and J. A. Hollings - 1976

EERC 76-15 "Reinforced Concrete Frame 2: Seismic Testing and Analytical Correlation," by R. W. Clough and J. Gidwani - 1976 (PB 261 323)A08

EERC 76-16 "Cyclic Shear Tests on Masonry Piers, Part II - Analysis of Test Results," by R. L. Mayes, Y. Omote, and R. W. Clough - 1976

EERC 76-17 "Structural Steel Bracing Systems: Behavior under Cyclic Loading," by E. P. Popov, K. Takanashi, and C. W. Roeder - 1976 (PB 260 715)A05

EERC 76-18 "Experimental Model Studies on Seismic Response of High Curved Overcrossings," by D. Williams and W. G. Godden - 1976

EERC 76-19 "Effects of Non-Uniform Seismic Disturbances on the Dumbarton Bridge Replacement Structure," by F. Baron and R. E. Hamati - 1976

EERC 76-20 "Investigation of the Inelastic Characteristics of a Single Story Steel Structure using System Identification and Shaking Table Experiments," by V. C. Matzen and H. D. McNiven - 1976 (PB 258 453)A07

EERC 76-21 "Capacity of Columns with Splice Imperfections," by E. P. Popov, R. M. Stephen and R. Philbrick - 1976 (PB 260 378)A04

EERC 76-22 "Response of the Olive View Hospital Main Building during the San Fernando Earthquake," by S. A. Mahin, V. V. Bertero, A. K. Chopra, and R. Collins," - 1976

EERC 76-23 "A Study on the Major Factors Influencing the Strength of Masonry Prisms," by N. M. Mostaghel, R. L. Mayes, R. W. Clough, and S. W. Chen - 1976

EERC 76-24 "GADFLEA - A Computer Program for the Analysis of Pore Pressure Generation and Dissipation during Cyclic or Earthquake Loading," by J. R. Booker, M. S. Rahman, and H. B. Seed - 1976 (PB 263 947)A04

EERC 76-25 "Rehabilitation of an Existing Building: A Case Study," by B. Bresler and J. Axley - 1976

EERC 76-26 "Correlative Investigations on Theoretical and Experimental Dynamic Behavior of a Model Bridge Structure," by K. Kawashima and J. Penzien - 1976 (PB 263 388)A11

EERC 76-27 "Earthquake Response of Coupled Shear Wall Buildings," by T. Srichatrapimuk - 1976 (PB 265 157)A07

EERC 76-28 "Tensile Capacity of Partial Penetration Welds," by E. P. Popov and R. M. Stephen - 1976 (PB 262 899)A03

EERC 76-29 "Analysis and Design of Numerical Integration Methods in Structural Dynamics," by H. M. Hilber - 1976 (PB 264 410)A06

EERC 76-30 "Contribution of a Floor System to the Dynamic Characteristics of Reinforced Concrete Buildings," by L. E. Malik and V. V. Bertero - 1976

EERC 76-31 "The Effects of Seismic Disturbances on the Golden Gate Bridge," by F. Baron, M. Arikan, R. E. Hamati - 1976

EERC 76-32 "Infilled Frames in Earthquake-Resistant Construction," by R. E. Klingner and V. V. Bertero - 1976 (PB 265 892)A13

UCB/EERC-77/01 "PLUSH - A Computer Program for Probabilistic Finite Element Analysis of Seismic Soil-Structure Interaction," by M. P. Romo Organista, J. Lysmer, and H. B. Seed - 1977

UCB/EERC-77/02 "Soil-Structure Interaction Effects at the Humboldt Bay Power Plant in the Ferndale Earthquake of June 7, 1975," by J. E. Valera, H. B. Seed, C.-F. Tsai, and J. Lysmer - 1977 (B 265 795)A04

UCB/EERC-77/03 "Influence of Sample Disturbance on Sand Response to Cyclic Loading," by K. Mori, H. B. Seed, and C. K. Chan - 1977 (PB 267 352)A04

UCB/EERC-77/04 "Seismological Studies of Strong Motion Records," by J. Shoja-Taheri - 1977 (PB 269 655)A10

UCB/EERC-77/05 "Testing Facility for Coupled Shear Walls," by L.-H. Lee, V. V. Bertero, and E. P. Popov - 1977

UCB/EERC-77/06 "Developing Methodologies for Evaluating the Earthquake Safety of Existing Buildings," No. 1 - B. Bresler; No. 2 - B. Bresler, T. Okada, and D. Zisling; No. 3 - T. Okada and B. Bresler; No. 4 - V. V. Bertero and B. Bresler - 1977 (PB 267 354)A08

UCB/EERC-77/07 "A Literature Survey - Transverse Strength of Masonry Walls," by Y. Omote, R. L. Mayes, S. W. Chen, and R. W. Clough - 1977

UCB/EERC-77/08 "DRAIN-TABS: A Computer Program for Inelastic Earthquake Response of Three Dimensional Buildings," by R. Guendelman-Israel and G. H. Powell - 1977

UCB/EERC-77/09 "SUBWALL: A Special Purpose Finite Element Computer Program for Practical Elastic Analysis and Design of Structural Walls with Substructure Option," by D. Q. Le, H. Petersson, and E. P. Popov - 1977

UCB/EERC-77/10 "Experimental Evaluation of Seismic Design Methods for Broad Cylindrical Tanks," by D. P. Clough - 1977

UCB/EERC-77/11 "Earthquake Engineering Research at Berkeley - 1976," - 1977

UCB/EERC-77/12 "Automated Design of Earthquake Resistant Multistory Steel Building Frames," by N. D. Walker, Jr. - 1977

UCB/EERC-77/13 "Concrete Confined by Rectangular Hoops and Subjected to Axial Loads," by J. Vallenas, V. V. Bertero, and E. P. Popov - 1977

UCB/EERC-77/14 "Seismic Strain Induced in the Ground during Earthquakes," by Y. Sugimura - 1977

UCB/EERC-77/15 "Bond Deterioration under Generalized Loading," by V. V. Bertero, E. P. Popov, and S. Viwathanatepa - 1977

UCB/EERC-77/16 "Computer-Aided Optimum Design of Ductile Reinforced Concrete Moment-Resisting Frames," by S. W. Zagajeski and V. V. Bertero - 1977

UCB/EERC-77/17 "Earthquake Simulation Testing of a Stepping Frame with Energy-Absorbing Devices," by J. M. Kelly and D. F. Tsztoo - 1977

UCB/EERC-77/18 "Inelastic Behavior of Eccentrically Braced Steel Frames under Cyclic Loadings," by C. W. Roeder and E. P. Popov - 1977

UCB/EERC-77/19 "A Simplified Procedure for Estimating Earthquake-Induced Deformation in Dams and Embankments," by F. I. Makdisi and H. B. Seed - 1977

UCB/EERC-77/20 "The Performance of Earth Dams during Earthquakes," by H. B. Seed, F. I. Makdisi, and P. de Alba - 1977

UCB/EERC-77/21 "Dynamic Plastic Analysis Using Stress Resultant Finite Element Formulation," by P. Lukkunaprasit and J. M. Kelly - 1977

UCB/EERC-77/22 "Preliminary Experimental Study of Seismic Uplift of a Steel Frame," by R. W. Clough and A. A. Huckelbridge - 1977

UCB/EERC-77/23 "Earthquake Simulator Tests of a Nine-Story Steel Frame with Columns Allowed to Uplift," by A. A. Huckelbridge - 1977

UCB/EERC-77/24 "Nonlinear Soil-Structure Interaction of Skew Highway Bridges," by M.-C. Chen and J. Penzien - 1977

UCB/EERC-77/25 "Seismic Analysis of an Offshore Structure Supported on Pile Foundations," by D.D.-N. Liou - 1977

UCB/EERC-77/26 "Dynamic Stiffness Matrices for Homogeneous Viscoelastic Half-Planes," by G. Dasgupta and A. K. Chopra - 1977

UCB/EERC-77/27 "A Practical Soft Story Earthquake Isolation System," by J. M. Kelly and J. M. Eidinger - 1977

UCB/EERC-77/28 "Seismic Safety of Existing Buildings and Incentives for Hazard Mitigation in San Francisco: An Exploratory Study," by A. J. Meltsner - 1977

UCB/EERC-77/29 "Dynamic Analysis of Electrohydraulic Shaking Tables," by D. Rea, S. Abedi-Hayati, and Y. Takahashi - 1977

UCB/EERC-77/30 "An Approach for Improving Seismic-Resistant Behavior of Reinforced Concrete Interior Joints," by B. Galunic, V. V. Bertero, and E. P. Popov - 1977

UCB/EERC-78/01 "The Development of Energy-Absorbing Devices for Aseismic Base Isolation Systems," by J. M. Kelly and D. F. Tsztoo - 1978

UCB/EERC-78/02 "Effect of Tensile Prestrain on the Cyclic Response of Structural Steel Connections," by J. G. Bouwkamp and A. Mukhopadhyay - 1978

UCB/EERC-78/03 "Experimental Results of an Earthquake Isolation System using Natural Rubber Bearings," by J. M. Eidinger and J. M. Kelly - 1978

UCB/EERC-78/04 "Seismic Behavior of Tall Liqiud Storage Tanks," by A. Niwa - 1978

UCB/EERC-78/05 "Hysteretic Behavior of Reinforced Concrete Columns Subjected to High Axial and Cyclic Shear Forces," by S. W. Zagajeski, V. V. Bertero, and J. G. Bouwkamp - 1978

UCB/EERC-78/06 "Inelastic Beam-Column Elements for the ANSR-I Program," by A. Riahi, D. G. Row, and G. H. Powell - 1978

UCB/EERC-78/07 "Studies of Structural Response to Earthquake Ground Motion," by O. A. Lopez and A. K. Chopra - 1978

UCB/EERC-78/08 "A Laboratory Study of the Fluid-Structure Interaction of Submerged Tanks and Caissons in Earthquakes," by R. C. Byrd - 1978

UCB/EERC-78/09 "Models for Evaluating Damageability of Structures," by I. Sakamoto and B. Bresler - 1978

UCB/EERC-78/10 "Seismic Performance of Secondary Structural Elements," by I. Sakamoto - 1978

UCB/EERC-78/11 "Case Study -- Seimsic Safety Evaluation of a Reinforced Concrete School Building," by J. Axley and B. Bresler - 1978

UCB/EERC-78/12 "Potential Damageability in Existing Buildings," by T. Blejwas and B. Bresler - 1978

UCB/EERC-78/13 "Dynamic Behavior of a Pedestal Base Multistory Building," by R. M. Stephen, E. L. Wilson, J. G. Bouwkamp, and M. Button - 1978

UCB/EERC-78/14 "Seismic Response of Bridges - Case Studies," by R. A. Imbsen, V. Nutt, and J. Penzien - 1978

UCB/EERC-78/15 "A Substructure Technique for Nonlinear Static and Dynamic Analysis," by D. G. Row and G. H. Powell - 1978

UCB/EERC-78/16 "Seismic Performance of Nonstructural and Secondary Structural Elements," by I. Sakamoto - 1978

UCB/EERC-78/17 "Model for Evaluating Damageability of Structures," by I. Sakamoto and B. Bresler - 1978

UCB/EERC-78/18 "Response of K-Braced Steel Frame Models to Lateral Loads," by J. G. Bouwkamp, R. M. Stephen, and E. P. Popov - 1978

UCB/EERC-78/19 "Rational Design Methods for Light Equipment in Structures Subjected to Ground Motion," by J. L. Sackman and J. M. Kelly - 1978

UCB/EERC-78/20 "Testing of a Wind Restraint for Aseismic Base Isolation," by J. M. Kelly and D. E. Chitty - 1978